Western Australian School of Mines
Department of Mining Engineering and Metallurgical Engineering

Removal of Arsenic from Alkaline Process Water of Gold Cyanidation by Use of Functionalised Magnetic Adsorbents

Chong Feng

This thesis is presented for the Degree of
Doctor of Philosophy
of
Curtin University

August 2017

Declaration

To the best of my knowledge and belief this thesis contains no material previously published by any other person except where due acknowledgment has been made.

This thesis contains no material which has been accepted for the award of any other degree or diploma in any university.

Signature: .....

Date: 09.08.2017

Abstract

As is well-known, arsenic is a notorious toxic element, posing a severe threat to both human health and nature. Meanwhile, arsenic is also a vexing issue in gold industry, leading to a number of undesirable outcomes during gold cyanidation, such as retardation or prevention of gold dissolution, influence on gold adsorption onto activated carbon, etc. Although a great variety of techniques have been proposed for removing arsenic from aqueous solutions in the past few decades, none of them is completely competent under all conditions. Adsorption in particular, is a promising approach, but nearly all relevant methods have concentrated on water purification under neutral or acidic conditions. In alkaline process waters of gold cyanide leaching system, these adsorbents tend to be less effective. Inspired by previous researches, in this study, three types of functionalised magnetic adsorbents with different core-shell structures, namely Fe_3O_4@SiO_2@TiO_2, γ-Fe_2O_3@ZrO_2 and Fe_3O_4@CeO_2/$Ce(OH)_4$, were successfully synthesised via uncomplicated synthetic processes and creatively used to extract arsenic species from alkaline gold cyanidation process waters.

In the first place, a series of analytical methods were employed to comprehensively characterise the synthesised adsorbents, including SEM-EDS for microstructure, morphology and elemental composition, XRD for phase composition, SQUID for magnetic properties, BET for specific surface area, etc. The analysis results showed that these adsorbents were microparticles with diameters ranging from 20 to 400 nm, and consisted of crystalline magnetite/maghemite and mostly amorphous titanium/zirconium/cerium oxide. All three ferromagnetic materials exhibited saturation magnetization in excess of 40 emu/g, readily allowing magnetic separation by an external magnetic field after adsorption. The specific surface areas of Fe_3O_4@SiO_2@TiO_2, γ-Fe_2O_3@ZrO_2 and Fe_3O_4@CeO_2/$Ce(OH)_4$ were determined to be 86.65, 140.03 and 91.38 m^2/g, respectively, which were sufficiently large to provide abundant active sites for arsenic adsorption.

Next, systematic adsorption tests were carried out to determine their adsorption behaviours towards both As(III) and As(V) under alkaline conditions, including

effect of pH on adsorption, adsorption kinetics, adsorption isotherms and competitive adsorption. Within the studied pH range of 7–11, generally speaking, good adsorption results were achieved but the adsorbed amounts of both As(III) and As(V) onto all three adsorbents decreased with increasing pH. Adsorption kinetics and isotherms were both performed at pH 9, which is typical of process water samples from a few gold mines located in Western Australia. For all three adsorbents, adsorption equilibrium could be achieved in approximately 4 h and the kinetic data were satisfactorily fitted by the pseudo-second-order kinetic model, indicating chemisorption was most likely involved. According to the experimental results from adsorption isotherms, all three adsorbents showed great adsorption performances, with the Langmuir maximum adsorption capacities of 31.4–79.1 mg/g for As(III) and 10.2–25.5 mg/g for As(V) in arsenic-only solutions. In competitive adsorption tests conducted in simulated process waters from gold cyanidation, the simultaneous arsenic adsorption capacities of Ti-based, Zr-based and Ce-based adsorbents were found to be 15.6, 42.3 and 51.2 mg/g, respectively, showing huge potential in the future industrial applications.

Last but not least, the possibility and feasibility of the synthesised adsorbents for regeneration and reuse were evaluated through multiple consecutive adsorption-desorption cycles with 1.0 mol/L NaOH solution as a regenerant. Over 60% of the initial adsorption capacities of all three materials were retained after four or five cycles of adsorption and desorption, revealing that a highly alkaline solution could liberate a certain amount of active adsorption sites for arsenic species to be reloaded again, which is highly conducive to cost reduction in consideration of the industrial practicability.

All in all, this thesis provides an entirely new way of thinking for removing arsenic species from alkaline process waters of gold cyanidation and establishes the solid foundation for future industrialisation.

List of Abbreviations and Acronyms

As(III)	arsenite
As(V)	arsenate
BET	Brunauer-Emmett-Teller
EDS	energy dispersive spectrometer
emu	electromagnetic unit
ICP-OES	inductively coupled plasma - optical emission spectrometer
Oe	oersted (unit of magnetic field strength equivalent to 79.58 A/m)
PZC	point of zero charge
SEM	scanning electron microscope
SQUID	superconducting quantum interference device
TBT	titanium(IV) butoxide
TEOS	tetraethyl orthosilicate
XRD	X-ray diffraction

Acknowledgements

It is an honour to thank the people who made this thesis possible.

It is difficult to overstate my gratitude to my supervisors: Prof. Chris Aldrich, Prof. Jacques Eksteen and Prof. Damien Arrigan. With their enthusiasm, their inspiration, and their great efforts to help me with all sorts of difficulties I encountered, they made research fun for me. Throughout my Ph.D. study, they provided encouragement, sound advice, good teaching and countless good ideas. I would have been lost without them.

I would like to thank my many student colleagues for providing an interesting and stimulating environment in which to learn and grow, especially Doyoung Choi, Bennson Tanda, Ngoie Mpinga, Alireza Rabieh and Nirmala Ilankoon.

I would also like to thank BASF Australia Limited for financial support and technical assistance, and Curtin University's John de Laeter Centre and CSIRO Mineral Resources at Waterford for accessing to analytical facilities.

I am grateful to my entire extended family, particularly my uncle, Dingwu Feng, for continued support.

Lastly, and most importantly, I wish to thank my parents, Jinhai Feng and Yunxia Zhu, and my wife, Yang Hou for their unconditional love. To them I dedicate this thesis.

Publications

The following publications have resulted from the research presented in this thesis:

- Feng, C., Aldrich, C., Eksteen, J. J., & Arrigan, D. W. M. (2017). Removal of arsenic from alkaline process waters of gold cyanidation by use of Fe_3O_4@SiO_2@TiO_2 nanosorbents. *Minerals Engineering*, 110, 40-46.

- Feng, C., Aldrich, C., Eksteen, J. J., & Arrigan, D. W. M. (2017). Removal of arsenic from alkaline process waters of gold cyanidation by use of γ-Fe_2O_3@ZrO_2 nanosorbents. *Hydrometallurgy*, 174, 71-77.

- Feng, C., Aldrich, C., Eksteen, J. J., & Arrigan, D. W. M. (2017). Removal of arsenic from gold processing circuits by use of novel magnetic nanoparticles. *Canadian Metallurgical Quarterly*. (In press)

- Feng, C., Aldrich, C., Eksteen, J. J., & Arrigan, D. W. M. (2017). Removal of arsenic from alkaline process waters of gold cyanidation by use of cerium-based magnetic microparticles. *Minerals Engineering*. (Under review)

- Feng, C., Aldrich, C., Eksteen, J. J., & Arrigan, D. W. M. (2017). Removal of arsenic from gold processing circuits by use of novel magnetic nanoparticles. World Gold, 27-30 August, Vancouver, BC, Canada.

Table of Contents

List of Tables

List of Figures

CHAPTER 1 INTRODUCTION

1.1. Background

It is widely known that arsenic is a carcinogenic, teratogenic, clastogenic poison posing a severe threat to human health. Arsenic constitutes approximately 0.00015% of the Earth's crust in the form of more than 300 minerals, making it the 53rd most abundant element (John Emsley, 2011). In general, the most common arsenic minerals in association with gold are sulfides, such as realgar (As_4S_4), orpiment (As_2S_3) and arsenopyrite (FeAsS).

During gold processing by cyanidation, arsenic is inevitably released into process waters and is able to adversely affect the gold extraction in various ways. In the strongly alkaline solutions used for gold leaching by cyanidation, arsenic sulfides can be oxidised to arsenite (AsO_3^{3-}) and arsenate (AsO_4^{3-}) with oxygen present, and the proportion of each is dependent on the solution composition, oxidation potential and pH (Kyle et al., 2012a). Oxidised and partially oxidised arsenic species influence cyanidation by consuming oxygen and retarding or preventing gold dissolution (Marsden and House, 2006). Arsenic may also affect gold recovery by competitive adsorption onto activated carbon (Lorenzen et al., 1995). Although limited information is available on the behaviour of arsenic in tailings dams, there is little doubt that arseniferous tailings are difficult to treat and seriously threatening human health and the environment (Liu et al., 2015). In addition, it is common knowledge that water is a valuable and expensive resource. The process water for gold cyanidation is recycled with adjustments. If not removed from the process water, the arsenic species could accumulate and the negative impact mentioned above could be exacerbated. Therefore, it is necessary to remove arsenic from the process waters.

In order to tackle arsenic contamination problems, numerous approaches have been proposed. Basically, these approaches can be broadly divided into three categories, i.e., precipitation/encapsulation, membrane technologies and adsorption.

It is known that in aqueous solutions, the arsenic species prevalently exist in the form of oxyanions arsenite (As(III)) and arsenate (As(V)) (Molinari and Argurio, 2017). According to a survey carried out on the gold cyanidation process waters from several Western Australian gold mines, it is found that the pH values of the process waters are basically within the range of 7.0–10.0. Under this condition, the most thermodynamically stable species for As(III) are H_3AsO_3 (pH<9.2 approximately) and $H_2AsO_3^-$ (9.2<pH<10), and $HAsO_4^{2-}$ for As(V). With the restrictions of arsenic species in combination with the presence of other substances, particularly cyanide, precipitation is generally inappropriate (Nishimura and Robins, 2000; Tahija and Huang, 2000). Membrane technologies seem to be an efficient way for arsenic removal with no toxic solid wastes produced, however, the treatment processes usually require high cost in capital, operating and maintenances and potentially long treatment time (Mohan and Pittman Jr, 2007; Nicomel et al., 2016). Adsorption, with the advantages of low-cost, easy handling, low energy requirement and satisfactory arsenic removal rate (Mohan and Pittman Jr, 2007), is considered to be a more suitable approach for As removal from the gold cyanidation process waters.

Various kinds of arsenic adsorbents were proposed and investigated for the remediation of drinking water or ground water systems, which had pH values near 7. Among them, the oxides/hydroxides of titanium, zirconium and cerium have attracted extensive attentions due to their high arsenic adsorption capacities, wide application pH ranges and easy regeneration/reuse abilities. In addition, the mechanisms of the arsenic adsorption on these adsorbents have been established by a number of research groups from macro and micro perspective of views (Cui et al., 2012; Guan et al., 2012; Sun et al., 2012). It was demonstrated that the surface hydroxyl groups of the metal oxides/hydroxides adsorbents were involved in the arsenic adsorption and inner-sphere complexes were formed between arsenic and the sorbents. Furthermore, via comparative studies of various arsenic adsorbents, Li et al. (2014) found that the ionic potential of a material could be used as a guidance for the selection of suitable arsenic adsorbents. They suggested that if the ionic potential of a material is within the range of (approximately) 4–7, it could be a suitable candidate for arsenic adsorption. Interestingly, the ionic potentials of Ti^{4+}, Zr^{4+} and Ce^{4+} are located right in the so-called criteria range.

Although numerous studies have been carried out regarding the arsenic adsorption performance of titannium, zirconium and cerium based adsorbents, there are no records for the treatment of gold cyanidation process waters under alkaline conditions.

Moreover, for the enhanced arsenic adsorption capacity, nano-sized adsorbents are pursued mainly because of the increased specific surface area. However, nanoparticles are too small to control confidently. They are very likely to be released into the natural environment especially water systems, posing a threat to the human health (Tang and Lo, 2013). Moreover, the preparation of nanoparticles tends to be more energy consuming and relatively expensive. Consequently, it is not always the best option to use nanoparticles to improve the adsorption capacities of the adsorbents.

In addition, considering the practical application of these adsorbents, separation of the spent sorbents from the water body is important. Conventionally, filtration or centrifugation was employed (Clifford et al., 1983). However, problems would arise if the filters became blocked or adsorbents lost (Reddy and Yun, 2016). More recently, the use of magnetic separation has attracted a lot of interests (Mehta et al., 2015). A large number of publications have reported the combination of arsenic adsorbents with magnetic materials such as magnetite (Fe_3O_4), maghemite (γ-Fe_2O_3) and zero valent iron to facilitate the rapid and efficient separation of the exhausted adsorbents from the aqueous medium.

On the basis of the above observations from various previous work, in this study, magnetic titanium, zirconium and cerium based adsorbents were synthesised and innovatively introduced to the gold cyanidation process waters for arsenic removal. Since the arsenic adsorption mechanisms have already been established by other researchers, the focus of this study is to investigate the performance of the Ti, Zr and Ce based adsorbents under alkaline conditions and to explore the application potential of the synthesised magnetic adsorbents in gold cyanidation process waters.

1.2. Objectives

The waters associated with the gold cyanidation process circuits are complicated owing to diverse water sources, various types of gold ores and different process flows, etc. Consequently, the actual process waters can be composed of a wide variety of chemical species. Moreover, since water is a valuable resource, it is generally recycled and reused. In this way, the ions present in the process waters can be accumulated, leading to high ionic concentrations and strength. In general, during the gold leaching by cyanidation, lime or sodium hydroxide are added to the leaching solution to prevent the unexpected consumption of cyanide species and the release of toxic HCN gas. Therefore, the pH of the process water is generally kept between 10–12. This alkaline condition renders most of the adsorbents dedicated for arsenic removal inefficient. However, after gold recovery with active carbon or resins, for instance, in the tailings dams, excessive free cyanides in the process water are destructed and the pH of the water is adjusted to around 7–9 for recycling. In order to prevent the arsenic species from accumulating in the cycled process water, this study aims to provide a potential adsorption method to remove arsenic species from alkaline process water of gold cyanidation by using functionalised magnetic adsorbents and lay the foundation for practical industrial application in the near future. The main targeted solutions were process waters after cyanide destruction with milder alkaline conditions. Specifically, the objectives of this study are achieved by following steps.

- Design and synthesise several types of functionalised magnetic particles for effectively adsorbing arsenic species from alkaline aqueous solutions.
- Determine their surface properties and structural characteristics by a series of analytical methods.
- Examine their adsorption capacities towards arsenic species in both arsenic-only solutions and simulated process waters from gold cyanidation.
- Explore the feasibility of regenerating and reusing the synthesised adsorbents.

1.3. Structure of thesis

This thesis consists of seven chapters, as outlined below.

CHAPTER 1 introduces the background and objectives of this study.

CHAPTER 2 firstly reviews the mineralogy and aqueous chemistry of arsenic and problems caused by its presence in gold cyanidation processes, followed by various techniques used to remove arsenic from aqueous medium. Adsorption method is highlighted through comparisons of different arsenic removal approaches and the properties of various adsorbents are compared. A number of factors relating to the application of the adsorbents are also reviewed, including pH, properties of the adsorbent materials, co-existing anions, separation and regeneration of the As-loaded adsorbents as well as the potential of reusing the regenerated adsorbents. Three types of arsenic adsorbents stand out, i.e. oxides/hydroxides of titanium, zirconium and cerium. Most of the literature focused on the remediation of drinking water or ground water with near neutral pH. Very few papers have investigated the arsenic adsorption in alkaline waters and none is found for the treatment of gold cyanidation process waters.

CHAPTER 3 provides the materials and methods used for the following three experimental chapters.

CHAPTER 4, CHAPTER 5 and CHAPTER 6 detail the synthesis, characterisation, adsorption tests and desorption tests of the titanium-based magnetic adsorbent ($Fe_3O_4@SiO_2@TiO_2$), the zirconium-based magnetic adsorbent (γ-$Fe_2O_3@ZrO_2$) and the cerium-based magnetic adsorbent ($Fe_3O_4@CeO_2/(OH)_x$), respectively.

CHAPTER 7 highlights the key findings for achieving the objectives of this thesis and makes reasonable suggestions for future work.

CHAPTER 2 LITERATURE REVIEW

2.1. Arsenic in gold processing by cyanidation

2.1.1. Impact of arsenic on environment and humans

Arsenic is widely distributed in the environment such as natural waters, soil, plants and air. Investigations (Brammer and Ravenscroft, 2009; Heikens et al., 2007) revealed that As can gradually build up in soil via irrigating with As rich water, which could adversely affect the sustainability of agriculture by degradation of soil and lowering of crop yield. Moreover, the accumulated arsenic could enter the food chain, imposing great threats to human health. Mining and metallurgical activities were found to be responsible for the arsenic contamination of river water, ground water and soil (Ashley and Lottermoser, 1999; Bissen and Frimmel, 2003). High concentrations of arsenic in groundwater and drinking water have been found in many countries, including Australia, Bangladesh, Chile, China, India, Mexico and USA, etc. (Singh et al., 2015; Argos et al., 2010).

It is commonly known that arsenic is toxic. However, the toxicity of arsenic depends on its binding form. In general, organic arsenic is less toxic than inorganic arsenic species and arsenite is more toxic than arsenate (Singh et al., 2015). The acute and chronic poisoning of arsenic on humans include respiratory, gastro-intestinal, cardio-vascular, nervous, and haematopoietic systems. Moreover, arsenic has been identified to be carcinogenic, inducing skin, lung and bladder cancers, etc. (Bissen and Frimmel, 2003; Bretzler et al., 2017).

2.1.2. Arsenic mineralogy

Arsenic is ubiquitous in the environment and over 300 different types of arsenic-bearing minerals have been found to occur in nature (Drahota and Filippi, 2009). Usually, these minerals can be classified into six primary categories, namely,

elemental arsenic, arsenides, arsenic sulfides, arsenic oxides, arsenites and arsenates. Examples of common arsenic-bearing minerals that fall under the above primary categories are listed in Table 2-1 (O'Day, 2006).

Among them, it is reported that around 60% are arsenates, around 20% are arsenic sulphides, 10% are arsenic oxides and the rest are elemental arsenic, arsenides and arsenites. Arsenopyrite (FeAsS), with 46% arsenic content, is one of the most common arsenic sulfide minerals. Arsenic also generally occurs in the structure of pyrite (FeS_2) as a coupled substitution (Arehart et al., 1993). Both arsenopyrite and pyrite can be associated with significant amounts of gold. Besides, arsenic is often found in copper sulfosalts as well, such as enargite (Cu_3AsS_4) and tennantite ($(Cu,Fe)_{12}As_4S_{13}$), which normally serve as an indicator of Cu-Au deposits (Asselin and Shaw, 2016). In a word, arsenic, the notorious toxic element, is closely bound up with gold-bearing minerals and ore bodies. It is unfortunate that, therefore, arsenic management becomes part and parcel of the entire gold industry including mining, metallurgy, etc. Regulations regarding the operations of mining and metallurgical industries are increasingly strict. The presence of arsenic in the processing circuits not only causes considerable increase in the production costs and decrease in the quality of products, but also potentially imposes great hazard on the environment. Therefore, removing arsenic from the processing circuits becomes utterly important.

Table 2-1. Classification of arsenic-bearing minerals and examples.

Category	Mineral	Formula
Elemental arsenic	Native arsenic	As
	Arsenolamprite	As
	Pararsenolamprite	As
Arsenides	Domeykite	Cu_3As
	Löllingite	$FeAs_2$
	Nickeline (aka Niccolite)	NiAs
	Rammelsbergite	$NiAs_2$
	Safflorite	$CoAs_2$
	Sperrylite	$PtAs_2$
Arsenic sulfides	Arsenopyrite	FeAsS
	Enargite	Cu_3AsS_4
	Cobaltite	CoAsS
	Gersdorffite	NiAsS
	Orpiment	As_2S_3
	Realgar	As_4S_4/AsS
Arsenic oxides	Arsenolite	As_2O_3
	Claudetite	As_2O_3
Arsenites	Leiteite	$ZnAs_2O_4$
	Reinerite	$Zn_3(AsO_3)_2$
	Gebhardite	$Pb_8(As_2O_5)_2OCl_6$
Arsenates	Johnbaumite	$Ca_5(AsO_4)_3(OH)$
	Austinite	$CaZn(AsO_4)(OH)$
	Scorodite	$FeAsO_4 \cdot 2H_2O$
	Hörnesite	$Mg_3(AsO_4)_2 \cdot 8H_2O$
	Barium-pharmacosiderite	$BaFe_4(AsO_4)_3(OH)_5 \cdot 5H_2O$
	Mixite	$BiCu_6(AsO_4)_3(OH)_6 \cdot 3H_2O$
	Sarmientite	$Fe_2(AsO_4)(SO_4)(OH) \cdot 5H_2O$
	Arsenuranylite	$Ca(UO_2)_4(AsO_4)_2(OH)_4 \cdot 6H_2O$

2.1.3. Aqueous chemistry of arsenic

It is well known that arsenic is present in aqueous solutions prevalently in the form of oxyanions arsenite (As(III)) and arsenate (As(V)) (Molinari and Argurio, 2017). Due to the slow kinetics of redox transformations, both arsenite and arsenate can coexist irrespective of the redox conditions (Masscheleyn et al., 1991). While arsenic speciation and proportion of each species highly rely on specific solution conditions, especially redox potential and pH. The Pourbaix diagram (also known as E_h-pH diagram) presenting the thermodynamically stable regions for inorganic arsenic species is shown in Figure 2-1.

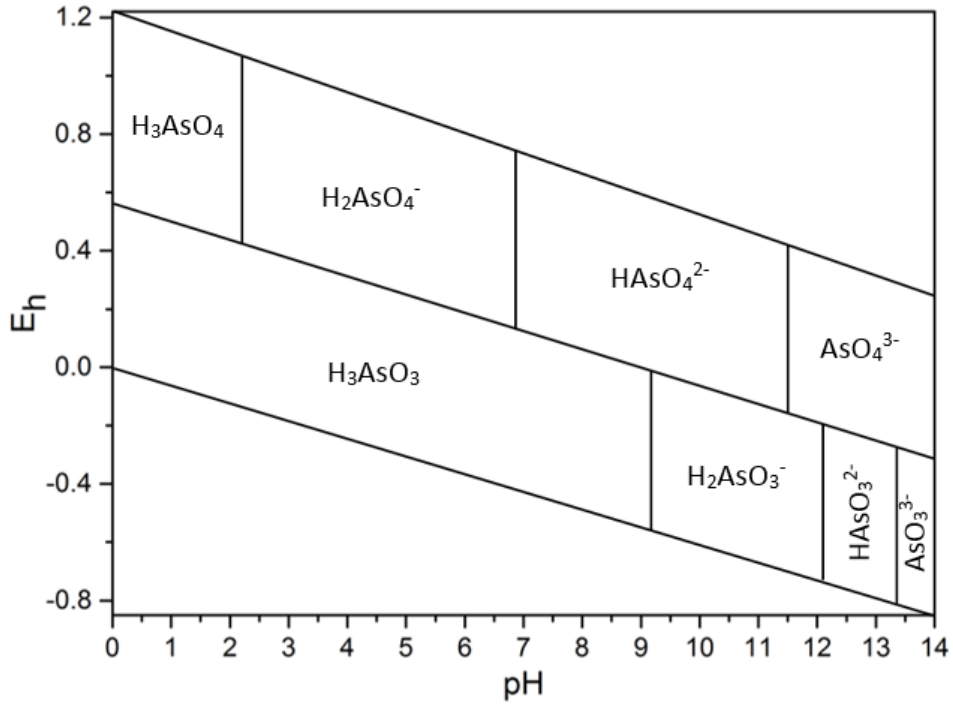

Figure 2-1. Pourbaix diagram for inorganic arsenic species.

According to our surveys, the pH values of the process water samples from several gold mines in Western Australia were basically within the alkaline range of 7.0–10.0. In combination with the acid dissociation constants of arsenious acid ($pK_{a1,2,3}$=9.2, 12.1, 13.4) and arsenic acid ($pK_{a1,2,3}$=2.2, 6.9, 11.5) (Palmer et al., 2006), it is apparent that the most thermodynamically stable species are H_3AsO_3 and $H_2AsO_3^-$ for As(III) and $HAsO_4^{2-}$ for As(V), respectively. In other words, these aqueous

arsenic species can be theoretically regarded as the main target adsorbates in this study.

Furthermore, arsenite has been confirmed to be much more toxic (Ferguson and Gavis, 1972; Singh et al., 2015), soluble and mobile (Deuel and Swoboda, 1972) than arsenate in water. Obviously, more attention should be paid to developing and enhancing the management of As(III) species.

2.1.4. Behaviours of arsenic in gold processing by cyanidation

Figure 2-2 shows a simplified gold cyanidation process flow chart, which was drawn according to the reviews by Kyle et al. (2012b) and Adams (2016). On the basis of this flow diagram, the possible influences of arsenic behaviours on the gold cyanidation circuits will be discussed.

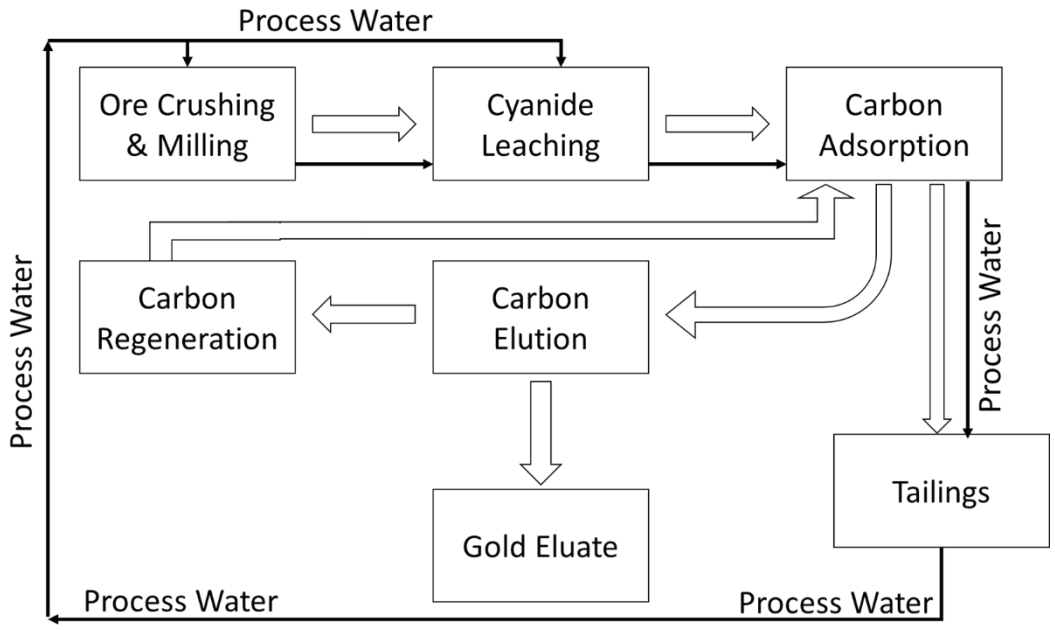

Figure 2-2. Simplified gold cyanidation process flow diagram.

To begin with, the As-bearing gold ores are crushed and milled to the specified particle size. If the ores are refractory in nature, which is often the case for arsenical gold ores, a preoxidation process is required to make the gold ores more amenable to cyanide leaching. Conventionally, roasting is carried out for this purpose. During

roasting, arsenic is converted to a volatile As_2O_3 which can be scrubbed in lime (Kyle et al., 2012b). Alternative approaches including high/low pressure acid and alkaline oxidation and bio-oxidation are also used (Adam, 2016; Robins and Jayaweera, 1992). The arsenic species remaining in solution could reach an extent of hundreds of mg/L in an acid oxidation process (Robins and Jayaweera, 1992). In the case of bacterial oxidation, mixed arsenite and arsenate were found in solution with a total concentration of 1 mg/L (Ehrlich, 1964).

During the cyanidation process, because of the alkaline conditions and the presence of oxygen, arsenic sulphides can be oxidised to arsenite (AsO_3^{3-}) and arsenate (AsO_4^{3-}), or partially oxidised to thioarsenites (AsS_3^{3-}) and thioarsenates (AsS_4^{3-}). Depending on the solution composition, oxidation potential and pH, the proportion of the oxidised arsenic species can vary (Kyle et al., 2012b). This oxidation process adversely affects the gold cyanidation process by consuming the oxygen that needed by the dissolution of gold (Marsden and House, 2006). Meanwhile, free cyanide is likely to be involved in the further oxidation of thioarsenites and thioarsenates to form thiocyanates (SCN^-), causing a loss of lixiviant (Hedley and Tabachnick, 1950). In addition, it is reported that the formed oxides could attach to the gold surface, which in part prevents the interaction of cyanide ions and oxygen with the gold (Kyle et al., 2012b). In the gold recovery stage, carbon-in-pulp (CIP) and carbon-in-leach (CIL) recoveries have been used widely (Staunton, 2016). While the gold-bearing species attaching to the activated carbon, arsenite and arsenate can also be weakly adsorbed, partially reducing the efficiency of the gold recovery (Kyle et al., 2012b).

In tailing dams, arsenic can be present at high concentrations in alkaline solutions (Kyle et al., 2012b). According to the literature (Haffert and Craw, 2008), the more toxic As(III) species is much more soluble than the As(V) species in tailings waters. McCreadie (1998) analysed the composition of the pore water of tailings from gold processing. It was indicated that the solution pH was in the range of 7–9 and the dissolved arsenic (mainly As(III)) concentration increased over a period of one year.

2.1.5. Technologies for removing arsenic from aqueous solutions

In order to prevent or reduce the adverse effects of arsenic species on the gold cyanidation processes and the health and safety threat of arsenic species to humans, arsenic must be removed from the aqueous systems. On the basis of literature survey, a variety of approaches have been proposed for arsenic removal, mostly targeting the treatment of drinking water or groundwater at a neutral or near neutral pH. Basically, these approaches can be divided into three categories, i.e., precipitation/encapsulation, membrane technologies and adsorption.

Precipitation/encapsulation

Precipitation is the most commonly used method for arsenic management in mining industry (Adam, 2016). The idea is to transform the soluble arsenic species into insoluble solids, subsequently separating the arsenic-containing solids from the water body by sedimentation and/or filtration. According to the arsenic chemistry in most water systems, the predominant form of As(III) is non-charged at pH below 9.2, making it difficult to precipitate. Therefore, an initial oxidation of arsenite to arsenate is usually necessary. In practice, atmospheric oxygen, chlorine, hydrogen peroxide, hypochlorite and so on are commonly used arsenic oxidants. The precipitants reported in literature and the corresponding chemical reactions for arsenic removal are presented in Table 2-2.

Table 2-2. Precipitants commonly used for arsenical removal and associated reactions.

Precipitant	Possible reaction	Reference
Ferric salts	$Fe^{3+} + AsO_3^{4-} \rightarrow FeAsO_4$ (s)	(Jadhav et al., 2015)
Aluminium sulphate	$Al^{3+} + H_2O \rightarrow Al(OH)_3 + H^+$ $H_2AsO_4^- + Al(OH)_3 \rightarrow$ Al–As complex (s)	(Baskan and Pala, 2010)
Lime	$Ca(OH)_2 + AsO_4^{3-} \rightarrow Ca_3(AsO_4)_2$ (s)	(Nazari et al., 2016)
Sulphides	$AsO_2^- + HS^- + H^+ \rightarrow As_2S_3$ (s)	(Opio, 2013)

The use of ferric ions to remove arsenic from hydrometallurgical process solutions and waste waters has been widely investigated. Under suitable conditions, the

positively charged Fe^{3+} and Al^{3+} in solution could form colloidal hydrolysed metal species, thereby interacting with the soluble arsenic by forming surface complexes. Through inclusion, occlusion or adsorption, these colloidal particles get larger, followed by bridging between the larger particles, leading to the formation of flocs. Afterwards, the arsenic-bearing flocs can be further precipitated and removed from the solution (Nicomel et al., 2015; Wang et al., 2014). Robins et al. (2001) reported that at low pH values, ferric arsenate could be formed at relatively high concentrations of Fe(III) and As(V), while the co-precipitation of ferrioxihydroxide occurred at lower concentrations of As(V). In the case of lime treatment, at high pH values, a number of calcium arsenate precipitates could be formed in the As(V)-bearing solutions (Nazari et al., 2016; Nishimura and Robins, 1998) and the arsenic concentration of the treated solution could be reduced to less than 0.01 mg/L with excess lime additions (Robins et al., 2001). However, the precipitates mentioned above are shown to be unstable under certain conditions, which could result in the release of arsenic species to the environment again. For example, the arsenical sulphides As_2S_3 can be easily oxidised and increasingly soluble when pH>4; calcium arsenates precipitating when pH>8 tend to be converted to calcium carbonate when exposed to CO_2 in the atmosphere.

To further immobilize the formed As-bearing precipitates, encapsulation is employed. Encapsulation is a method to isolate the As-bearing precipitates within an inert material which has a high structural integrity that minimises the possible exposure area of the pollutants to the environment. This technique usually involves three steps, i.e., chemical precipitation (lime-based, cement-based and phosphate-based), physical encapsulation and vitrification or thermoplastic polymer encapsulation (Conner and Hoeffner, 1998). Recently, Lalancette et al., (2015) proposed a new method for the arsenic sequestration. Firstly, As(III) was oxidised to As(V), followed by adding lime to the solution to form non-volatile (at the melting temperature of glass) calcium arsenate. Afterwards, recycled glass or glass forming components were introduced to the calcium arsenate residues. Finally, the mixture was vitrified at a temperature between 1000 °C to 1200 °C. It is claimed that the final products are very stable and insoluble.

Membrane technology

Recently, membrane technology has gained much attention in the field of water treatment due to its outstanding performance and high reliability (Jadhav et al., 2015). In principle, the membrane acts as a very specific filter that will let water flow through, while it catches the unwanted substances. The driving force of the water flow could be pressure, concentration gradient or an electric potential. There are various types of membrane-based approaches that have been applied for arsenic removal, such as nanofiltration (Figoli et al., 2010; Harisha et al., 2010; Košutić et al., 2005; Nguyen et al., 2009; Saitúa et al., 2005; Wang et al., 2016; Yoon et al., 2009), microfiltration (Pagana et al., 2008), ultrafiltration (Lohokare et al., 2008), hybrid filtration (Nguyen et al., 2009; Sen et al., 2010), reverse osmosis (Abejón et al., 2015; Akin et al., 2011; Chan and Dudeney, 2008; Chang et al., 2014; Gholami et al., 2006; Kang et al., 2000; Kang et al., 2001; Ning, 2002; Schmidt et al., 2016), forward osmosis (Mondal et al., 2014), distillation (Criscuoli et al., 2013; Dao et al., 2016; Manna et al., 2010; Pal and Manna, 2010; Qu et al., 2009) and electrodialysis (Litter et al., 2010; Ravenscroft et al., 2009), etc. Several examples of the arsenic removal performance by use of membrane based techniques are given in Table 2-3.

It can be seen that efficient removal of arsenic can be obtained at near-neutral pH values. Most of the studies were targeted at arsenate species rather than arsenite species, which could be attributed to the fact that at the typically used pH, arsenite exists as a neutral molecule in aqueous solutions, complicating its rejection by the membranes (Abejón et al., 2015). Consequently, when it comes to the issue with decontamination of As(III)-containing waters, a preoxidation process is often required. Nevertheless, the use of oxidants is not an easy task and it may cause damage to the membranes (Abejón et al., 2015). Although certain methods such as the one proposed by Dao et al. (2016) could avoid the oxidation step, its capital and energy costs should not be overlooked.

Table 2-3. Examples of arsenic retention by membrane based techniques.

Membrane	Technique	pH	As species	Initial As concentration	Type of water	Rejected	Reference
DK/DL (GE Osmonics)	Nanofiltration	8.0	As(V)	1–50 μg/L	NaCl solution	≥80%	(Fang and Deng, 2014)
NF270 (Filmtec DOW)	Nanofiltration	7.85	As(V)	100 μg/L	Drinking water	98%	(Košutić et al., 2005)
BE (Woongjin Chemical) / UTC 80B (Toray)	Reverse osmosis	neutral	As(V)	100 μg/L	Drinking water	98%	(Abejón et al., 2015)
FO membrane (Hydration Technology Innovation)	Forward osmosis	neutral	As(V)	500 μg/L	$MgSO_4$ solution	>98%	(Mondal et al., 2014)
PTFE (Millipore Corporation)	Distillation	6.8	As(III)	0.3–2 mg/L	Ground water	>98%	(Dao et al., 2016)

Adsorption

Adsorption is amongst the best and time-honored technologies for As removal from aqueous systems. As long ago as 1500 B.C., the Egyptians had used carbonized wood as a medical adsorbent and purifying agent (Mohan and Pittman, 2007). The arsenic species in aqueous systems could interact with the suitable adsorbents either physically or chemically. Physical adsorption is usually driven by van der Waals forces between the adsorbates and the adsorbents. This kind of force is relatively weak and easy to break simply by solvent exchange, calcination or sonication. By contrast, for chemisorption, there is true chemical bonds formed between the adsorbates and adsorbents. As a result, the regeneration of the spent adsorbents usually involves chemical treatment (Nicomel et al., 2015).

Various adsorbents have been reported for removing arsenic species from waters, such as activated carbon, ion-exchange resins, metal oxides, industrial by-products/wastes and biosorbents, etc. More detailed review on the arsenic adsorbents and their performance will be illustrated in section 2.2.

Comparison of main arsenic removal technologies

All the aforementioned arsenic removal technologies have advantages and disadvantages. For the precipitation methods, their superiorities lie in the operational simplicity, applicability in a wide range of pH and low-cost (Mondal et al, 2013) but they also suffer from some drawbacks, such as the need of preoxidation of arsenite to arsenate and the production of high amount of toxic sludge (Ungureanu et al., 2015a). With regard to the membrane technologies (Mohan and Pittman, 2007), very high costs in capital, operation and maintenance are required and the interferences of the co-existing ions are also problematic. Nevertheless, membrane technologies are usually found to be quite efficient in arsenic removal, as can be seen from Table 2-3. Compared to the precipitation and membrane technologies, adsorption approaches share the merits (Mohan et al., 2007) of low-cost, easy handling, low energy requirement and high arsenic removal rate. Meanwhile, the application of adsorption methods for arsenic removal can also be limited by their disadvantages (Mondal et al., 2013), e.g. production of toxic solid wastes, subjection to the interferences of co-

existing ions and dependence on solution pH. However, these disadvantages can be overcome by selecting suitable arsenic adsorbents. Section 2.2 will systematically review the adsorption methods for arsenic removal.

2.2. Arsenic removal by adsorption

Adsorption is considered to be superior to other techniques for decontamination in regards to its comparatively low cost, a wide range of applications, simplicity of design, easy operation, low harmful secondary products and simple regeneration of the adsorbents (Khan, et al., 2013; Gu et al., 2005; Rahaman et al., 2008). The following sections will discuss the theories for adsorption processes, various kinds of adsorbents found in literatures and their potential application in the treatment of gold cyanidation process waters.

2.2.1. Adsorption theories

The arsenic adsorption mechanisms for different adsorbents may vary from case to case, but in theory, each adsorption process can be fitted to certain kinetic and equilibrium isotherm models. A number of kinetic and isotherm models have been used by researchers to characterise the adsorption processes, as shown in Table 2-4 and Table 2-5. Among the various models, the most widely used in literature are pseudo-first-order and pseudo-second-order models for kinetics and Langmuir and Freundlich models for equilibrium isotherms. Since the Langmuir model estimates the maximum adsorption capacity, most of the literatures describe the adsorption performance of their adsorbents by fitting experimental data to the Langmuir model and report the Q_m values.

Table 2-4. Adsorption reaction kinetic models used for arsenic removal.

Kinetic model	Differential equation	Integrated equation	Assumptions	Reference
Pseudo-first-order	$\frac{dq_t}{dt} = k_{p1}(q_e - q_t)$ q_t(mg/g): Adsorption capacity at time *t*; q_e(mg/g): Adsorption capacity at equilibrium; t (min): Time; k_{p1}(min^{-1}): Rate constant;	$\ln\left(\frac{q_e}{q_e - q_t}\right) = k_{p1}t$	1. Sorption only occurs on localized sites and involves no interaction between the sorbed ions. 2. The energy of adsorption is not dependent on surface coverage. 3. Maximum adsorption corresponds to a saturated monolayer of adsorbates on the adsorbent surface. 4. The concentration of adsorbate is considered to be constant. 5. The adsorbate uptake on the adsorbents is governed by a first-order rate equation.	(Ho and McKay, 1998; Lagergren, 1898; Largitte and Pasquier, 2016)
Pseudo-second-order	$\frac{dq_t}{dt} = k_{p2}(q_e - q_t)^2$	$\frac{t}{q_t} = \frac{1}{k_{p2}q_e^2} + \frac{1}{q_e}t$	Same as above except that the adsorbate uptake on the adsorbents is governed by a second-order rate equation.	(Ho and McKay, 1998; Largitte and Pasquier, 2016; Qiu et al., 2009)
Elovich's equation	$\frac{dq}{dt} = ae^{-\alpha q}$ q: Amount of adsorbates uptake on the adsorbents at time t; a: Desorption constant; α: Initial adsorption rate.	$q = \alpha \ln(a\alpha) + \alpha lnt$ $a\alpha t \gg 1$	1. Sorption only occurs on localized sites and involves interaction between the sorbed ions. 2. The energy of adsorption increases linearly with the surface coverage. 3. The adsorbate concentration is considered to be constant. 4. Adsorbate uptake is governed by a zero-order rate equation.	(Asmel et al., 2017; Largitte and Pasquier, 2016; Qiu et al., 2009)

Table 2-5. Adsorption isotherms models used for arsenic removal.

Isotherm	Non-linear form equation	Linear form equation	Remarks	Reference
Langmuir	$Q_e = Q_m(\frac{K_L C_e}{1 + K_L C_e})$ Q_e (mg/g): Amount of adsorbates on the surface of adsorbents at equilibrium; Q_m (mg/g): Maximum adsorption capacity; C_e (mg/L): Adsorbate concentration at equilibrium; K_L (L/mg): Adsorption constant.	$\frac{C_e}{Q_e} = \frac{C_e}{Q_m} + \frac{1}{K_L Q_m}$	This isotherm model assumes: 1. Monolayer adsorption which can only occur at a finite (fixed) number of definite localized sites. 2. Homogeneous adsorption, i.e., all sites possess equal affinity for the adsorbate, with no transmigration of the adsorbate in the plane of the surface.	(Kundu and Gupta, 2006; Pérez-Marín et al., 2007; Vijayaraghavan et al., 2006)
Freundlich	$Q_e = K_F C_e^{\frac{1}{n}}$ K_F: Freundlich constant, representing adsorption capacity at unit concentration of adsorbate; n: Constant, representing adsorption intensity.	$logQ_e = logK_F + \frac{1}{n} logC_e$	The Freundlich isotherm describes both monolayer and multilayer adsorptions onto both homogeneous as well as heterogeneous surfaces.	(Foo and Hameed, 2010)
Dubinin–Radushkevich	$Q_e = Q_s e^{-k_{ad}\varepsilon^2}$ Q_s (mg/g): Theoretical monolayer saturation adsorption capacity; k_{ad} (mol^2/J^2): Constant, relating to the mean free energy of adsorption; ε: Polanyi potential, relating to the equilibrium concentration.	$lnQ_e = lnQ_s - k_{ad}\varepsilon^2$	It does not assume a homogeneous surface or constant adsorption potential, making it more general than Langmuir model. This isotherm has been extensively used to distinguish the physical and chemical adsorption.	(Chaudhry et al., 2017)

Table 2-5. Continued.

Isotherm	Non-linear form equation	Linear form equation	Remarks	Reference
Tempkin	$Q_e = \frac{RT}{b_T} lnA_T C_e$ R: 8.314 J/K/mol, universal gas constant; T (K): Temperature; A_T (L/g): Constant, relating to maximum binding energy; b_T (kJ/mol): Constant, referring to the heat of adsorption.	$Q_e = \frac{RT}{b_T} lnA_T + \frac{RT}{b_T} lnC_e$	This model assumes that the heat of adsorption decreases linearly with the surface coverage of the adsorbent due to the interaction between adsorbates and adsorbents.	(Tempkin and Pyzhev, 1940)
Flory–Huggins	$\frac{\theta}{C_o} = K_{FH}(1-\theta)^{n_{FH}}$ θ: The degree of surface coverage; K_{FH} and n_{FH} are the equilibrium constant and model exponent;	$\log\left(\frac{\theta}{C_o}\right) = logK_{FH} + n_{FH}\log(1-\theta)$	It can indicate the feasibility and spontaneous nature of an adsorption process.	(Foo and Hameed, 2010)
Redlich-Peterson	$Q_e = \frac{K_R C_e}{1 + a_R C_e^{\beta}}$ K_R, β and a_R are constants.	$\ln\left(K_R \frac{C_e}{Q_e} - 1\right) = \beta ln(C_e) + \ln(a_R)$	It is a hybrid isotherm featuring both Langmuir and Freundlich isotherms.	(Redlich and Peterson, 1959)
Sips	$Q_e = \frac{K_S C_e^{\beta_S}}{1 + a_S C_e^{\beta_S}}$	$\beta_S lnC_e = -\ln\left(\frac{K_S}{Q_e}\right) + lna_S$	Combined form of Langmuir and Freundlich isotherms for predicting the heterogeneous adsorption systems.	(Foo and Hameed, 2010)

2.2.2. Arsenic adsorbents

A wide variety of arsenic adsorbents have been studied. In this review, arsenic adsorbents are broadly divided into four classes: activated carbon, metal-based adsorbents, biosorbents and other sorbents.

Activated carbon

Activated carbon is a material with highly porous structure and large surface area, which are commonly prepared from wood, coal, lignite, coconut shell and peat (Mohan and Pittman Jr, 2007). The adsorption capacity of the activated carbon depends on its own properties, chemical properties of adsorbates, temperature, pH and ionic strength. Table 2-6 presents the adsorption capacities of some activated carbons used for arsenic removal from water in literature of recent five years.

Most of the studies listed in Table 2-6 were aimed at the decontamination of drinking/ground water at near neutral pH values. The adsorption tests were carried out with different initial arsenic concentrations ranging from 0.01–10 mg/L to 1–100 mg/L. A variety of activated carbons, either commercial or laboratory synthesised, were used for arsenic removal. Basically, nude activated carbons showed very low arsenic adsorption capacities especially in the presence of competitive ions in natural or simulated mineral water samples. Iron impregnation is the most frequently used approach for activated carbon modification thereby improving the arsenic removal rate. Other modification methods such as CeO_2, Mn, La and alumina doping were also investigated. Arcibar-Orozco et al. (2014) studied the As(V) removal by a set of activated carbons with and without modification. They found that the surface charge and iron content on the surface of the activated carbons played the most significant roles in As(V) uptake. In addition, the high porous volumes and large specific surface area also contributed to the elevated arsenate adsorption capacities, as reported by Lodeiro et al. (2013). It is also noted that in some cases, the arsenic uptake is mainly attributed to the metal oxides/hydroxides deposited on the surface of the activated carbons, although those oxides/hydroxides may benefit from the structural properties of the activated carbon to achieve the satisfactory adsorption

results. It seems that the activated carbons were mainly used as support materials to facilitate the separation of the As-loaded adsorbents from the treated water.

Table 2-6. Adsorption capacities of some activated carbons used for arsenic removal.

Adsorbent	Remarks	Adsorbate	pH	Adsorption capacity	Reference
$PyrC_{350}$®	Developed from pyrolytic-tire char.	As(III)	4–8.5	31.0 mg/g	(Mouzourakis et al., 2017)
Filtrasorb 400 (Calgon Carbon Corporation)	A commercial granular activated carbon; CeO_2 modified.	As(III)	5	36.8 mg/g	(Yu et al., 2017)
		As(V)	5	43.6 mg/g	
PSAC (Bravo Green Sdn Bhd, Kuching, Malaysia)	Palm shell-based activated carbon; Magnetized and coated with La.	As(V)	6	228 mg/g	(Jais et al., 2016)
GAC (Sinopharm Chemical Reagent, Shanghai, China)	Coal-based granular activated carbon impregnated with iron hydroxide.	As(V)	5	108-141 mg/g(Fe)	(Xu et al., 2016)
Viscose rayon carbon cloth ("Vinča" Institute of Nuclear Sciences, Serbia)	Mechanochemically activated.	As(V)	7	5.50 mg/g	(Matović et al., 2016)
ACAL11	Waste tire rubber derived activated carbon–alumina composites.	As(III)	9	14.3 mg/g	(Karmacharya et al., 2016)
		As(V)	3	23.8 mg/g	

Table 2-6. Continued.

Adsorbent	Remarks	Adsorbate	pH	Adsorption capacity	Reference
CAC	Chemical activated carbon, prepared from jute stick particles.	As(III)	7	0.0550 mg/g	(Asadullah et al., 2014)
FCAC	Iron-modified chemical activated carbon.			0.0970 mg/g	
Charcoal activated (Merck Millipore)	The activated charcoal was only used as support for iron oxide nanoparticles.	As(V)	6–8	27.8 mg/g	(Yürüm et al., 2014)
Coal-based mesoporous activated carbon	Adsorption tests were conducted at 7 °C.	As(III)	6	1.49 mg/g	(Li et al., 2014)
		As(V)		1.76 mg/g	
Aquacarb 207EA™	Originated from bituminous coals.	As(V)	7	0.100 mg/g	(Natale et al., 2013)
Activated carbon fibre (ACF, Nantong Senyou Carbon Fiber Co., Ltd., Nantong, China)	As received ACF	As(V)	7	<2.00 mg/g	(Sun et al., 2013)
	Mn-modified ACF			23.8 mg/g	
F400	Bituminous filtrasorb-400 from Calgon	As(V)	7	1.01 mg/g	(Rodriguez and Mendez, 2013)
CAZ	From Agave salmiana bagasse and chemically modified with $ZnCl_2$.	As(V)	7	0.250 mg/g	
CAP	From Agave salmiana bagasse and chemically modified with H_3PO_4.	As(V)	7	0.167 mg/g	

Metal-based adsorbents

The metal-based adsorbents mainly include metal oxides/hydroxides adsorbents and zero valent iron.

Efficient metal oxides/hydroxides arsenic adsorbents reported in literature include manganese oxides, activated alumina, iron oxides/hydroxides, titanium dioxide, zirconium oxide and cerium oxide/hydroxide as well as their binary mixtures. In general, high affinity between arsenic species and the unique hydroxyl groups formed on the oxides surface in aqueous solutions is the key to arsenic removal (Chen et al., 2014; Tang et al., 2011; Dutta et al., 2004; Luo et al., 2013). It has been demonstrated that arsenic could interact with the metallic-OH group to form an inner-sphere complex (Manning et al., 1998; Zhang et al., 2009). Additionally, it is believed that larger surface area of the metal oxides can provide more adsorption sites for arsenic species (Lata and Samadder, 2016). The metal oxides/hydroxides adsorbents have showed excellent arsenic removal performance in many studies, especially those associated with titanium, zirconium and cerium, as indicated by Table 2-7.

Table 2-7. Removal of arsenic by metal oxides/hydroxides-based adsorbents.

Adsorbent	pH	Adsorbate	Adsorption capacity	Reference
Manganese oxide	6	As(III)/As(V) mixture	7.27 mg/g	(Hou et al., 2017)
MnO_2-loaded resin	6.0	As(III)	53.0 mg/g	(Lenoble et al., 2004)
		As(V)	22.0 mg/g	
Mesoporous alumina	6.6	As(V)	36.6 mg/g	(Han et al., 2013)
Fe_3O_4 nanoparticles	6	As(III)	5.68 mg/g	(Luther et al., 2012)
		As(V)	4.78 mg/g	
Fe_2O_3 nanoparticles		As(III)	20.0 mg/g	
		As(V)	4.90 mg/g	
Iron hydroxide	8	As(V)	11.2 mg/g	(Mahmood et al., 2014)
TiO_2	7	As(III)	32.4 mg/g	(Bang et al., 2005)
		As(V)	41.4 mg/g	
Hydrous zirconium oxide	7	As(V)	88.7 mg/g	(Pan et al., 2014)
Hydrous cerium oxide	7	As(III)	172 mg/g	(Li et al., 2012)
		As(V)	107 mg/g	
Hybrid iron oxide silicates	7	As(III)/As(V) mixture	300 mg/g	(El-Moselhy et al., 2017)
Fe-Mn bimetal oxides	3	As(III)	67.9 mg/g	(Wen et al., 2014)
		As(V)	93.5 mg/g	
Ce-Mn bimetal oxide	7	As(V)	18.7 mg/g	(Gupta et al., 2011)
Fe(III)-Ti(IV) binary mixed oxide	7	As(III)	85.0 mg/g	(Gupta and Ghosh, 2009)
		As(V)	14.0 mg/g	
Iron-Zirconium Binary Oxide-Coated Sand	7	As(V)	45.1 mg/g	(Chaudhry et al., 2017)
Cerium incorporated manganese oxide	7	As(III)	34.9 mg/g	(Gupta et al., 2012)

Zero valent iron was also considered to be an effective arsenic adsorbent (Bhowmick et al., 2014; Liu et al., 2016; Sun et al., 2017; Tanboonchuy et al., 2012). On the surface of the Fe^0, there is usually a thin layer of oxides/hydroxides in the presence of oxygen. According to the recent research by Ling and Zhang (2014), As(V) is firstly attracted to the adsorbent surface via electrostatic interactions and then chemically reduced to elemental arsenic As^0 by the Fe^0 core. As a result, arsenic can be trapped between the Fe^0 core and its oxidised shell. Similar mechanism also applies to the adsorption of As(III) onto the zero valent iron adsorbents (Yan et al., 2012).

Alijani and Shariatinia (2017) synthesised nanoscale zero valent iron doped multiwall carbon nanotubes using natural α-Fe_2O_3 as precursor and studied the arsenic adsorption behaviour of this material. They claimed that the synthesised particles had a maximum arsenic adsorption capacity of 200 mg/g for As(III) and 250 mg/g for As(V) by fitting a Langmuir isotherm model at a near neutral pH. Wang et al. (2017) investigated the adsorptive removal of arsenate by biochar supported zero valent iron. Batch adsorption tests showed that, at pH 4.1, the arsenate adsorption equilibrium could be reached within an hour and the Langmuir maximum adsorption capacity was 124.5 mg/g.

Biosorbents

Biosorbents have attracted a lot of attention because they are inexpensive and eco-friendly (Podder and Majumder, 2015). Table 2-8 lists some of the biosorbents used for arsenic removal in literature.

Table 2-8. Biosorbents for arsenic removal from aqueous solutions.

Adsorbent	pH	Adsorbate	Capacity	Reference
Thiol-functionalised chitin nanofibers	7	As(III)	149 mg/g	(Yang et al., 2015)
Functionalized nanocrystalline cellulose	7.5	As(III)	10.6 mg/g	(Singh et al., 2015)
	2.5	As(V)	12.1 mg/g	
Chitosan goethite bionanocomposite beads	5	As(III)	8.46 mg/g	(He et al., 2016)
		As(V)	11.3 mg/g	
Stem of Tecomella undulata	7	As(III)	0.108 mg/g	(Brahman et al., 2016)
		As(V)	0.159 mg/g	
Functionalised saccharum officinarum bagasse	7	As(III)	28.6 mg/g	(Gupta et al., 2015)
		As(V)	34.5 mg/g	
Chitosan-coated ceramic alumina	4	As(III)	56.5 mg/g	(Boddu et al., 2008)
		As(V)	96.5 mg/g	

Chitin, chitosan and cellulose are natural biopolymers with similar molecular structures (Figure 2-3). The abundant amine and hydroxyl groups provide potential opportunities for further modifications in order to facilitate the adsorption of aqueous arsenic species. For instance, Kwok et al., (2014) reported that the amine groups in chitosan molecules can be protonated in aqueous medium thus interacting with anionic arsenic species via electrostatic attraction. Yang et al. (2015) prepared chitin nanofibers with positively charged amine groups through a combination of acid, base and mechanical treatments. The protonated amine groups were able to interact with the oppositely charged arsenic species through electrostatic attraction and with neutral arsenic species via van der Waals forces. Further modification of the amine groups by cysteine grafting promoted the arsenic adsorption capacity of the chitin nanofiber due to the formation of As-thiolate complex. In the investigation of cellulose as efficient arsenic adsorbent, Singh et al. (2015) firstly prepared dialdehyde nanocrystalline cellulose by sodium periodate oxidation, followed by diethylene triamine grafting to yield amine derivatives. The functionalised nanocrystalline cellulose biosorbents showed satisfactory arsenic uptake capacities.

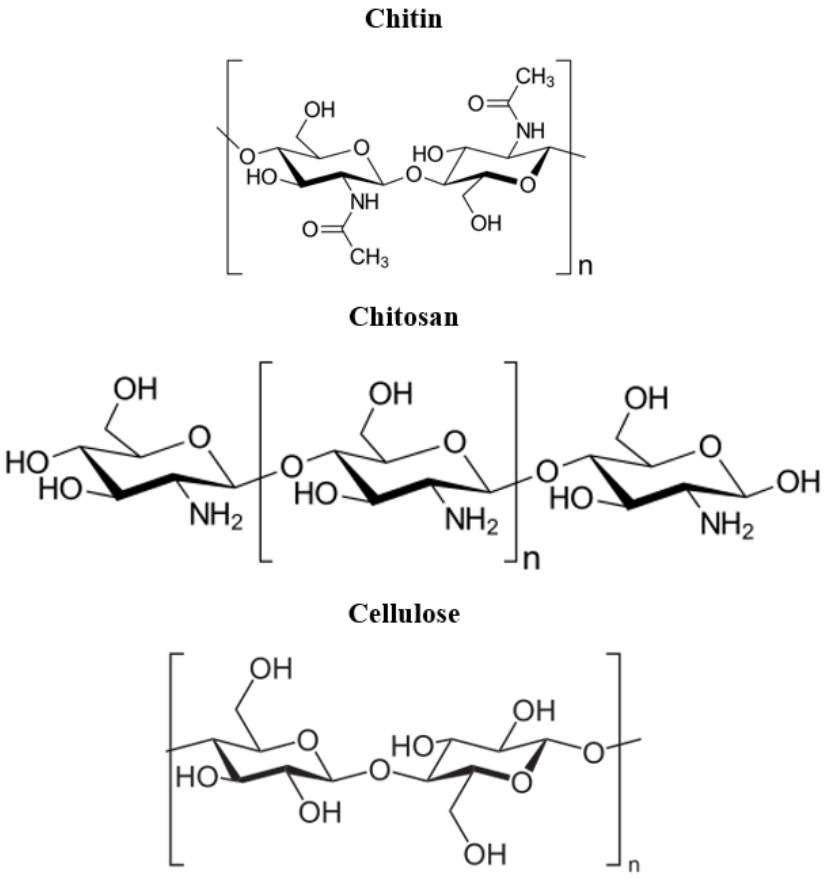

Figure 2-3. Structures of chitin, chitosan and cellulose.

Another interesting way for arsenic removal is the combination of biosorption and bioaccumulation through microorganisms. Podder and Majumder (2016) immobilized the Corynebacterium glutamicum MTCC 2745 biofilm onto granular activated carbon/$MnFe_2O_4$ composite and used it as arsenic adsorbent. They proposed that the presence of functional groups such as –OH on the cell wall surface of the biomass were responsible for arsenic removal proved by FT–IR analysis.

Other sorbents

Other arsenic adsorbents include:

- Agricultural products/by-products such as rice husks (Amin et al., 2006; Khalid et al., 1998);
- Industrial wastes/by-products like biochar from fast wood and bark pyrolysis during bio-oil production (Mohan et al., 2007; Vithanage et al., 2017), red mud formed during alumina production (Akin et al., 2012), blast furnace slags from

steel plants (Ahn et al., 2003) and fly ash from coal combustion (Diamadopoulos et al., 1993; Rodella et al., 2014);

- Sand (Smith et al., 2017; Trois and Cibati, 2015) and clay minerals (Bentahar et al., 2016; Doušová et al., 2011), etc.
- Anion exchange resins (Barakat and Ismat-Shah, 2013; Donia et al., 2011; Lin et al., 2006).

According to Amin et al. (2006), the rice husks removed 96% of As from the contaminated groundwater of Bangladesh. The adsorption of arsenic species could be attributed to the hydroxyl groups present on the carbon surface which exchanged for As(V) anions in the solution and the van der Waals forces between neutral As(III) species and the rice husks.

The adsorption of arsenic on biochars is due to the presence of various functional groups such as amine and carboxyl, etc. (Mohan et al., 2007). Similar to the chitin, chitosan and cellulose biosorbents, the protonated amine groups are capable of interacting with the oppositely charged arsenic species through electrostatic attraction and with the neutral arsenic species via van der Waals forces.

Diamadopoulos et al. (1993) examined the possible use of fly ash as a means of removing As(V) from aqueous solutions. The fly ash obtained from Kardia thermal power plant contained mainly CaO, SiO_2, Al_2O_3, Fe_2O_3 and MgO. It was suggested that the strong adsorption of As(V) at pH 4 was due to ferric and aluminum oxides while adsoption at pH 10 was because of calcium and magnesium oxides.

The anion exchange resin are usually supplied in chloride form with trimethylbenylammonium group as exchange sites for arsenic species (Lin et al., 2006). When treated with arsenic contaminated water, anionic arsenic species could replace the Cl^- and attach to the trimethylbenylammonium group of the resin by electrostaic attractions. However, it is because of this physical adsorption mechanism, the resins are found to be inefficient for As(III) removal since the predominant form of As(III) in solutions with pH<9.2 is non-charged H_3AsO_3.

Comparison of various adsorbents

Although most of the adsorbents exhibited satisfactory arsenic uptake capacities as presented in Table 2-6, Table 2-7 and Table 2-8, it is still difficult to make direct comparisons of the various kinds of adsorbents due to the lack of consistency of experimental conditions in literature. Nevertheless, from the adsorption mechanism analyses in those literatures, it is found that, for the majority of the adsorbent types, electrostatic attractions and van der Waals forces between arsenic species and the effective constituents (e.g. amine groups) of the adsorbents were the dominant driving forces for arsenic adsorption. In contrast, the arsenic adsorptions onto the metal oxides/hydroxides adsorbents were resulted from the formation of an inner-sphere complex in addition to the physical attractions.

2.2.3. Titanium, zirconium and cerium based arsenic adsorbents

As discussed before, the metal oxides/hydroxides adsorbents have showed high affinity to arsenic (formation of inner-sphere complex) and excellent arsenic adsorption performance. However, problems still exist for some adsorbents of this kind, such as the need for preoxidation of As(III), low optimum pH and potential dissolution of the adsorbents in the treated water bodies. Considering the alkline condition of the targeted process water and its complex chemical composition, titanium, zirconium and cerium based adsorbents stand out compared to the other same-type arsenic scavengers, owing to their chemical inertness, negligible toxicity, insolubility in water, abundant resource and wide applicable pH range. Besides, they are inexpensive and easy to prepare (Cui et al., 2012; Li et al., 2012; Andjelkovic et al., 2015).

Titanium, zirconium and cerium based materials have been widely investigated for arsenic removal. Recently, a review by Yan et al. (2016) indicated that over the past 20 years, the number of publications on arsenic removal by TiO_2-based adsobents had increased dramatically especially in the recent five years. Furthermore, over 700 papers in this regard were cited in the year of 2015 alone. Similarly, more and more attentions have been paid to the zirconium (Bortun et al., 2010; Chaudhry et al., 2017;

Cui et al., 2012; Kwon et al., 2016; Luo et al., 2013; Ma et al., 2011; Pan et al., 2014) and cerium (Li et al., 2012; Sun et al., 2012; Yu et al., 2017; Zhang et al., 2016) based adsorbents for removing arsenic from water systems.

The mechanisms of arsenic adsorption on the Ti, Zr and Ce based oxides/hydroxides adsorbents were studied by various research groups (Pena et al., 2006; Cui et al., 2012; Li et al., 2012) through both macroscopic and microscopic analytical methods. All the analyses came to an agreement that the formation of an inner-sphere complex in addition to the physical attractions between the arsenic species and the adsorbents should be accounted for the exceptional arsenic adsorption performance of the titanium, zirconium and cerium based adsorbents.

The mechanism of arsenic adsorption on Ti-based adsorbents has been well established over a decade ago. Pena et al. (2006) used electrophoretic mobility measurements, extended X-ray absorption fine structure spectroscopy and Fourier transform infrared spectroscopy to explore the As(III)/As(V) interactions at the solid-water interface of TiO_2. The point of zero charge of TiO_2 decreased from 5.8 to 5.2 after arsenic adsorption, indicating negatively charged inner-sphere surface complexes were formed during adsorption for both As(III) and As(V). According to the extended X-ray absorption fine structure analyses, an average Ti-As(III) bond distance of 3.35 Å and Ti-As(V) bond distance of 3.30 Å confirmed the formation of bidentate binuclear surface complexes for both As(III) and As(V). Additionally, the Fourier transform infrared spectroscopy bands caused by vibrations of the adsorbed arsenic species remained at the identical energy levels at various pH values. As a result, the unchanged nonprotonated complexes were maintained on the surface of TiO_2 at pH 5-10, and the main arsenic species were $(TiO)_2AsO^-$ and $(TiO)_2AsO_2^-$ for As(III) and As(V), respectively.

The adsorption mechanism of ZrO_2 in removing arsenic species from water was deeply investigated by Cui et al. (2012), via both the macroscopic techniques, including the ionic strength effect on the adsorption behavior and the electrophoretic mobility measurements on ZrO_2, and the microscopic technique, i.e. Fourier transform infrared spectroscopy. During the study on the ionic strength effect on arsenic adsorption, the adsorption amounts of both As(III) and As(V) were found to

increase with the increasing ionic strength, demonstrating that the arsenic adsorption onto ZrO_2 follows the inner-sphere complex mechanism at pH 7. Based on the electrophoretic mobility study, the isoelectric point of ZrO_2 was determined at pH 5.9, but decreased to 5.4 and 5.0 with the adsorption of As(III) and As(V), respectively, evidencing that the inner-sphere As(III) or As(V) anionic charged surface complexes were formed on the surface of ZrO_2. The mechanism was further researched with Fourier transform infrared spectroscopy before and after arsenic adsorption. The formation of As-OZr bond manifested that the As(III)/As(V) adsorption onto ZrO_2 is in line with the inner-sphere complex mechanism and the analytical results also showed that the substitution of Zr-OH groups by arsenic species plays a crucial part.

Li et al. (2012) employed similar technical methods to investigate the arsenic adsorption mechanism onto CeO_2. Through examining the effects of ionic strength on arsenic adsorption, it could be inferred that the arsenic adsorption on CeO_2 follows the inner-sphere complex mechanism at near-neutral pH. The futher investigation of Fourier transform infrared spectroscopy confirmed the formation of the As-OCe bond which is similar to the As-OZr bond mentioned above, proving again that the adsorption of both As(III) and As(V) onto CeO_2 follows the inner-sphere complex mechanism.

Furthermore, a few Ti/Zr/Ce-based polynary oxide adsorbents have been studied and nearly the same arsenic adsorption mechnisms were reported in the literature. For example, Li et al. (2010) studied the adsorption mechanism of As(V) and As(III) on Ce-Ti bimetal oxide. Through measuring the point of zero charge of the adsorbent before and after arsenic uptake, it was found that the pH_{pzc} decreased after arsenic was loaded on the adsorbents, indicating the formation of inner-sphere complexes. Furthermore, the Fourier transform infrared spectroscopy indicated that the hydroxyl groups on the adsorbent surface were involved in arsenic adsorption, while X-ray photoelectron spectroscopy provided further evidence for the involvement of hydroxyl groups in the adsorption and the formation of monodentate and bidentate complexes on the adsorbent surface.

Recently, the intrinsic property of a material – ionic potential (IP) – was proposed as a general criterion for the selection of highly efficient arsenic adsorbents by a research group in China (Li et al., 2014). Through the arsenic adsorption mechanism studies on various arsenic adsorbents, they suggested that if the ionic potential of a material was in the range of approximately 4–7, the metal-O bond was optimal in terms of the relative balance between the requirements for the desorption of surface hydorxyl groups and the adsorption of arsenic species. Interestingly, most of the arsenic adsorbents with good adsorption performance shown in Table 2-7 are located in the region where IP values are between 4 and 7, including oxides/hydroxides of cerium, zirconium and titanium.

On account of the above observations, titanium, zirconium and cerium based adsorbents were selected as the candidate arsenic adsorbents for the treatment of gold cyanidation process waters in this study.

2.2.4. Factors relating to the application of arsenic adsorbents

The diverse adsorption performance of various arsenic adsorbents can be attributed to a number of factors, such as pH, properties of the adsorbents including crystallinity, size/specific area and porosity and co-existing anions. According to the purpose of the studies, different researchers carried out their adsorption tests with different conditions.

pH

In all the literatures presented in the Tables 2-6, 2-7 and 2-8, the adsorption capacities were reported with certain pH values. Most of the tests were conducted at neutral or near neutral pH values because the target was drinking water and/or groundwater. In a few cases, acidic pH values were used as it was believed to be optimal for arsenic to be adsorbed onto the adsorbents. The effects of pH on the arsenic uptake efficiency are embodied in two aspects, i.e. adsorbate and adsorbent.

On one hand, the aqueous arsenic species vary with pH. As discussed in section 2.1.3, arsenic exists in aqueous solutions in the form of oxyanions arsenite (As(III)) and arsenate (As(V)). According to the E_h-pH diagram (Figure 2-1), for As(III), when the solution pH is less than 9.2, the dominant form is uncharged H_3AsO_3 while $H_2AsO_3^-$ becomes predominant when 9.2<pH<12. As to As(V), in extreme acidic solution (pH<2), the dominant species is uncharged H_3AsO_4; when the pH ranges between 2 and 7, $H_2AsO_4^-$ will predominate; if the pH value is higher than 7, $H_2AsO_4^{2-}$ becomes predominate. Additionally, AsO_4^{3-} may be present in extremely high alkaline solutions (approximately pH>12), which is usually not the case in natural waters. On the other hand, the variation of pH affects the surface charge of the adsorbents (Li et al., 2012; Cui et al., 2012; Pena et al., 2006). When the pH value is below the point of zero charge (pzc) of the adsorbents, the adsorbents will be positively charged, making them more attractive to anions. On the contrary, when the pH value is above the pzc of the adsorbents, the surface of the adsorbents will be negatively charged. As a result, the anions will be repelled from the adsorbents. Naturally, the arsenic adsorption process is affected by the variation of pH.

For example, Wang et al. (2014) investigated the effect of pH on the adsorption of arsenic on the synthesised adsorbent Fe_3O_4@$Zr(OH)_4$-impregnated chitosan beads. The results showed that when the solution pH value was above 9 (higher than the zpc of the adorbents), the As(III) uptake decreased. Because the negatively charged $H_2AsO_3^-$ increased and so did the negatively charged surface sites of the adsorbents, the repulsive effect between the adsorbates and adsorbents was enhanced. Similar effects were observed for the adsorption of As(V) which was present in the solution with predominant forms of $H_2AsO_4^-$ and $HAsO_4^{2-}$ when pH was above 7. In addition, since the number negatively charged As(V) species was more than that of As(III) species, the adsorption performance for As(V) was more strongly affected by the increase of pH values. By contrast, when pH value was within the range of 5–7, the surface of the adsorbents was positively charged and the As(V) adsorption was facilitated by the electrostatic attractions.

Co-existing anions

In the real-world waters, such as groundwater and industrial waters, there are many other anions co-existing with the arsenic contaminants. Most of the studies have taken this into consideration when evaluating the adsorption performance of the arsenic adsorbents. Some of the co-existing anionic species were reported to have adverse effects on the arsenic adsorptioin on metal oxides/hydroxides sorbents.

Ramos et al. (2016) studied the effect of co-existing anions Cl^-, SO_4^{2-} and NO_3^- on the As(V) adsorption capacity of TiO_2 reinforced chitin hydrogel. The results demonstrated that SO_4^{2-} significantly reduced the As(V) uptake while the presence of Cl^- and NO_3^- had little influences on the As(V) adsorption provided their concentrations were kept below the EPA drinking water standards (i.e. 250 mg/L for Cl^- and 10 mg/L for NO_3^-). The interference of these co-existing anions could be overcome by increasing the dosage of sorbents. Investigations carried out by Babu et al. (2016) suggested that the chloride, sulfate and nitrate anions with a concentration of 30 mg/L had no significant interference for As(V) and As(III) adsorption on mesoporous Fe_2O_3/TiO_2 nanoparticles supported by reduced graphene oxide, while the presence of 20 mg/L phosphate would significantly reduce the As(III) adsorption. Similar observations were made by Uppal et al. (2016) with graphene oxide-zirconium (GO-Zr) nanocomposite as arsenic adsorbent. High level of carbonate (1-200 ppm) or sulfite did not influence the As adsorption strongly either. In addition, the As(V) uptake on a zirconium based nanosorbent can be hindered by the presence of silicate (SiO_3^{2-}) (Ma et al., 2011).

Separation of the exausted adsorbents from water

No matter what types of adsorbents are used for arsenic removal, the exhausted As-loaded adsorbents have to be separated from the aqueous solutions and regenerated. Conventionally, this is resolved by filtration or centrifugation (Clifford et al., 1983). However, problems would arise if the filters became blocked or adsorbents lost (Reddy and Yun, 2016). In recent years, the use of magnetic adsorbents has attracted extensive attention (Mehta et al., 2015). With the help of an external magnetic field, the magnetic adsorbents can be easily and rapidly separated from the aqueous

medium. This is especially useful for the nano-sized and micro-sized adsorbents which are usually suspended in the solution and difficult to separate from the water. A summary of the applications of magnetic arsenic adsorbents in water treatment reported in literature over the past five years has been presented in Table 2-9.

Table 2-9. Arsenic adsorption performance of magnetic adsorbents.

Adsorbent	Size	Adsorbate	pH	Adsorption	Reference
Magnetic iron oxide/ CNT composites	11 nm	As(III)	7.5	8.13 mg/g	(Ma et al., 2013)
		As(V)	4	9.74 mg/g	
$MnFe_2O_4$	8-12 nm	As(III)	6.9	27.3 mg/g	(Xu et al., 2013b)
$CuFe_2O_4$	60 nm	As(III)	4.2	41.2 mg/g	(Tu et al., 2013)
$Mg_{0.27}Fe_{2.50}O_4$	3.7 nm	As(III)	7	127 mg/g	(Tang et al., 2013)
		As(V)		83.2 mg/g	
Magnetic nanoparticles modified with Fe-Mn binary oxide	20-50 nm	As(III)	7	47.8 mg/g	(Shan and Tong, 2013)
γ-Fe_2O_3	<10 nm	As(V)	7	45.0 mg/g	(Kilianová et al., 2013)
γ-Fe_2O_3-TiO_2	25-35 nm	As(III)	7	33.0 mg/g	(Yu et al., 2013)
Magnetic biochar	50-1000 nm	As(V)	-	3.15 mg/g	(Zhang et al., 2013)
Phosphonium-silane modified magnetic nanoparticles	8-15 nm	As(V)	3	50.5 mg/g	(Badruddoza et al., 2013)
Fe^{2+} loaded activated carbon	0.15-0.5 mm	As(V)	3	2.02 mg/g	(Tuna et al., 2013)
Fe^{3+} loaded activated carbon		As(V)		3.01 mg/g	
$MnFe_2O_4$	11 nm	As(III)	6.5	97.0 mg/g	(Kumar et al., 2014)
		As(V)	4	136 mg/g	
Graphene oxide-$MnFe_2O_4$	-	As(III)	6.5	146 mg/g	
		As(V)	4	207 mg/g	

Table 2-9. Continued.

Adsorbent	Size	Adsorbate	pH	Adsorption	Reference
$MnFe_2O_4$	11 nm	As(III)	6.5	97.0 mg/g	(Kumar et al., 2014)
		As(V)	4	136 mg/g	
Graphene oxide-$MnFe_2O_4$	-	As(III)	6.5	146 mg/g	
		As(V)	4	207 mg/g	
Zero-valent iron impregnated chitosan-caboxymethyl-β-cyclodextrin composite beads		As(III)	6	18.5 mg/g	(Sikder et al., 2014)
		As(V)		13.5 mg/g	
Fe_3O_4 nanoparticles from tea waste	5-25 nm	As(III)	7	189 mg/g	(Lunge et al., 2014)
		As(V)		154 mg/g	
Arginine modified Fe_3O_4	10 nm	As(V)	6	29.1 mg/g	(Zhang et al., 2014)
Lysine modified Fe_3O_4	10 nm	As(V)	6	23.9 mg/g	
Magnetic Kans grass biochar	-	As(III)	7	2.00 mg/g	(Baig et al., 2014)
		As(V)		3.10 mg/g	
Magnetic Fe_3O_4@$Zr(OH)_4$ impregnated chitosan beads	2.5 mm	As(III)	6.8	35.3 mg/g	(Wang et al., 2014)
		As(V)		35.7 mg/g	
Fe-Mn biochar composites	-	As(V)	7.5	3.44 mg/g	(Wang et al., 2015)
Magnetic biochar prepared from pinewood and natural hematite	38-75 μm	As(V)	7	0.400 mg/g	(Wang et al., 2015)
$NiFe_2O_4$	<10 nm	As(III)	7	169 mg/g	(Liu et al., 2015)
		As(V)		90.1 mg/g	

Table 2-9. Continued.

Adsorbent	Size	Adsorbate	pH	Adsorption	Reference
Magnetic nanoparticle activated microfibrillated cellulose	<10 nm	As(V)	2	184 mg/g	(Hokkanen et al., 2015)
Nanocomposite of α-Fe_2O_3 and γ-Fe_2O_3	15-25 nm	As(III)	7	46.5 mg/g	(Cheng et al., 2015)
Magnetite nanoparticles	34 nm	As(III)	5	16.6 mg/g	(Liu et al., 2015)
		As(V)		16.0 mg/g	
Graphene oxide-$MnFe_2O_4$	12-15 nm	As(V)	1-2	240 mg/g	(Huong et al., 2016)
Magnetite-graphene oxide	-	As(III)	7	42.9 mg/g	(Yoon et al., 2016)
		As(V)		18.8 mg/g	
Magnetite-reduced graphene oxide	-	As(III)		29.8 mg/g	
		As(V)		8.42 mg/g	
Fe_3O_4@$Cu(OH)_2$	250 nm	As(V)	5	35.7 mg/g	(Peng et al., 2016)
Europium doped magnetic graphene oxide-MWCNT nanohybrid	-	As(III)	7	320 mg/g	(Roy et al., 2016)
		As(V)		298 mg/g	
Mag-FMBO in clay-reinforced KGM aerogels	-	As(III)	7	16.0 mg/g	(Ye et al., 2016)
Magnetic gelatin-modified biochar	-	As(V)	4	45.8 mg/g	(Zhou et al., 2017)
Magnetic CuO-Fe_3O_4 nanoparticles	30 nm	As(III)	7	118. mg/g	(Sun et al., 2017)

It can be seen that most of the magnetic adsorbents were prepared or synthesised as nanoparticles or microparticles and showed excellent arsenic adsorption performance. In addition, magnetite (Fe_3O_4) was the most frequently used magnetic constituent of the adsorbents, followed by maghemite (γ-Fe_2O_3) and zero valent iron. After

adsorption, the As-loaded adsorbents could be easily and efficiently separated from the liquid phase with the help of a hand-held magnet, as depicted in Figure 2-4.

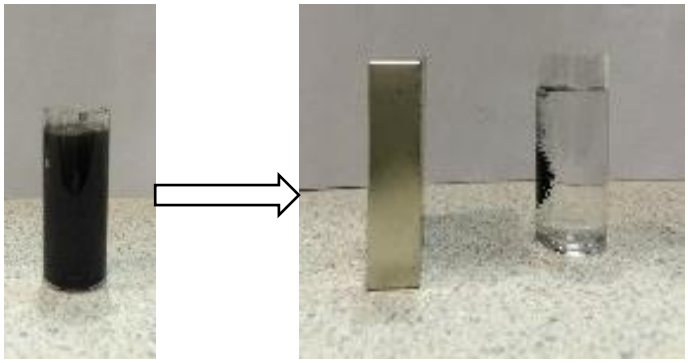

Figure 2-4. Illustration of magnetic separation of solid adsorbents from liquid.

Properties of the adsorbents

Guan et al. (2012) reviewed the arsenic adsorption on various crystal forms of TiO_2 based adsorbents, e.g. crystalline anatase, rutile and amorphous TiO_2. It was revealed that, in general, the adsorption capacity of TiO_2-based adsorbents increased with increasing the specific surface area and decreasing the degree of crystallinity.

With the increase of the specific area, the active reaction sites on the surface of the adsorbents for arsenic species tend to be increased, leading to the enhanced adsorption capacity (Tang and Lo, 2013). For example, Feng et al. (2012) and Zhang et al. (2007) investigated the arsenic adsorption capacities of two different adsorbents, namely ascorbic acid-coated Fe_3O_4 nanoparticles with BET surface area of 179 m^2/g and amorphous Fe–Mn binary oxide with BET surface area of 265 m^2/g, respectively. Under similar test conditions (i.e. pH=5.0 and initial arsenic concentration range was 0–50 mg/L), the Fe–Mn binary oxide showed a much higher adsorption capacity (132.8 mg/g) than the ascorbic acid-coated Fe_3O_4 nanoparticles (46.5 mg/g).

In order to increase the specific surface area, reducing the adsorbent particle size to nanoscale is commonly used. Nano-sized adsorbents were reported to have large removal capacities, fast kinetics and high reactivity for contaminant removal due to

their extremely small particle sizes and high surface-area-to-volume ratios (Lata and Samadder, 2016). However, nanoparticles are too small to control confidently. They are very likely to be released into the natural environment especially water systems, posing a threat to the human health (Tang and Lo, 2013). Moreover, the preparation of nanoparticles tends to be more energy consuming and relatively expensive. Therefore, it is not always the best option to use nanoparticles to improve the adsorption capacities of the adsorbents (Ungureanu et al., 2015; Lata and Samadder, 2016).

Jegadeesan et al. (2010) investigated the crystallinity effects of TiO_2 particles on the arsenic adsorption and suggested that the amorphous TiO_2 could be useful in improving the arsenic adsorption due to the large surface area, disordered structure and possible altered chemical and physical properties compared to crystalline TiO_2.

Regeneration and reuse of the adsorbents

The regeneration and reuse abilities of an adsorbent are critical considerations and contributors from the cost perspective of view. Generally, the regeneration of the spent arsenic adsorbents can be easily achieved by alkali or acid wash (Mohan and Pittman Jr., 2007). Most of the titanium, zirconium and cerium based adsorbents can be regenerated and reused for a number of adsorption-desorption cycles with considerable arsenic adsorption capacities retained. For example, in a typical study using granular TiO_2 to remediate wastewater with a high concentration of As(III), the As-loaded TiO_2 particles were washed with 5 M NaOH solution in triplicate. The total desorption rate of As(III) was in the range of 76%−93% in ten treatment cycles, and the regenerated TiO_2 adsorbent restored its full As(V) adsorption capacity, which was 162±20 mg/g. Luo et al. (2013) used 2 M HNO_3 for the regeneration of a Zr-based arsenic adsorbent. After five treatment cycles, the adsorption capacity remained stable. He et al. (2012) reported a 97% of As(V) desorption rate from the Ce-loaded resin by use of 0.5 M NaOH solution.

2.3. Summary

Several key points can be summarised from the above literature review:

- The process waters associated with gold cyanidation are usually characterised with alkaline pH conditions, complex chemical compositions and various concentrations of ions. Arsenic contained in the gold ores can be released to the process waters and form arsenites and arsenates, causing detrimental effects on the gold cyanidation and recovery processes.
- A number of techniques have been proposed for arsenic removal from aqueous systems. In gold processing circuits, precipitation of arsenic with ferric ions and lime are most widely employed. However, preoxidation of arsenite to arsenate is usually required and a large number of toxic residues are produced from this practice. By contrast, adsorption methods show outstanding prospect in terms of high efficiency, low cost and minimum sludge production in addition to a wide applicable pH range.
- Titanium, zirconium and cerium based adsorbents exhibited excellent arsenic adsorption performance and wide application foreground. The adsorption of arsenic onto these adsorbents was attributed to the hydroxyl groups present on the surface of the adsorbents and followed the inner-sphere complex mechanism in addition to electrostatic attractions. The particle size, surface morphology and specific surface area of the adsorbents are important factors influencing their arsenic adsorption capacities. These properties of the adsorbents can be characterised using scanning electron microscopy (SEM) and Brunauer–Emmett–Teller (BET) method.
- The combination of magnetic cores with the Ti, Zr and Ce based adsorbents could facilitate easy separation of the As-loaded adsorbents from aqueous solutions. The magnetism of the synthesised adsorbents could be evaluated by superconducting quantum interference device (SQUID).
- It is possible to desorb the arsenic species from the adsorbents by using NaOH solution with extremely high pH values, providing a possible way to regenerate and reuse the adsorbents.

The management of arsenic is an ongoing challenge for gold industry. With the decline in resources, the gold mining industry is likely to work with more arsenical ores and higher arsenic levels. Additional research into the handling of arsenic containing solutions is in need. Extensive investigations have been carried out regarding the adsorptive removal of arsenic by titanium, zirconium and cerium based adsorbents from drinking water or ground water at near-neutral pH with highly promising results. Nevertheless, fewer studies were found using the Ti, Zr and Ce based magnetic adsorbents and clearly none was related to the treatment of the alkaline waters of gold cyanide leaching process. Therefore, it is worthwhile to explore:

1. Is it possible to coat the Ti, Zr and Ce based adsorbents onto magnetic cores?
2. Can the synthesised adsorbents still be effective towards As(III) and As(V) under alkaline conditions (pH = 7–11)?
3. How fast the adsorption equilibrium can be reached?
4. Will the adsorption capacities of these adsorbents vary with the pH of the solutions?
5. What are their maximum arsenic adsorption capacities?
6. Will the complex ions present in the gold processing liquors affect their arsenic adsorption performance?
7. Can the adsorbents be regenerated and reused? If so, how will their performance vary after repeated regeneration cycles?

The following sections of the thesis will discuss all these questions in detail with experimental data.

CHAPTER 3 MATERIALS AND METHODS

3.1. Materials

All the chemicals were purchased from Sigma-Aldrich Co. LLC. (Australia) and used without further treatment, unless otherwise stated. All the solutions were prepared with deionised water (resistivity>18 MΩ·cm at 25 °C).

Commercial grade magnetite (Fe_3O_4) and maghemite (γ-Fe_2O_3) nanoparticles were selected as magnetic core materials. According to the official specification sheets, the magnetite nanoparticles have a diameter of 50–100 nm and the maghemite nanoparticles are no larger than 50 nm in diameter based on SEM and BET tests, respectively.

Tetraethyl orthosilicate (i.e. TEOS, $Si(OC_2H_5)_4$), titanium(IV) butoxide (i.e. TBT, $Ti(OCH_2CH_2CH_2CH_3)_4$), ammonium hydroxide (NH_4OH) and ethanol (C_2H_5OH) were used to synthesise $Fe_3O_4@SiO_2@TiO_2$ microparticles. Zirconyl chloride octahydrate ($ZrOCl_2·8H_2O$), ammonium hydroxide (NH_4OH) and ethanol (C_2H_5OH) were the main raw materials for the preparation of γ-$Fe_2O_3@ZrO_2$ microparticles. As for $Fe_3O_4@CeO_2/(OH)_x$ microparticles, the cerium-based shells on the surface of magnetite nanoparticles were achieved by the chemical reaction between cerium(III) nitrate hexahydrate ($Ce(NO_3)_3·6H_2O$) and sodium hydroxide (NaOH).

Stock solutions of As(III) and As(V) were prepared from sodium (meta)arsenite ($NaAsO_2$) and sodium arsenate dibasic heptahydrate ($Na_2HAsO_4·7H_2O$), respectively, at a concentration of 1 g/L. Hydrochloric acid (HCl) and sodium hydroxide (NaOH) solutions (both 0.1 mol/L) were used for pH adjustment.

3.2. Synthesis of the functionalised magnetic microparticles

3.2.1. Fe_3O_4@SiO_2@TiO_2 microparticles

The Fe_3O_4@SiO_2@TiO_2 microparticles were prepared via a conventional sol-gel technique (Kang et al., 2014; Ng et al., 2014) with a few modifications, as depicted in Figure 3-1.

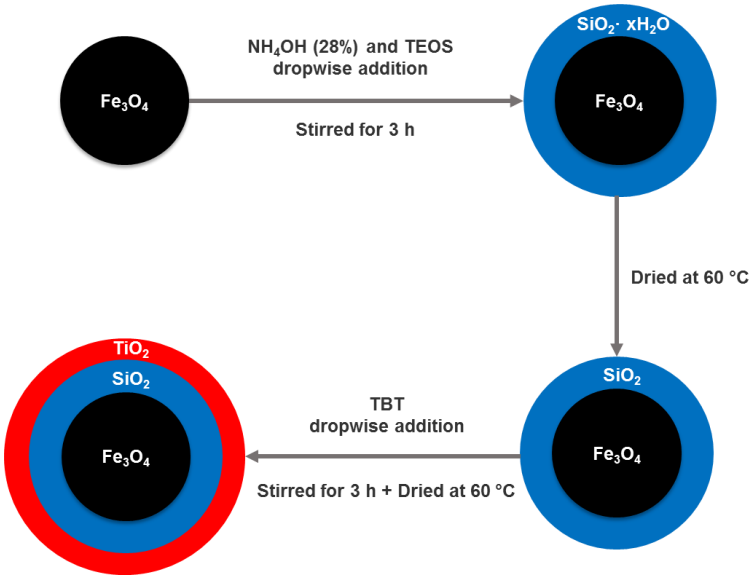

Figure 3-1. Schematic of Fe_3O_4@SiO_2@TiO_2 preparation.

As a first step, Fe_3O_4@SiO_2@TiO_2 microparticles were synthesised by introducing a layer of SiO_2 onto the surface of Fe_3O_4 nanoparticles based on the Stöber method (Stöber et al., 1968), as follows. 65 mL of ethanol (100%) and 35 mL of deionised water were injected into a 250 mL beaker, after which 5 g of Fe_3O_4 nanoparticles were added. The suspension was treated by a handheld ultrasonic homogeniser for 2 min. Following this, 15 mL of ammonium hydroxide (28%) and 5 mL of TEOS were added dropwise. The suspension was mechanically mixed at 600 rpm for 3 h, followed by solid-liquid separation with a neodymium magnet. After rinsing the particles several times with ethanol and deionised water alternately, the resultant product, Fe_3O_4@SiO_2, was dried at 60 ℃ overnight.

Next, the dried $Fe_3O_4@SiO_2$ particles (approximately 6.5 g) were redispersed in 200 mL of ethanol (99%) by ultrasound, and 10 mL of TBT was added dropwise. The suspension was stirred at 600 rpm for 3 h. After a similar rinsing and drying procedure as mentioned above, approximately 8.5 g of $Fe_3O_4@SiO_2@TiO_2$ microparticles were obtained as the final product. Therefore, it is clear that the molar ratio of Fe:Si:Ti was around 2.6:1:1 in the synthesised $Fe_3O_4@SiO_2@TiO_2$ microparticles.

3.2.2. γ-Fe_2O_3@ZrO_2 microparticles

With regard to the preparation of γ-Fe_2O_3@ZrO_2 microparticles, ZrO_2 was directly coated onto the surface of γ-Fe_2O_3 nanoparticles by the hydrolysis of $ZrOCl_2 \cdot 8H_2O$ based on a previous study with a few modifications (Peng et al., 2015). Figure 3-2 shows the preparation process schematically.

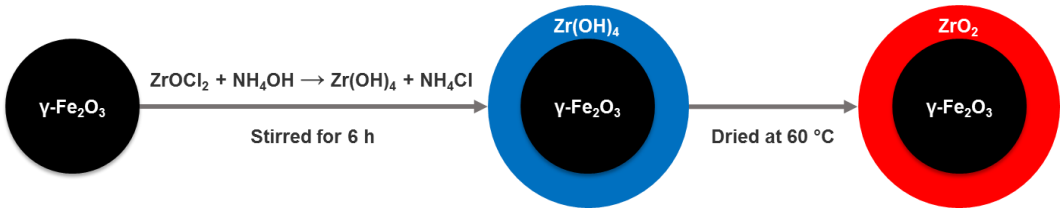

Figure 3-2. Schematic diagram for the synthetic process of γ-Fe_2O_3@ZrO_2.

Specifically, 1 g of γ-Fe_2O_3 nanoparticles were ultrasonically dispersed in a solution containing 400 mL deionised water, 300 mL ethanol and 10 mL ammonia water (28%) to form a homogeneous suspension. Next, an aqueous solution of $ZrOCl_2 \cdot 8H_2O$ (1.5 g dissolved in 10 ml of deionised water) was added dropwise for 10 min and then the mixture was stirred mechanically at 800 rpm for 6 h. After that, the product was collected by a hand-held magnet and rinsed repeatedly with ethanol and deionised water. The resultant particles were dried in an oven at 60 °C overnight. The final weight of γ-Fe_2O_3@ZrO_2 microparticles was approximately 1.7 g, making the molar ratio of Fe to Zr around 2.2:1.

3.2.3. Fe_3O_4@CeO_2/$(OH)_x$ microparticles

Fe_3O_4@CeO_2/$(OH)_x$ microparticles were synthesised via a simple chemical precipitation method at room temperature, as shown in Figure 3-3.

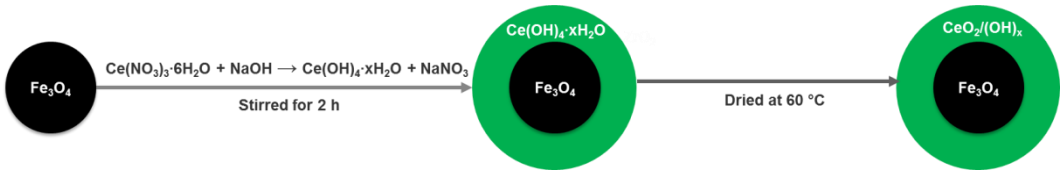

Figure 3-3. Schematic diagram for the synthetic process of Fe_3O_4@CeO_2/$(OH)_x$.

First of all, 1 g of Fe_3O_4 nanoparticles were ultrasonically dispersed in a 200 mL aqueous solution of 0.025 mol/L $Ce(NO_3)_3 \cdot 6H_2O$, followed by adding a 100 mL aqueous solution of 0.25 mol/L NaOH dropwise under mechanical stirring (800 rpm) for 2 h. After that, the resultant particles were separated magnetically and rinsed repeatedly with deionised water. Eventually, the final product of approximately 2 g, Fe_3O_4@CeO_2/$(OH)_x$ microparticles, was dried in an oven at 60 °C overnight. In other words, the synthesised microparticles had a 1:1 mass ratio between the magnetic magnetite cores and the nonmagnetic cerium species shells.

It should be noted that the final form of the cerium species could not be completely determined by the analytical methods adopted in this study. It could be a mixture of ceria and its hydrated forms. Therefore, the final adsorbent is denoted as Fe_3O_4@CeO_2/$(OH)_x$. Detailed explanation can be found in CHAPTER 6.

3.3. Analytical characterisation of the functionalised magnetic microparticles

3.3.1. Microstructure, morphology and elemental composition

A scanning electron microscope - energy dispersive spectrometer (SEM-EDS, Zeiss Neon 40ESB) was employed to visualise the microstructure, morphology and

elemental composition of the synthesised microparticles, which provided the most basic information about the three functionalised magnetic adsorbents.

To be specific, a small number of dried particles were firstly dispersed in a small quantity of deionised water by ultrasonication, and then one drop of the suspension was dripped on an aluminium stub and air dried, prior to the sputter coating with 3 nm of platinum. Afterwards, the prepared samples were analysed by SEM at an acceleration voltage of 5 or 15 kV at various magnifications and eventually the EDS analysis was conducted at an acceleration voltage of 30 kV.

3.3.2. Phase composition

X-ray diffraction technique (XRD, Panalytical Empyrean) was used to analyse the phase composition of the microparticles qualitatively and quantitatively. It is of great significance to reveal the information about the structure of crystalline materials, contributing to a comprehensive understanding of the synthesised adsorbents. The powder samples were scanned by an applied current of 40 mA and a voltage of 45 kV with scattering angles of 5 - 90 °2θ by means of Co Kα radiation.

3.3.3. Magnetic properties

The magnetic properties of the microparticles were studied on a superconducting quantum interference device (SQUID, Quantum Design MPMS 3) without any sample pretreatment at room temperature, which played a decisive role in the magnetic separability of the synthesised adsorbents. The entire instrument is shown in Figure 3-4.

3.3.4. Specific surface area

Given that surface area measures how much exposed area there is on the synthesised particles, surface area can be considered as a key to a quality adsorbent. The Brunauer-Emmett-Teller method (BET, Micromeritics TriStar 3000) was employed

to study the specific surface areas of the microparticles with N_2 as the adsorbate, at -195.85 °C.

3.3.5. Zeta potential

Point of zero charge describes the condition when the electrical charge density on a surface is zero, which is often associated with the adsorption mechanism thus is very meaningful in the area of adsorption. Zetasizer Nano ZS (Malvern Instruments) was used to measure the surface zeta potentials of the microparticles for approximate determination of the points of zero charge.

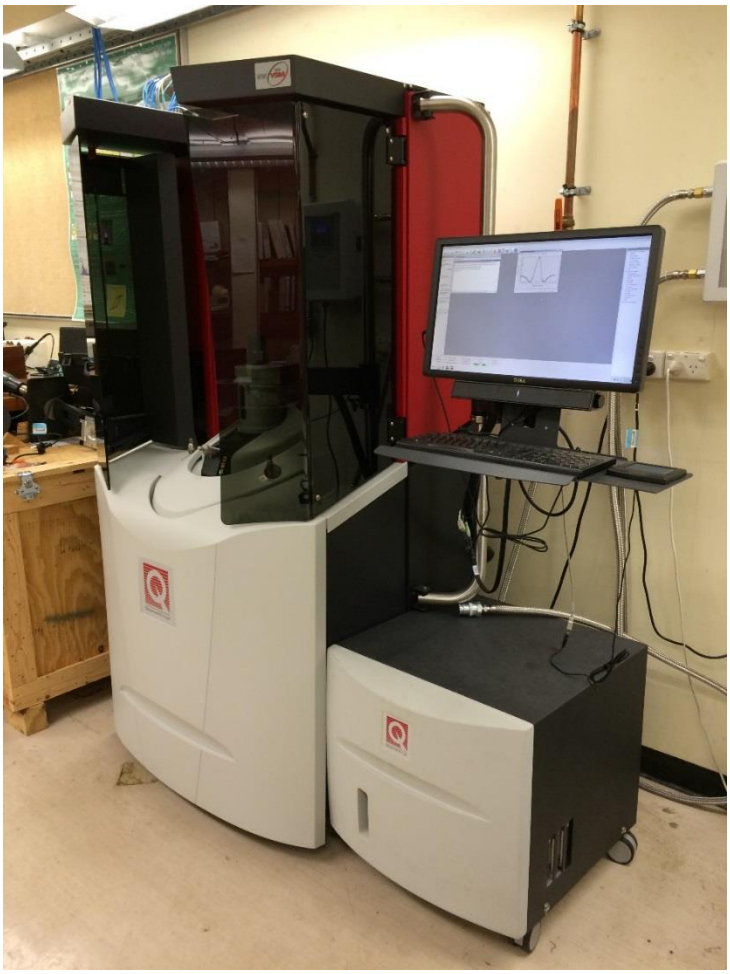

Figure 3-4. Quantum Design MPMS 3 SQUID magnetometer.

3.4. Adsorption tests

Generally speaking, all the adsorption tests throughout the study were carried out based on much the same experimental procedures. To put it simply, under room temperature, 0.05 g of microparticles were agitated with 50 mL of an arsenic-containing aqueous solution in a sealed 125 mL Erlenmeyer flask which was fixed in a shaking bath, as shown in Figure 3-5. After adsorption tests, the adsorbents were separated magnetically from the suspension, and the arsenic concentrations before and after adsorption in the supernatant were determined by use of an inductively coupled plasma - optical emission spectrometer (ICP-OES, Agilent 735-ES). Each test was performed in duplicate and average values were recorded. Additionally, a supplementary material which serves as a foil to the advantages of the synthesised adsorbents, is provided in the Appendix, showing roughly the adsorption performances of the magnetic core materials, i.e. Fe_3O_4 and γ-Fe_2O_3, as well as commercial TiO_2, ZrO_2 and CeO_2 particles.

Figure 3-5. The experimental setup for adsorption tests.

3.4.1. Effect of pH

As(III)-only (100 mg/L) and As(V)-only (100 mg/L) solutions with pH values ranging from 7 to 11 were used to investigate the effect of pH on the adsorption behaviours of the synthesised microparticles. The contact time was set as 24 h.

3.4.2. Adsorption kinetics

In the study of adsorption kinetics, the solutions containing 100 mg/L either As(III) or As(V) were treated with the synthesised microparticles for 0.5 h, 1 h, 2 h, 4 h, 6 h, 12 h and 24 h, respectively, at pH 9.

After tests, the data were fitted by a pseudo-second-order kinetic model using OriginPro 2015. The pseudo-second-order kinetic model is based on the assumption that the rate-limiting step might be chemisorption involving sharing or exchange of electrons between adsorbent and adsorbate (Azizian, 2004). It is expressed as equation (3-1),

$$\frac{t}{q_t} = \frac{1}{k_2 q_e^2} + \frac{t}{q_e} \tag{3-1}$$

where q_t (mg/g) is the adsorption capacity at time t (min), q_e (mg/g) is the equilibrium adsorption capacity, and k_2 (g/mg·min) is the rate constant. The goodness of fit of the experimental data to the pseudo-second-order kinetic model is quantified via squared correlation coefficient (R^2).

3.4.3. Adsorption isotherms

For the adsorption isotherms, the adsorption tests were conducted for 24 h in the As(III)-only and As(V)-only solutions with different initial arsenic concentrations. As the target of this study is to apply the adsorbents to treat the arsenic-containing process water associated with gold cyanidation circuits, of which the pH is 9, the experiments on arsenic adsorption isotherms were performed at room temperature and pH 9.

Both Langmuir (Equation (3-2)) and Freundlich (Equation (3-3)) models were used to fit the test data,

$$Q_e = Q_m \left(\frac{K_L C_e}{1 + K_L C_e} \right) \tag{3-2}$$

$$Q_e = K_F C_e^{\frac{1}{n}} \tag{3-3}$$

where C_e (mg/L) is the equilibrium arsenic concentration, and Q_e (mg/g) represents the arsenic concentration on the surface of the adsorbent. The Langmuir parameter Q_m (mg/g) estimates the maximum adsorption capacity at equilibrium, K_L (L/mg) is the Langmuir constant proportional to the energy of adsorption, and n and K_F ($mg^{1-1/n}L^{1/n}g^{-1}$) are parameters of the Freundlich model.

These models could estimate the relationships between the amounts of As(III)/As(V) adsorbed onto the synthetic adsorbents and their equilibrium concentrations. Similar to the kinetic studies, the fitting was implemented using OriginPro 2015 software and the goodness of fit was quantified by squared correlation coefficient (R^2).

3.4.4. Competitive adsorption

In order to investigate the potential influence of coexisting ions present in process waters from gold cyanidation on arsenic adsorption by the synthesised microparticles, a simulated solution was firstly prepared with the recipe given in Table 3-1. This recipe was based on the chemical composition analysis of a process water sample from a Western Australian gold mine. Afterwards, this solution was spiked with arsenite and arsenate in a 1:1 molar ratio of As(III) to As(V). The total arsenic concentration in the final solution was determined to be approximately 90 mg/L by ICP-OES. The pH of the synthetic process water sample was found to be 8.8, which is very close to that of the original process water sample (pH=9).

Table 3-1. The chemical composition of a process water sample from a gold mine in Western Australia.

Analyte	Mg^{2+}	Ca^{2+}	K^{+}	Na^{+}	Cl^{-}	SO_4^{2-}	NO_3^{-}	SCN^{-}	$Fe(CN)_6^{4-}$
Concentration (mg/L)	45	1700	250	11000	18000	2600	70	140	36

The competitive adsorption tests were performed using the synthetic solution abovementioned under the identical experimental setup used in all the other adsorption tests. The adsorption time was 24 h.

3.5. Regeneration and reuse

Multiple consecutive adsorption-desorption cycles were performed in duplicate to evaluate the possibility and feasibility of the synthesised microparticles for regeneration and reuse. The adsorption tests were conducted in arsenic-only solutions or synthetic process waters of gold cyanidation containing both As(III) and As(V) until equilibrium was achieved. Thereafter, the magnetically separated microparticles were gently rinsed with deionised water repeatedly, followed by redispersion in 50 mL of the regenerant, i.e. 1.0 mol/L NaOH solution (pH≈13), and shaken for another 2 h. Prior to the next adsorption cycle, the treated microparticles were washed with deionised water thoroughly until the solution reached a pH of 7. The adsorption-desorption cycles were repeated for several times with the arsenic adsorption capacities analysed and recorded.

CHAPTER 4 TITANIUM-BASED MAGNETIC ADSORBENT

4.1. Introduction

It is well-known that TiO_2 is a promising material for arsenic removal from aqueous solutions, owing to its physical and chemical stability, negligible toxicity, corrosion resistance (Nabi et al., 2009), as well as easy preparation and high affinity for arsenic (Balaji and Matsunaga, 2002). Most previous studies regarding TiO_2-based materials have focused on the photocatalytic oxidation of arsenite to arsenate and adsorption of arsenate (Guan et al., 2012), since the dominant form of arsenite under neutral or acidic conditions is uncharged H_3AsO_3 that exhibits poorer affinity for most TiO_2-based removal methods (Ungureanu et al., 2015a). However, few studies have considered the removal of arsenic by use of TiO_2 adsorbents under alkaline conditions.

As a consequence, the use of a magnetic TiO_2 adsorbent, $Fe_3O_4@SiO_2@TiO_2$ microparticles, for the removal of arsenic from gold cyanidation process waters is considered in this investigation. Given that the aqueous environment in gold cyanidation is alkaline (Díaz and Caizaguano, 1999), the preoxidation process causes adverse effects instead, owing to the change in electrostatic interactions between TiO_2 and arsenic species, i.e. arsenite is adsorbed more readily by TiO_2 than arsenate under alkaline conditions. Therefore, in this study, all experiments with As(III) were done in the dark to prevent the photocatalytic oxidation of As(III) to As(V), given that the adsorption capacity of titania for the latter is lower than for the former.

The magnetic core of the composite adsorbent allows it to be readily separated by an external magnetic field after adsorption (Tang and Lo, 2013). The intermediate layer of SiO_2 reduces interaction between the inner Fe_3O_4 and the outer TiO_2, and also stabilises the magnetic core (Liu et al., 2011). The $Fe_3O_4@SiO_2@TiO_2$ adsorbent

was characterised by a series of analytical methods, systematic adsorption tests were conducted, and its reusability was studied.

4.2. Results and discussion

4.2.1. Characterisation of Fe_3O_4@SiO_2@TiO_2

SEM-EDS

Figure 4-1 shows the SEM image of the Fe_3O_4@SiO_2@TiO_2 microparticles. It can be clearly seen that the well-dispersed particles were spheroidal, with diameters ranging from 200 to 400 nm. This is evidently larger compared with other Ti-based adsorbents (Guan et al., 2012), because the diameter of the magnetic core Fe_3O_4 nanoparticles is large.

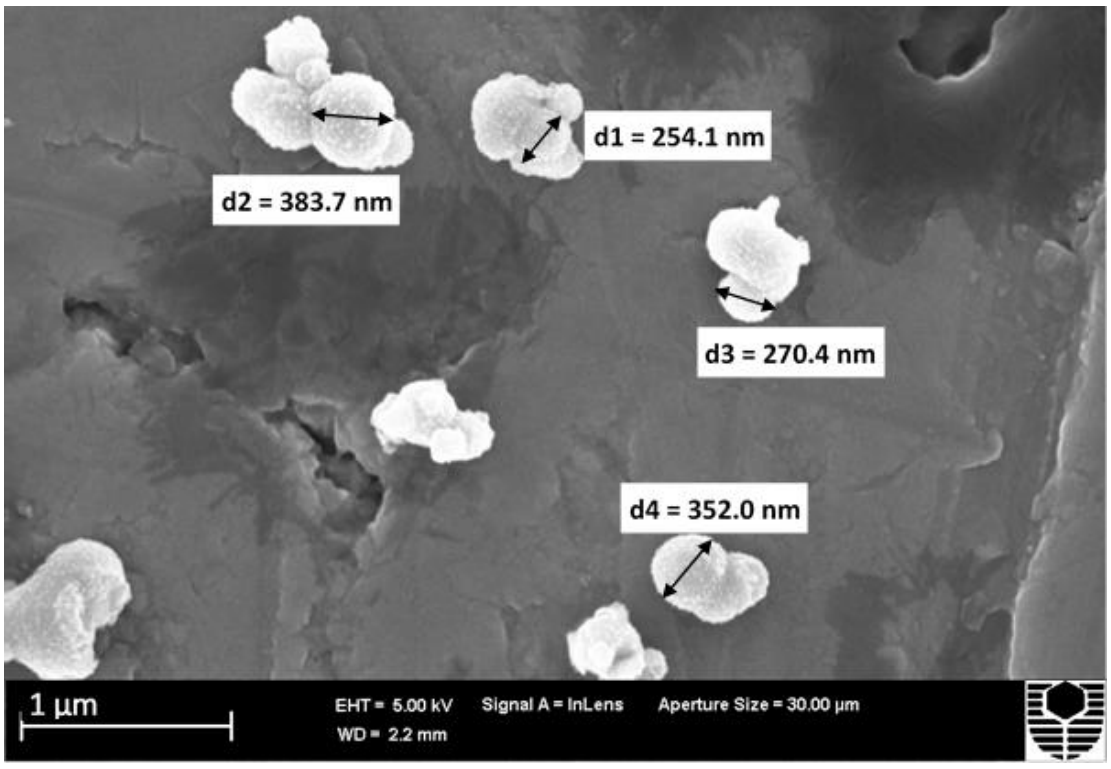

Figure 4-1. SEM image of Fe_3O_4@SiO_2@TiO_2.

Figure 4-2 shows the EDS spectra of Fe_3O_4@SiO_2 and Fe_3O_4@SiO_2@TiO_2 particles. Al originating from the aluminium substrate was detected, as well as Fe and O from

both the $Fe_3O_4@SiO_2$ and $Fe_3O_4@SiO_2@TiO_2$ particles, while Ti was also found in the latter. This indicates that the synthesis of the $Fe_3O_4@SiO_2@TiO_2$ microparticles via a two-step hydrolysis method was achieved.

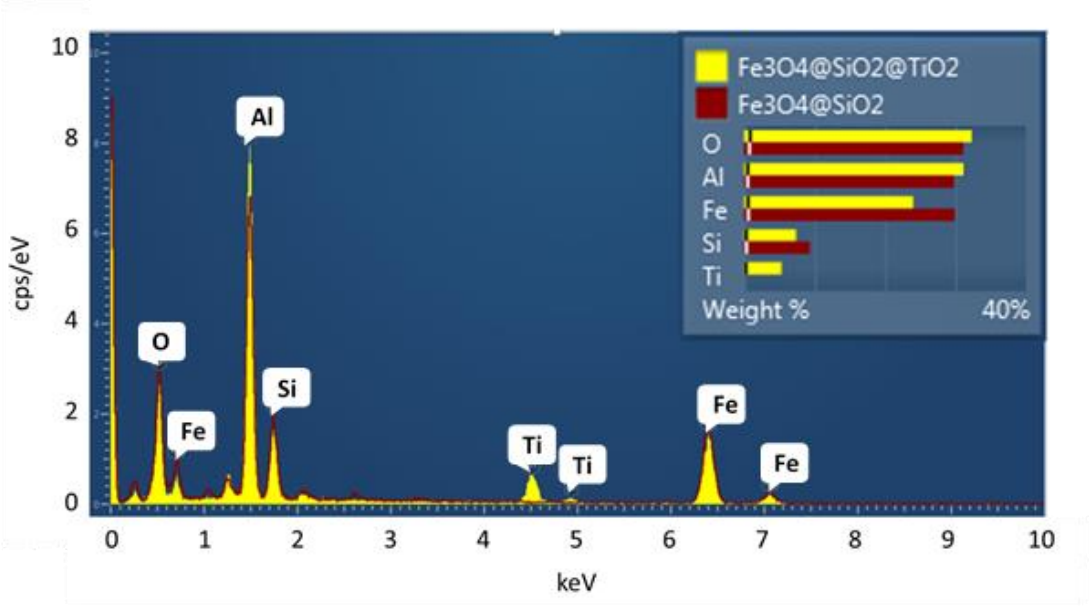

Figure 4-2. EDS spectra of $Fe_3O_4@SiO_2$ (yellow) and $Fe_3O_4@SiO_2@TiO_2$ (red).

XRD

It was reported that calcination crystallised the surface TiO_2 of the $Fe_3O_4@SiO_2@TiO_2$ particles (Ng et al., 2014). Table 4-1 shows the semi-quantitative XRD results of untreated and calcined (400 °C for 1 h) $Fe_3O_4@SiO_2@TiO_2$ microparticles. The diffraction portion of the untreated $Fe_3O_4@SiO_2@TiO_2$ microparticles was almost exclusively magnetite with a trace of anatase present. Some of the magnetite appeared to contain substitution. There was a broad peak around the main peak position for anatase, suggesting that a significant amount of amorphous titanium oxide was likely present. The diffraction portion of the calcined $Fe_3O_4@SiO_2@TiO_2$ microparticles contained predominantly maghemite, which appeared to contain some substitution by Ti.

Table 4-1. Semi-quantitative XRD results of Fe_3O_4@SiO_2@TiO_2.

Mineral	Mass%	
	Fe_3O_4@SiO_2@TiO_2	**Calcined Fe_3O_4@SiO_2@TiO_2**
Hematite (+ Ti)	0	1
Maghemite (+ Ti)	0	88
Magnetite (+ Ti)	99	0
Anatase	1	9
$Ti_{3-x}Fe_xO_5$	0	2

The TiO_2 present was still partially amorphous and in part nanocrystalline, with five to six distinct types of anatase present, each showing some distortion of the lattice. A mixed oxidation state of titanium oxide was identified, with the approximate composition of Ti_3O_5 with only a trace of Fe. Part of the maghemite had started to recrystallise and some hematite was present, most likely containing some titanium as well.

From this, it can be concluded that the TiO_2 on the surface of the untreated Fe_3O_4@SiO_2@TiO_2 microparticles was mostly amorphous and could be partially transformed into anatase by calcination under the above conditions. The innermost magnetite core could be oxidised to maghemite almost completely, with negligible loss in magnetism of the material.

Based on some preliminary adsorption tests (Table 4-2), the calcined Fe_3O_4@SiO_2@TiO_2 microparticles were less efficient than the untreated ones, which supported the point of view that amorphous TiO_2 might be beneficial for increased arsenic adsorption (Jegadeesan et al., 2010). Therefore, the Fe_3O_4@SiO_2@TiO_2 microparticles employed in this study were not calcined.

Table 4-2. **Preliminary adsorption results calcined and untreated $Fe_3O_4@SiO_2@TiO_2$ particles for As(III) and As(V) (Experimental conditions: 0.05 g adsorbent; As concentration=100 pm; T=25 °C; pH=9; 24 h).**

	As (III) adsorbed (mg/g)		As (V) adsorbed (mg/g)	
	Untreated $Fe_3O_4@SiO_2$ $@TiO_2$	Calcined $Fe_3O_4@SiO_2$ $@TiO_2$	Untreated $Fe_3O_4@SiO_2$ $@TiO_2$	Calcined $Fe_3O_4@SiO_2$ $@TiO_2$
Test	31.3	12.8	5.7	3.0
Repeat	28.7	10.9	7.9	2.5

SQUID

The magnetic properties of the raw and functionalised Fe_3O_4 particles were determined with a SQUID magnetometer. The magnetic field dependent magnetization plots of Fe_3O_4, $Fe_3O_4@SiO_2$ and $Fe_3O_4@SiO_2@TiO_2$ particles exhibit ferromagnetic behaviour, as shown in Figure 4-3. The maximum magnetization of Fe_3O_4, $Fe_3O_4@SiO_2$ and $Fe_3O_4@SiO_2@TiO_2$ particles were found to be approximately 80, 60 and 40 emu/g, respectively. As can be seen in Figure 4-4, despite a certain loss, the $Fe_3O_4@SiO_2@TiO_2$ microparticles still have strong magnetic responsiveness and could be separated easily from solutions with the help of an external magnetic force.

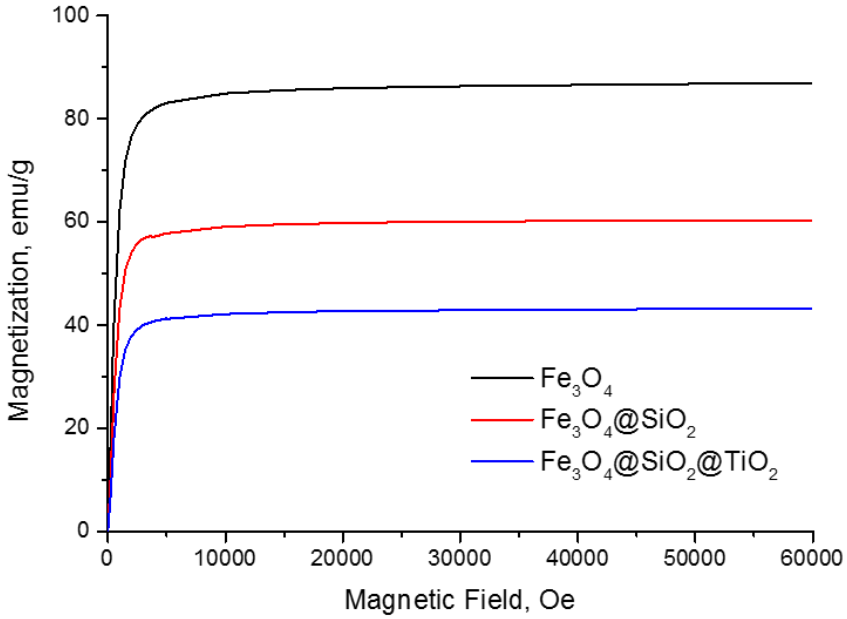

Figure 4-3. Magnetization curves of Fe_3O_4, $Fe_3O_4@SiO_2$ and $Fe_3O_4@SiO_2@TiO_2$.

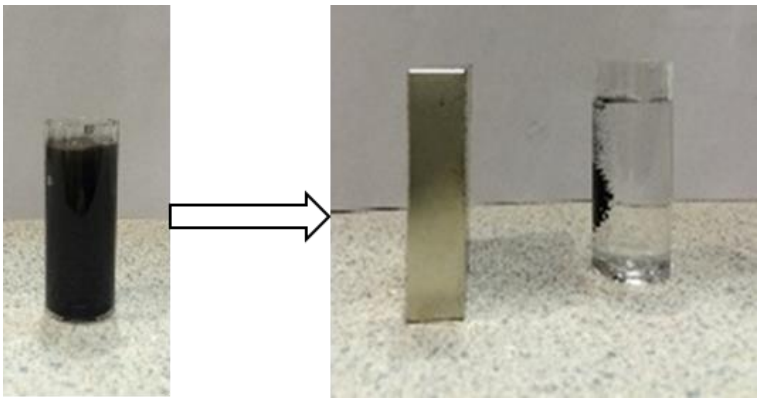

Figure 4-4. $Fe_3O_4@SiO_2@TiO_2$ microparticles dispersed in an aqueous solution (left), and magnetic separation of $Fe_3O_4@SiO_2@TiO_2$ microparticles (right) in the presence of a magnetic field.

BET

The specific surface area of the $Fe_3O_4@SiO_2@TiO_2$ microparticles determined by BET was 86.65 m^2/g, which was limited by the core material of Fe_3O_4 (100–200 nm). Theoretically, increasing the specific surface area by decreasing the particle size would enhance the adsorption capacity of adsorbents. However, other factors, such

as cost, the separability of the loaded particles, etc., would also have to be accounted for.

4.2.2. Adsorption tests

Effect of pH

Figure 4-5 shows the experimental conditions and the calculated results derived from ICP-OES analysis of adsorption tests. The differences between the designed As concentration and the ICP-OES measured values were within ± 2 mg/L. Overall, the Fe_3O_4@SiO_2@TiO_2 adsorbent showed good adsorption of both As(III) and As(V) under neutral and alkaline conditions. However, the adsorbed amount of As(III) on the Fe_3O_4@SiO_2@TiO_2 adsorbent decreased sharply with an increase of pH, and the highest specific adsorption of 30.6 mg/g was achieved at a pH of 8. By contrast, the Fe_3O_4@SiO_2@TiO_2 adsorbent had a lower adsorption capacity for As(V), which decreased only marginally over the entire pH range studied.

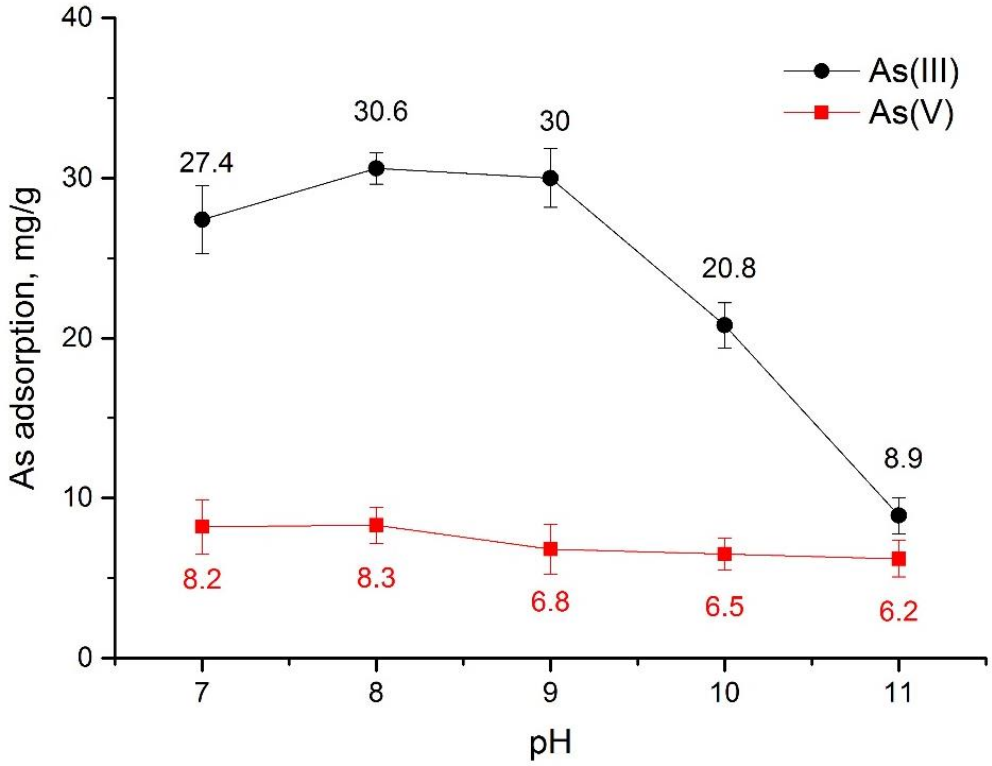

Figure 4-5. Effect of pH on arsenic adsorption (As concentration: 100 mg/L; contact time: 24 h). Average values from two parallel adsorption tests are presented. Bars indicate standard deviations.

Adsorption kinetics

The experimental conditions and the processed experimental data of adsorption kinetics tests are summarised in Figure 4-6. The kinetic data of the Fe_3O_4@SiO_2@TiO_2 adsorbent was fitted to a pseudo-second-order rate kinetic model:

$$\frac{t}{q_t} = \frac{1}{k_2 q_e^2} + \frac{t}{q_e} \quad (1)$$

where q_t (mg/g) is the adsorption capacity at time t (min), q_e (mg/g) is the amount of solute adsorbed at equilibrium, and k_2 (g·mg^{-1}·min^{-1}) is the rate constant. The suitability of the pseudo-second-order rate kinetic model is quantified by the squared correlation coefficient (R^2).

As shown in Figure 4-6, the kinetic behaviour of arsenic adsorption onto the Fe_3O_4@SiO_2@TiO_2 adsorbent was represented satisfactorily by the abovementioned model, with q_e=29.5 mg/g, k_2=0.001 min^{-1} and R^2=0.97 for As(III) and q_e=7.3 mg/g,

k_2=0.005 min^{-1} and R^2=0.98 for As(V). It can be seen clearly that the adsorption equilibrium could be achieved within around 4 h for both As(III) and As(V).

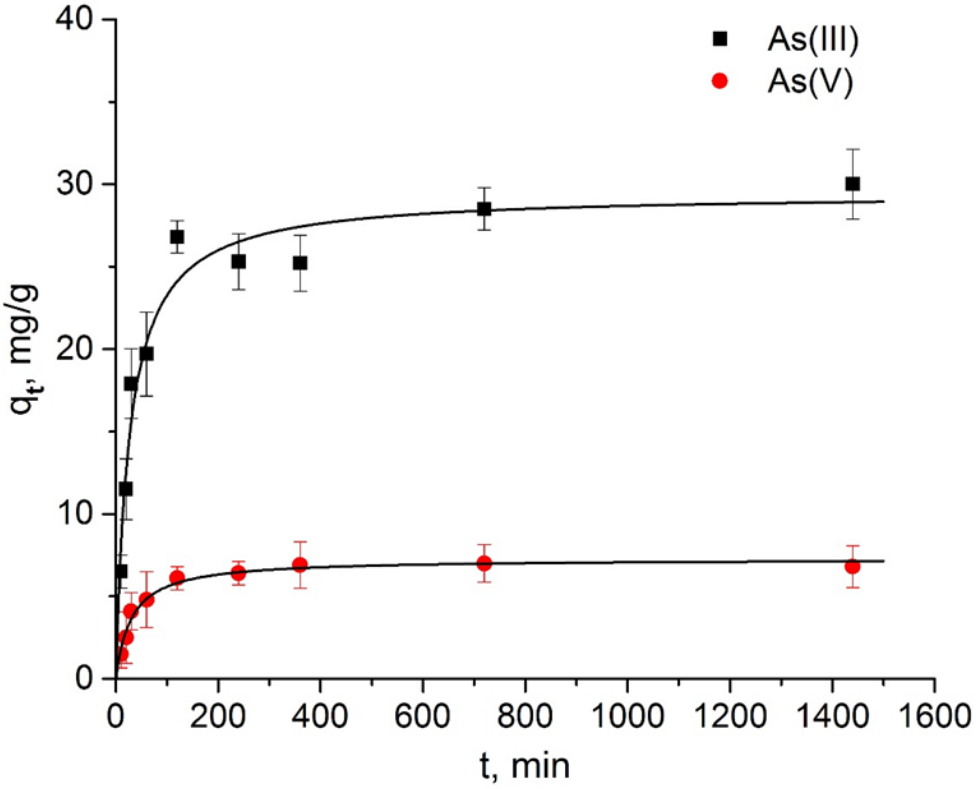

Figure 4-6. Adsorption kinetics data fitted by eq. (1) (As concentration: 100 mg/L; pH: 9). Average values from two parallel adsorption tests are presented. Bars indicate standard deviations.

Adsorption isotherms

Adsorption isotherm tests of arsenic on the Fe_3O_4@SiO_2@TiO_2 adsorbent were performed at 25 °C, and the results were fitted by the Langmuir isotherm model:

$$Q_e = Q_m \left(\frac{K_L C_e}{1 + K_L C_e} \right) \quad (2)$$

where C_e (mg/L) is the equilibrium arsenic concentration, Q_e (mg/g) is the adsorption capacity, the parameter Q_m (mg/g) estimates the maximum adsorption capacity at equilibrium when the adsorbent is saturated, and the constant K_L (L/mg) is proportional to the energy of adsorption (Artioli, 2008).

The Langmuir isotherms for both As(III) and As(V) under the above conditions are given in Figure 4-7. The Langmuir model satisfactorily explained the adsorption of arsenic onto the Fe_3O_4@SiO_2@TiO_2 adsorbent with model parameters Q_m =31.4 mg/g, K_L=0.25 L/mg and R^2=0.99 for As(III), and Q_m=10.2 mg/g, K_L=0.02 L/mg and R^2=0.99 for As(V).

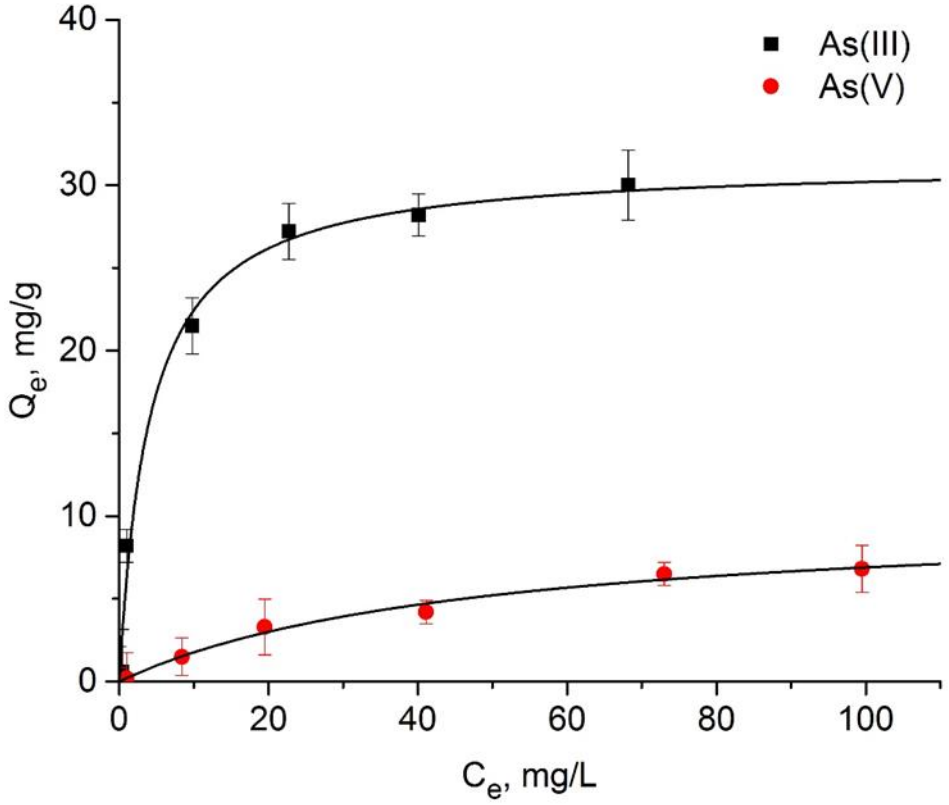

Figure 4-7. Adsorption isotherm data fitted by eq. (2) (pH: 9; contact time: 24 h). Average values from two parallel adsorption tests are presented. Bars indicate standard deviations.

In recent studies, a resin coated with nickel and nickel boride nanoparticles exhibited maximum adsorption capacities of 23.4 mg/g and 17.8 mg/g for As(III) and As(V), respectively, at pH 6 (Çiftçi and Henden, 2015), a mixed ferrite and hausmannite nanomaterial was reported to have maximum adsorption capacities of 41.5 mg/g and 13.9 mg/g for As(III) and As(V), respectively, at pH 3 (Garcia et al., 2014), while leonardite char achieved maximum adsorption capacities of 4.46 mg/g and 8.4 mg/g for As(III) and As(V), respectively, at pH 7 (Chammui et al., 2014). Zhang et al. (2013) reported maximum adsorption capacities of 122.3 mg/g and 82.7 mg/g for

As(III) and As(V), respectively, at pH 7 by use of a Fe-Cu binary oxide sorbent. The performance of $Fe_3O_4@SiO_2@TiO_2$ adsorbent in this study should be compared bearing in mind that the above studies were for drinking water, underground water, etc., which are closer to neutral rather than alkaline pH.

It is generally known that H_3AsO_3 and $H_2AsO_3^-$ are the dominant As(III) species and the main form of As(V) is $HAsO_4^{2-}$ in the pH range of 7–11 (Mohan & Pittman Jr, 2007). Moreover, the point of zero charge (PZC) of the $Fe_3O_4@SiO_2@TiO_2$ adsorbent was determined to be at a pH value of approximately 4.0. This is similar to the value of 4.5 reported for amorphous TiO_2 by Yan et al. (2016), and indicates that the surface of the adsorbent is negatively charged in the alkaline pH range studied here. Therefore, from the point of view of surface interactions driving the adsorption process, electrostatic attraction hardly exists in the studied adsorption system.

At a pH ranging from 7 to 9, the electrostatic repulsion between the neutral H_3AsO_3 and the negatively charged adsorbent is significantly less than that between negatively charged $HAsO_4^{2-}$ and adsorbent, which may explain the significant difference in the adsorption capacity for As(III) and As(V).

However, when the pH value exceeds 9.2, i.e. the acid dissociation constant of arsenous acid (pK_{a1}), the adsorption capacity of the $Fe_3O_4@SiO_2@TiO_2$ adsorbent for As(III) decreased significantly and was close to the value for As(V) at pH 11 (8.9 and 6.2 mg/g, respectively), as shown in Figure 4-5. This can be explained by the increase in the electrostatic repulsion between the dominant As(III) species ($H_2AsO_3^-$ and even $HAsO_3^{2-}$) and the negatively charged adsorbent, which inhibited the adsorption.

Thus, there must be a strong chemical bonding present between arsenic and the $Fe_3O_4@SiO_2@TiO_2$ adsorbent, in spite of the electrostatic repulsion. According to the literature (Jegadeesan et al., 2010; Jegadeesan et al., 2006; Jing et al., 2009; Niu et al., 2009; Pena et al., 2006), a general consensus has been reached on the adsorption mechanisms of arsenic species on TiO_2-based adsorbents.

In brief, both As(III) and As(V) can form negatively charged inner-sphere surface complexes with the involvement of the hydroxyl groups on the surface of TiO_2, which are mainly bidentate binuclear $(TiO)_2AsO^-$ and $(TiO)_2AsO_2^-$ for As(III) and As(V), respectively. It is worth mentioning that the adsorption of As(III) and As(V) slightly decreased the point of zero charge of the $Fe_3O_4@SiO_2@TiO_2$ adsorbent from 4.0 to 3.5 in our study, which reconfirms the formation of negatively charged inner-sphere surface complexes for both arsenic species.

Competitive adsorption

In order to test the adsorption capacity of the $Fe_3O_4@SiO_2@TiO_2$ adsorbent in the real environment of gold cyanidation, a simulated solution, consisting of 90 mg/L As(III)/As(V), 45 mg/L Mg^{2+}, 1700 mg/L Ca^{2+}, 250 mg/L K^+, 11000 mg/L Na^+, 18000 mg/L Cl^-, 2600 mg/L SO_4^{2-}, 70 mg/L NO_3^-, 140 mg/L SCN^- and 36 mg/L $Fe(CN)_6^{4-}$, was prepared and used for competitive adsorption tests under the same conditions described above. Note that the initial pH of the simulated solution was approximately 9 and no further pH adjustment was conducted in the adsorption tests.

Under such conditions, an average 15.6 mg/g combined adsorption performance for As(III) and As(V) was obtained. Hence it can be concluded that high ionic strength and the complex chemical environment of the simulated solution do not appreciably affect arsenic adsorption onto the $Fe_3O_4@SiO_2@TiO_2$ adsorbent, making this application promising.

4.2.3. Regeneration and reuse

Considering the industrial practicability of the $Fe_3O_4@SiO_2@TiO_2$ adsorbent, another important performance criterion is its reusability, which is highly beneficial for cost reduction. On the basis of Figure 4-5, it could be extrapolated that a strong alkaline solution would be favourable for arsenic desorption, and indeed the increased concentration of OH^- could compete greatly with the already adsorbed arsenic species on TiO_2-based adsorbents (Arumugam et al., 2013). Consequently, a regenerant of 1.0 mol/L NaOH solution was tentatively employed to elute arsenic

from the arsenic loaded microparticles. Four consecutive adsorption-regeneration cycles were conducted and positive results were obtained, as shown in Figure 4-8.

As can be seen, the Fe_3O_4@SiO_2@TiO_2 adsorbent still retained over 60% of its initial adsorption capacity for both As(III) and As(V) after four cycles of adsorption and regeneration. Coupled with some mass loss in particles during regeneration, it can be concluded that part of the adsorbed arsenic on the surface could be desorbed by highly alkaline solution (pH>13) and the adsorbent could be employed for repeated use without significant performance loss.

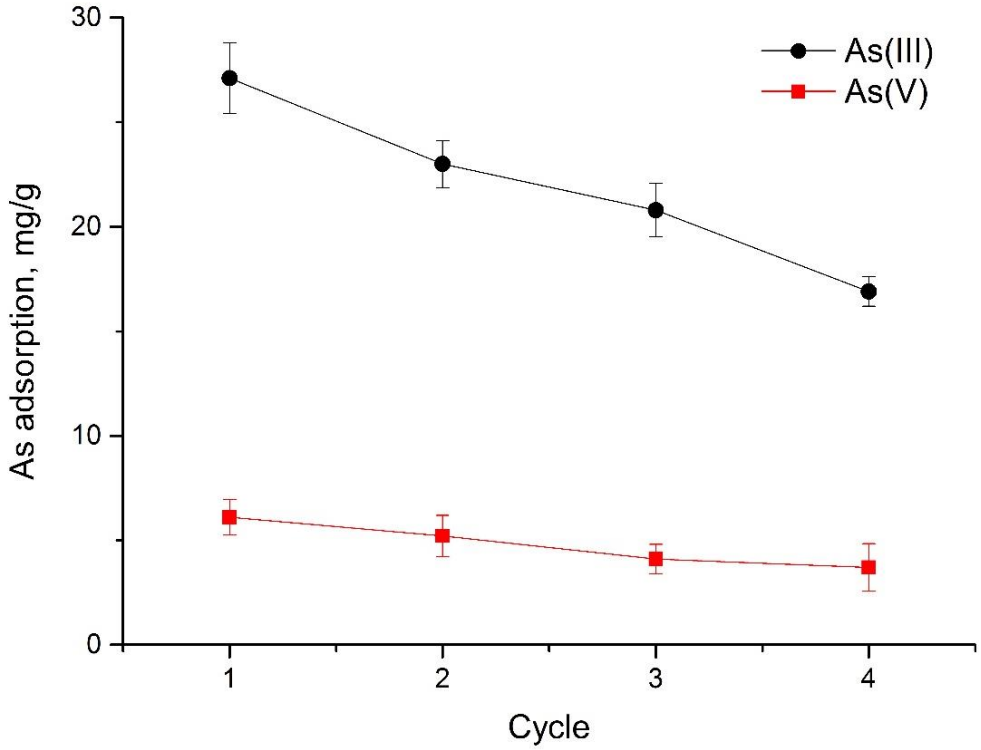

Figure 4-8. Regeneration and reuse of Fe_3O_4@SiO_2@TiO_2 (As concentration: 100 mg/L; pH: 9). Average values from two parallel adsorption tests are presented. Bars indicate standard deviations.

4.3. Summary

- A magnetic TiO_2-based adsorbent was successfully synthesised by a two-step process, i.e. synthesis of $Fe_3O_4@SiO_2$ based on the Stöber method, followed by synthesis of $Fe_3O_4@SiO_2@TiO_2$ through a sol-gel method. Characterisation of the particles showed that the diameter of the $Fe_3O_4@SiO_2@TiO_2$ adsorbent ranged from 200 to 400 nm and the surface layer of TiO_2 was mostly amorphous.
- Magnetic measurements indicated that the microparticles were ferromagnetic and the maximum magnetization was in excess of 40 emu/g, readily allowing magnetic separation. In addition, the BET surface area of the adsorbent was approximately 86.7 m^2/g.
- Based on the experimental results for arsenic adsorption, the $Fe_3O_4@SiO_2@TiO_2$ adsorbent was identified as a promising arsenic adsorbent. It showed good removal capacity and favourable adsorption kinetics and could potentially be used in the alkaline waters of gold cyanidation processes.
- The reusability of $Fe_3O_4@SiO_2@TiO_2$ was confirmed by four consecutive adsorption-regeneration cycles with a strong base as regenerating agent.

CHAPTER 5 ZIRCONIUM-BASED MAGNETIC ADSORBENT

5.1. Introduction

Zirconia (ZrO_2) is a known adsorbent of arsenic in water (Cui et al., 2012; Xu et al., 2013a; Zheng et al., 2012; Zheng et al., 2012). In this chapter, the use of composite microparticles consisting of magnetite cores functionalised with zirconia to remove arsenic from simulated mining process waters is considered. Zirconium dioxide, is an inexpensive, nontoxic, chemically unreactive and water-insoluble inorganic material, and is widely recognized as a strong adsorbent for arsenic species, particularly As(III) species (Cui et al., 2012; Luo et al., 2013).

The adsorption mechanism of arsenic species onto zirconium oxide follows the inner-sphere complex mechanism, where both As(III) and As(V) can form negatively charged inner-sphere complexes with the involvement of hydroxyl groups on the surface of ZrO_2 during adsorption (Cui et al., 2012). To extend these previous studies, a functionalised magnetic adsorbent (γ-Fe_2O_3@ZrO_2) was synthesised and its use in the removal of arsenic from process waters of gold cyanidation was evaluated.

Owing to the alkaline environment of process water from gold cyanide leaching, the adsorption tests on the effect of pH in this study were conducted within a pH range of 7 to 11, while adsorption kinetics and isotherms were carried out at pH 9, which is typical of process water samples from local gold mines in Western Australia. Moreover, a simulated solution with high ionic strength and complex chemistry was used to validate the adsorption performance of γ-Fe_2O_3@ZrO_2.

5.2. Results and discussion

5.2.1. Characterisation of γ-Fe_2O_3@ZrO_2

SEM-EDS

Figure 5-1 shows the SEM image of γ-Fe_2O_3@ZrO_2. The zirconia coated maghemite microparticles were near-spherical, with diameters ranging from 20 to 200 nm and partly aggregated, which greatly depends on the morphology of the maghemite microparticles purchased from Sigma-Aldrich. The surface coating of zirconium species was confirmed by the EDS spectrum of that area, as shown in Figure 5-2. It should be noted that element Al was also detected according to the spectrum, which originated from the substrate used for electron microscopy analysis.

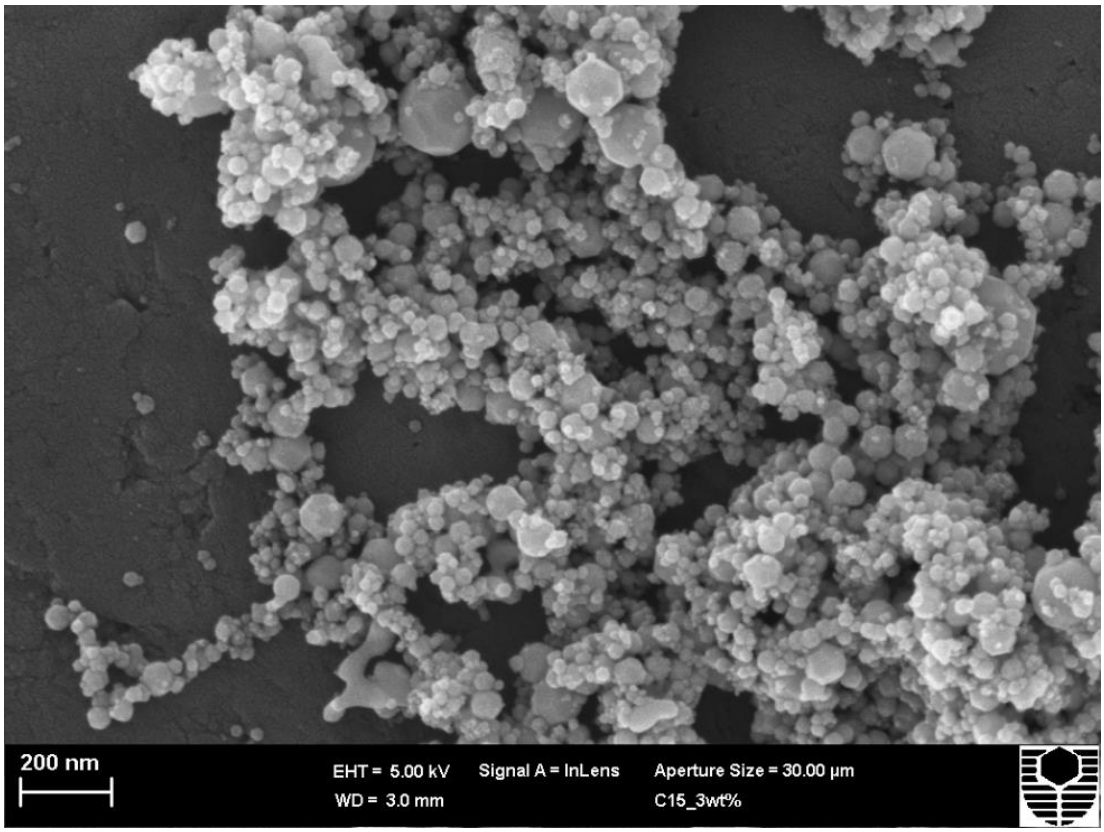

Figure 5-1. SEM image of γ-Fe_2O_3@ZrO_2.

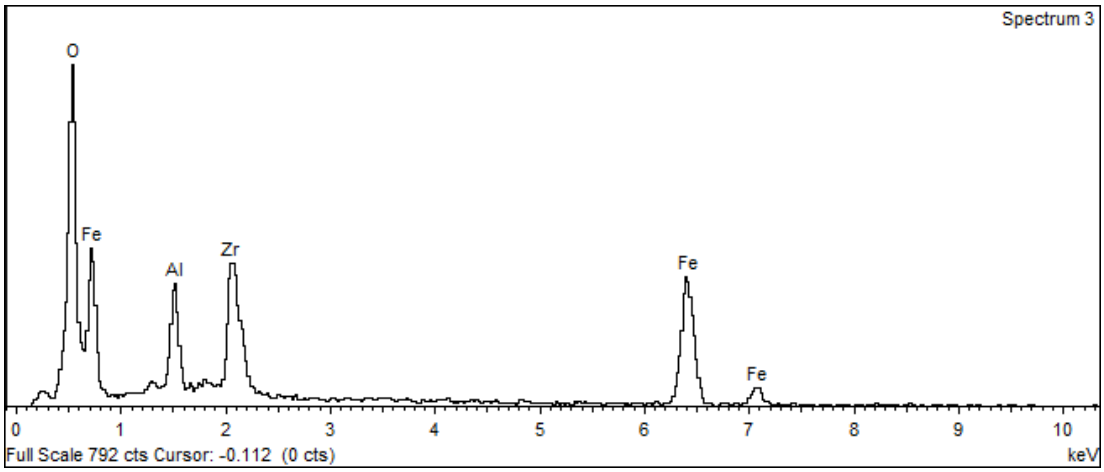

Figure 5-2. EDS spectrum of γ-Fe_2O_3@ZrO_2.

XRD

Figure 5-3 shows the XRD pattern of γ-Fe_2O_3@ZrO_2. The major crystalline phase detected was maghemite, i.e. the core material appears to be mostly crystalline γ-Fe_2O_3. Hematite and baddeleyite (ZrO_2) were also identified, but the peaks corresponding to these phases were fairly small. Given that peak area is correlated with concentration, the small peak area assigned to baddeleyite indicates that the concentration of crystalline ZrO_2 is small relative to the maghemite. In addition, the diffraction pattern displays a broad hump between 25 and 45 °2θ. This feature most likely corresponds to poorly ordered or amorphous material.

As a consequence, the surface coating of zirconium species can be further identified as ZrO_2, confirming the synthesis mechanism mentioned above. Moreover, the ZrO_2 on the surface of the maghemite cores was mainly amorphous, which is similar to the TiO_2 on the surface of the Fe_3O_4@SiO_2@TiO_2 microsized adsorbent in our previous study. It should be noted that the qualitative XRD pattern can only indicate that the crystalline ZrO_2 is less than the amorphous phases, but there is no way to estimate their exact fractions under current investigations.

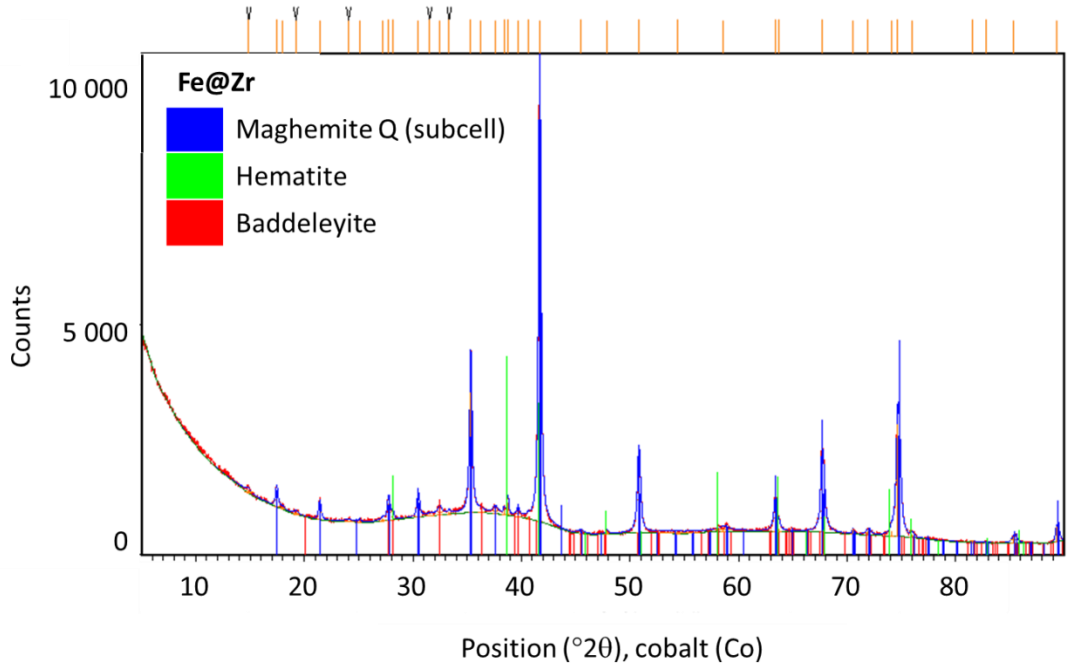

Figure 5-3. XRD pattern of γ-Fe_2O_3@ZrO_2.

Additionally, a set of adsorption tests was carried out with roasted γ-Fe_2O_3@ZrO_2 microparticles in both As(III)-only (100 mg/L) and As(V)-only (100 mg/L) solutions at pH 9. For roasting, a Muffle furnace was preheated to 400 °C in air before the samples were introduced. Then the temperature was held at 400 °C for 1 h, followed by cooling down naturally. The preliminary adsorption results with roasted and unroasted γ-Fe_2O_3@ZrO_2 microparticles are compared in Table 5-1.

Table 5-1. Preliminary adsorption results with roasted and unroasted γ-Fe_2O_3@ZrO_2 microparticles for As(III) and As(V)

	As (III) adsorbed (mg/g)		As (V) adsorbed (mg/g)	
	Unroasted γ-Fe_2O_3@ZrO_2	Roasted γ-Fe_2O_3@ZrO_2	Unroasted γ-Fe_2O_3@ZrO_2	Roasted γ-Fe_2O_3@ZrO_2
Test	69	47.2	20.6	12.8
Repeat	66.2	46	20.1	13.5

Clearly, after roasting, the γ-Fe_2O_3@ZrO_2 had poorer adsorption performance for both As(III) and As(V). According to previous work on TiO_2 adsorbents (Ng et al., 2014) and our investigations (see CHAPTER 4), roasting may increase the crystallinity of the particles thus reducing the amorphous phases. Therefore, it is

inferred that the nature of the amorphous state of zirconia could benefit the arsenic adsorption. As a consequence, further experiments were all carried out using unroasted γ-Fe_2O_3@ZrO_2.

SQUID

The magnetization curves shown in Figure 5-4(a) confirm both γ-Fe_2O_3 and γ-Fe_2O_3@ZrO_2 were typically ferromagnetic, and furthermore the saturation magnetization of the magnetic material reduced from approximately 70 emu/g to 40 emu/g after the surface coating of zirconium species onto the naked maghemite. Despite losing some of the magnetism, γ-Fe_2O_3@ZrO_2 still could be separated quickly and thoroughly with a handy magnet, as can be seen in Figure 5-4(b).

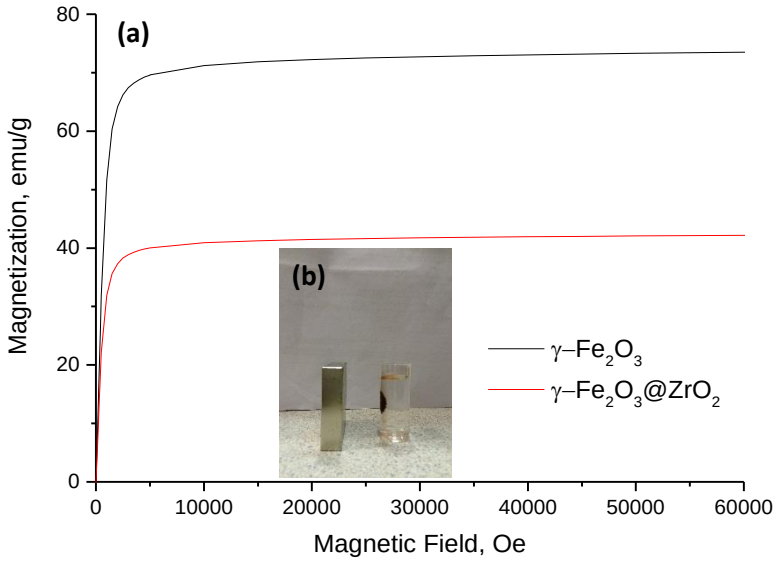

Figure 5-4. Magnetic properties: (a) magnetization curves of γ-Fe_2O_3 and γ-Fe_2O_3@ZrO_2; (b) magnetic separation of γ-Fe_2O_3@ZrO_2.

BET

The specific surface area of γ-Fe_2O_3 determined by BET was 33.29 m^2/g and this increased to 140.03 m^2/g after coating with ZrO_2. However, the pore volume and pore size did not change very much, as shown in Table 5-2. The surface area of the

synthesized γ-Fe_2O_3@ZrO_2 particles was sufficiently large to provide abundant active sites for arsenic adsorption, as was verified by the adsorption tests described in the following section.

Table 5-2. Characterisation of the γ-Fe_2O_3 and γ-Fe_2O_3@ZrO_2 particles determined by BET.

Particles	BET surface area, m^2/g	Pore volume, cm^3/g	Pore size, nm
γ-Fe_2O_3	33.29	0.12	14.07
γ-Fe_2O_3@ZrO_2	140.03	0.37	10.63

5.2.2. Adsorption tests

Effect of pH

In order to evaluate the effect of pH on arsenic adsorption, batch adsorption tests were conducted over a period of 24 h, at initial pH values ranging from 7 to 11. The experimental results shown in Figure 5-5 shows the adsorption of As(V) decreasing monotonically from more than 30 mg/g to approximately 11 mg/g over this pH range. By contrast, the adsorption of As(III) remains constant over a pH range of 7 to 9, before starting a rapid decrease with an increase in pH between 9 and 11. Moreover, it is evident that considerably more As(III) is adsorbed by γ-Fe_2O_3@ZrO_2 than As(V) over the entire pH range studied.

The different adsorption behaviours of As(III) and As(V) can be explained by the influence of pH on the surface charges of the adsorbents and adsorbates. To begin with, the point of zero charge of γ-Fe_2O_3@ZrO_2 was determined to be at a pH value of approximately 5, indicating that the surface of the adsorbent was negatively charged over the entire pH range studied. According to the arsenic speciation diagram (Lehmann et al., 2013), H_3AsO_3 (pH<9.2) and $H_2AsO_3^-$ (9.2<pH<12.1) were the dominant As(III) species and the main form of As(V) was $HAsO_4^{2-}$ (6.9<pH<11.5) in the pH range of 7 to 11.

Therefore, it is likely that there was hardly any electrostatic attraction present in the studied adsorption system. The electrostatic repulsion between $HAsO_4^{2-}$ and negatively charged γ-Fe_2O_3@ZrO_2 is always stronger than that between H_3AsO_3/$H_2AsO_3^-$ and negatively charged γ-Fe_2O_3@ZrO_2, which accounts for the marked difference in the adsorption capacities for As(III) and As(V). Moreover, since negatively charged arsenic species increase with increasing pH for As(V), the electrostatic repulsion increases, leading to the decrease in arsenic adsorption. In comparison, in the pH range of 7 to 9.2, the dominant As(III) species H_3AsO_3 barely interacts electrostatically with γ-Fe_2O_3@ZrO_2, thus pH values have little effect on the arsenic adsorption. However, in the pH range from 9.2 to 11, the decrease in adsorption of As(III) can be attributed to the increasing electrostatic repulsion between the dominant As(III) species $H_2AsO_3^-$ and negatively charged γ-Fe_2O_3@ZrO_2.

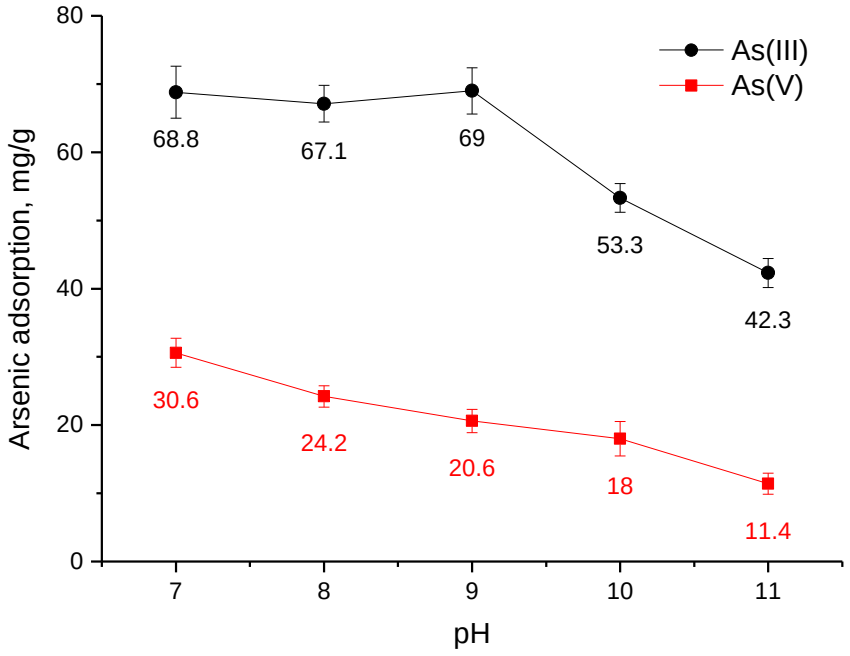

Figure 5-5. Effect of pH on arsenic adsorption in independent As (III) and As (V) solutions (As (III) or As (V): 100 mg/L; contact time: 24 h). Bars indicate standard deviations.

Adsorption kinetics

Figure 5-6 shows that arsenic adsorption takes place rapidly and over 90% of arsenic species are removed in the first hour. In addition, for all practical purposes, adsorption equilibrium can be achieved within 4 h for both As(III) and As(V).

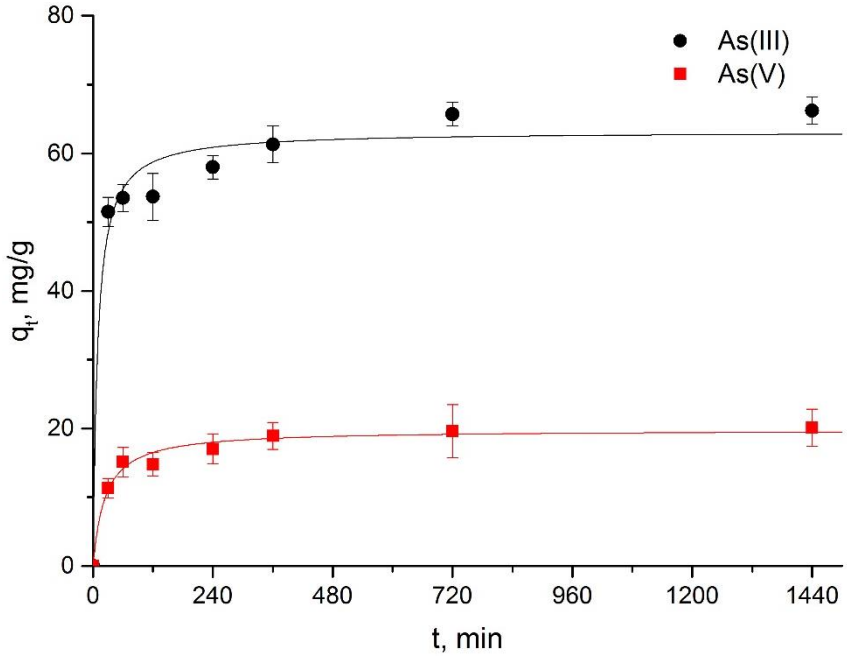

Figure 5-6. Adsorption kinetics data fitted by the pseudo-second-order equation (Test solution: independent As (III) and As (V) solutions with initial concentration of 100 mg/L in each; pH: 9). Bars indicate standard deviations.

To further investigate the adsorption kinetics, a pseudo-second-order kinetic model was used to represent the arsenic adsorption onto γ-Fe_2O_3@ZrO_2. This model can be expressed as:

$$\frac{t}{q_t} = \frac{1}{k_2 q_e^2} + \frac{t}{q_e} \quad (1)$$

where q_t (mg/g) is the adsorption capacity at time t (min), q_e (mg/g) is the equilibrium adsorption capacity, and k_2 (g/mg·min) is the rate constant. The applicability of the pseudo-second-order kinetic model is quantified by the squared correlation coefficient (R^2). The pseudo-second-order kinetic model is based on the assumption that the rate-limiting step might be chemisorption involving sharing or exchange of electrons between adsorbent and adsorbate (Azizian, 2004).

The kinetic parameters obtained are summarised in Table 5-3. It can be seen that the kinetic data for arsenic adsorption onto γ-Fe_2O_3@ZrO_2 could be satisfactorily fitted by the pseudo-second-order model, with q_e=63.2 mg/g, k_2=0.00175 g/mg·min and R^2=0.976 for As(III) and q_e=19.8 mg/g, k_2=0.00212 $g.mg^{-1}\cdot min^{-1}$ and R^2=0.979 for As(V). This indicates the adsorption of As(III)/As(V) to γ-Fe_2O_3@ZrO_2 involves chemisorption. Similar observations have been reported by Cui et al. (2012) on the study of amorphous ZrO_2 nanoparticles, Gupta et al. (2008) on iron(III)-zirconium(IV) binary mixed oxide nanoparticles and Pena et al. (2006) on nanocrystalline TiO_2. In fact, as mentioned in the Introduction, the adsorption mechanism has been established by Cui et al. (2012), who found that both As(III) and As(V) can form negatively charged inner-sphere complexes with the involvement of hydroxyl groups on the surface of ZrO_2 during adsorption.

Table 5-3. Kinetic parameters for arsenic adsorption onto γ-Fe_2O_3@ZrO_2.

Arsenic species	q_e, mg/g	k_2, g/mg·min	R^2
As(III)	63.2	0.00175	0.976
As(V)	19.8	0.00212	0.979

Adsorption isotherms

As the focus of this paper is to apply the adsorbents to treat the arsenic-containing gold cyanidation process waters, of which the pH is 9, the experimental study on arsenic adsorption isotherms was performed at room temperature and pH 9. Both Langmuir and Freundlich models were used to describe the relationships between the amounts of As(III)/As(V) adsorbed onto γ-Fe_2O_3@ZrO_2 and their equilibrium concentrations, which are represented, respectively, by

$$Q_e = Q_m\left(\frac{K_L C_e}{1 + K_L C_e}\right) \tag{2}$$

$$Q_e = K_F C_e^{\frac{1}{n}} \tag{3}$$

where C_e (mg/L) is the equilibrium arsenic concentration, and Q_e (mg/g) represents the arsenic concentration on the surface of the adsorbent. The Langmuir parameter Q_m (mg/g) estimates the maximum adsorption capacity at equilibrium, K_L (L/mg) is the Langmuir constant proportional to the energy of adsorption, and n and K_F (mg^{1-}

$^{1/n}L^{1/n}g^{-1}$) are parameters of the Freundlich model. The values of these parameters are summarised in Table 5-4.

Table 5-4. Isotherms parameters for arsenic adsorption onto γ-Fe_2O_3@ZrO_2.

	Langmuir isotherm			Freundlich isotherm		
	Q_m, mg/g	K_L, L/mg	R^2	n	K_F, $mg^{1-1/n}L^{1/n}g^{-1}$	R^2
As(III)	62.2	0.259	0.977	3.38	19.7	0.987
As(V)	18.3	2.11	0.891	7.16	10.8	0.954

As shown in Figure 5-7, the adsorption data could be fitted satisfactorily with both Langmuir and Freundlich isotherms. As to the big difference between the Langmuir constants K_L for As(III) and As(V) shown in Table 5-3, it might suggest that As(V) is more strongly adsorbed onto the γ-Fe_2O_3@ZrO_2 adsorbents than As(III). Nevertheless, the fitting correlation coefficient of Langmuir model for As(V) was only 0.891. Therefore, the K_L value may not be accurately estimated.

Nevertheless, since the maximum adsorption capacity Q_m in the Langmuir model facilitates the direct comparison of the adsorption capacity among various arsenic adsorbents, it was decided to use this parameter to compare with other arsenic adsorbents reported in the literature under similar conditions. Some examples are shown in Table 5-5. As can be seen, this synthesised adsorbent γ-Fe_2O_3@ZrO_2 has a higher or at least comparable capacity to other arsenic adsorbents in alkaline conditions.

Table 5-5. Maximum adsorption capacities (Q_m) reported in the literature for arsenic removal.

Adsorbate	Adsorbent	pH	Q_m (mg/g)	Reference
As (III)	Biochar (derived from rice husk)	8	26.9	(Samsuri, Sadegh-Zadeh, & Seh-Bardan, 2013)
As (V)			22.6	
As (III)	Iron(III)-loaded chelating resin	9	62.9	(Matsunaga, Yokoyama, Eldridge, & Bolto, 1996)
As (V)	MnO_2-loaded resin	7-8.5	22	(Lenoble et al., 2004)

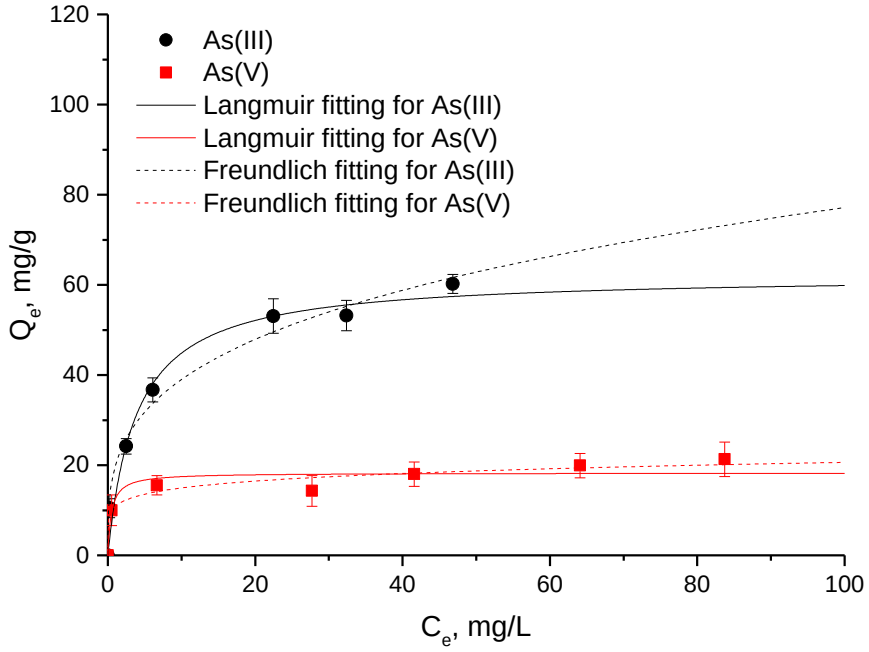

Figure 5-7. Adsorption isotherms data fitted by Langmuir and Freundlich isotherms (Test solution: Independent As (III) and As (V) solutions with initial concentration of 100 mg/L in each; pH: 9; contact time: 24 h). Bars indicate standard deviations.

Competitive adsorption

In order to investigate the potential influence of coexisting ions present in gold cyanidation solutions on arsenic adsorption by γ-Fe_2O_3@ZrO_2, a simulated solution was prepared with composition as shown in Table 5-6. This composition was based

on analysis of a sample of process water from a gold mine in Western Australia. This solution was spiked with arsenite and arsenate in a 1:1 molar ratio of As(III) to As(V). In the final synthetic solution, the total arsenic was determined to be approximately 90 ppm, while the pH was approximately 9, i.e. similar to that of the original process water sample.

Table 5-6. The chemical composition of a process water sample from a gold mine in Western Australia.

Analyte	Mg^{2+}	Ca^{2+}	K^{+}	Na^{+}	Cl^{-}	SO_4^{2-}	NO_3^{-}	SCN^{-}	$Fe(CN)_6^{4-}$
Concentration (mg/L)	45	1700	250	11000	18000	2600	70	140	36

The competitive adsorption tests were conducted the abovementioned solution under the same experimental conditions as those used for all the other adsorption tests. A simultaneous adsorption of 42.3 mg/g for As(III) and As(V) was achieved, hence it can be concluded that the competing effects of the components in process water from gold cyanide leaching on arsenic adsorption onto γ-Fe_2O_3@ZrO_2 were negligible. This suggests that these magnetic microparticles could form the basis for promising industrial applications.

5.2.3. Regeneration and reuse

As far as the industrial practicability of γ-Fe_2O_3@ZrO_2 is concerned, the study on the reusability becomes necessary, which is highly beneficial for cost reduction. Inspired by the effect of pH on arsenic adsorption, as shown in Figure 5-5, it could be inferred that a strong alkaline solution would possibly facilitate the arsenic desorption. On this basis, a regenerant of 1.0 mol/L NaOH solution (pH≈13) was used to elute arsenic from the spent γ-Fe_2O_3@ZrO_2 after adsorption tests in the simulated process waters of gold cyanidation. Five consecutive adsorption-desorption cycles were carried out and acceptable results were obtained, as shown in Figure 5-8.

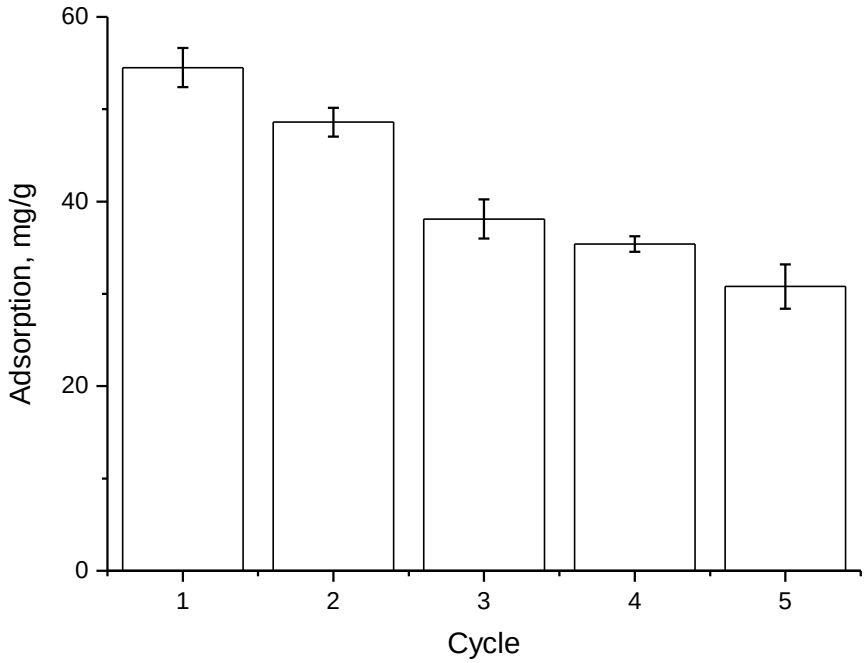

Figure 5-8. Regeneration and reuse of γ-Fe_2O_3@ZrO_2 (As concentration: 90 mg/L; pH≈9; contact time: 24 h). Bars indicate standard deviations.

It is clear that γ-Fe_2O_3@ZrO_2 still retained approximately 80% of its original adsorption capacity after 5 cycles of adsorption and desorption, indicating that part of the adsorbed arsenic on the surface can be desorbed with the help of a highly alkaline aqueous solution hence this adsorbent can be used repeatedly without significant performance loss.

5.3. Summary

- The magnetic ZrO_2-based microsized adsorbent could be synthesised successfully by use of a two-step process, i.e. via hydrolysis of $ZrOCl_2 \cdot 8H_2O$ in a suspension of magnetite nanoparticles, followed by drying of the coated particles. This yielded near-spherical, partly aggregated zirconia coated maghemite particles with diameters ranging from 20 to 200 nm.
- The ferromagnetic microparticles exhibited maximum magnetization in excess of 40 emu/g, readily allowing magnetic separation. In addition, the BET surface area of the adsorbent was approximately 128.4 m^2/g.
- Experimental results showed that the $Fe_3O_4@ZrO_2$ adsorbent had a Langmuir adsorption capacity for As(III) and As(V) at pH 9 of approximately 62.2 mg/g and 18.3 mg/g, respectively.
- Finally, the reusability of $Fe_3O_4@ZrO_2$ adsorbent was confirmed by five consecutive adsorption-regeneration cycles at a pH of approximately 13. This makes it a potentially useful adsorbent of arsenic in the alkaline process waters of gold cyanidation.

CHAPTER 6 CERIUM-BASED MAGNETIC ADSORBENT

6.1. Introduction

Adsorption is one of the most commonly used methods for removing arsenic species from aqueous solutions, but the vast majority of related studies only aimed at drinking water under near neutral pH other than the alkaline conditions applied in gold cyanidation. It was reported that cerium oxide is an efficient arsenic adsorbent over a wide pH range from 3 to 11 (Li et al., 2012), showing an outstanding adsorption performance particularly towards As(III) under alkaline conditions. As for the adsorption mechanism, both As(III) and As(V) can be adsorbed onto the surface of cerium oxide by the formation of negatively charged inner-sphere complexes with the surface hydroxyl groups.

To facilitate the separability, in this chapter, cerium oxide was innovatively coated on the surface of magnetic magnetite nanoparticles via a simple chemical precipitation method. The synthesised cerium-based magnetic microparticles (Fe_3O_4@CeO_2/$(OH)_x$) were used for studying on removing arsenic species from both arsenic-only solutions and simulated process waters of gold cyanidation. Moreover, the desorption tests were also conducted to evaluate the reusability of Fe_3O_4@CeO_2/$(OH)_x$.

6.2. Results and discussion

6.2.1. Characterisation of $Fe_3O_4@CeO_2/(OH)_x$

SEM-EDS

Figure 6-1 shows the SEM image of $Fe_3O_4@CeO_2/(OH)_x$, which demonstrates that these synthesised particles have an average particle size of approximately 300 nm in diameter. They have a cubic inverse spinel structure determined by the morphology of the core material, i.e. magnetite. It can be seen clearly that these particles were still aggregated to some extent despite some efforts made to disperse them during the preparation process, such as ultrasonication and strong agitation.

The EDS spectrum of the area in Figure 6-1 is shown in Figure 6-2. As expected, elements Fe, Ce and O were observed, indicating that the cerium species were coated onto the magnetite nanoparticles successfully. Additionally, element Al was also found in the spectrum, owing to the aluminium substrate used for analysis.

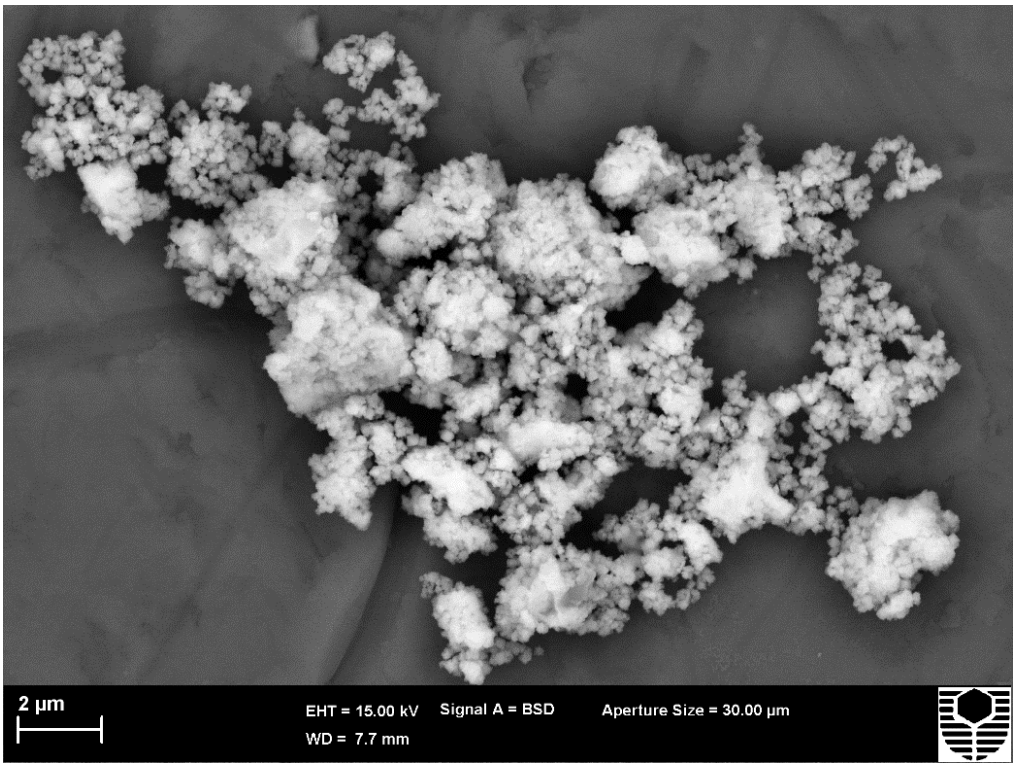

Figure 6-1. SEM image of $Fe_3O_4@CeO_2/(OH)_x$.

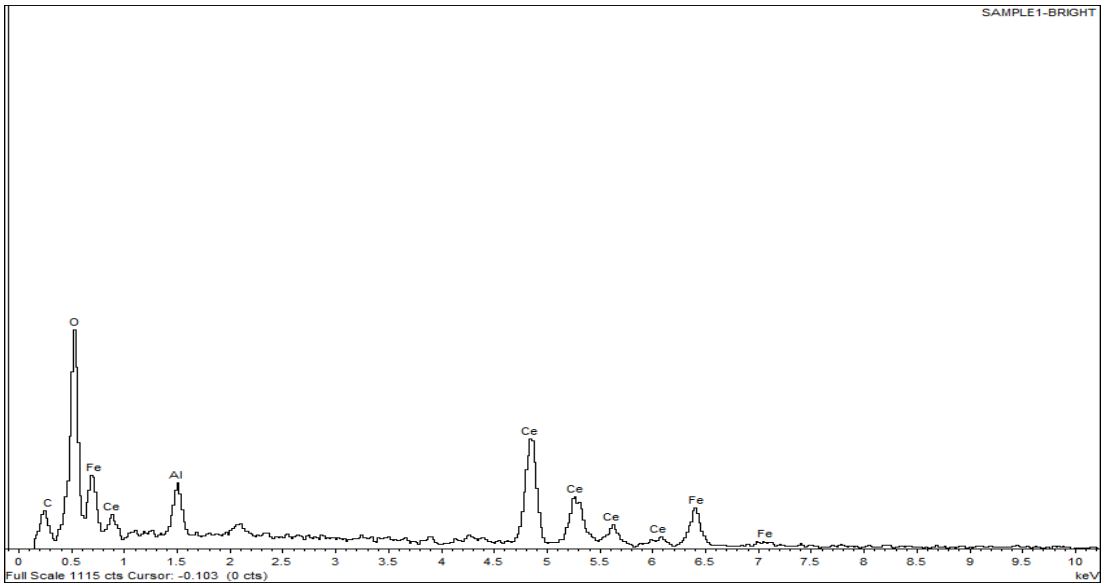

Figure 6-2. EDS spectrum of Fe_3O_4@CeO_2/$(OH)_x$.

XRD

Figure 6-3 shows the XRD pattern of Fe_3O_4@CeO_2/$(OH)_x$. Evidently, well-ordered crystalline magnetite was identified. By contrast, very broad peaks corresponding to cerium oxide were identified. The width of these peaks indicate that the cerium oxide was poorly ordered. The peaks width is consistent with grain sizes well below 100 nm. No crystalline cerium hydroxide was detected, but amorphous cerium hydroxide cannot be ruled out by this analysis. In addition, peaks corresponding to a metallic iron nickel alloy are a contribution from the sample holder due to the small quantity of sample available for analysis.

Theoretically, cerium hydroxide should be firstly formed on the surface of magnetite nanoparticles based on the aforementioned synthetic method. After the drying process at relatively low temperature (60 °C), the cerium hydroxide could be transformed to CeO_2 partially. However, only poorly ordered cerium oxide was identified in the present work. Therefore, it can be reasonably inferred that the cerium species might be a mixture of cerium oxides and amorphous cerium hydroxides, which is represented as CeO_2/$(OH)_x$ in this study. A further calcination process could turn cerium hydroxide to cerium oxide (Ketzial and Nesaraj, 2011), making the form of the final product more clear. However, similar to the previous work with the synthesised magnetic adsorbents Fe_3O_4@SiO_2@TiO_2 and γ-

Fe_2O_3@ZrO_2, a set of preliminary adsorption tests (Table 6-1) showed that the arsenic adsorption performance of Fe_3O_4@CeO_2/$(OH)_x$ after calcination was greatly compromised.

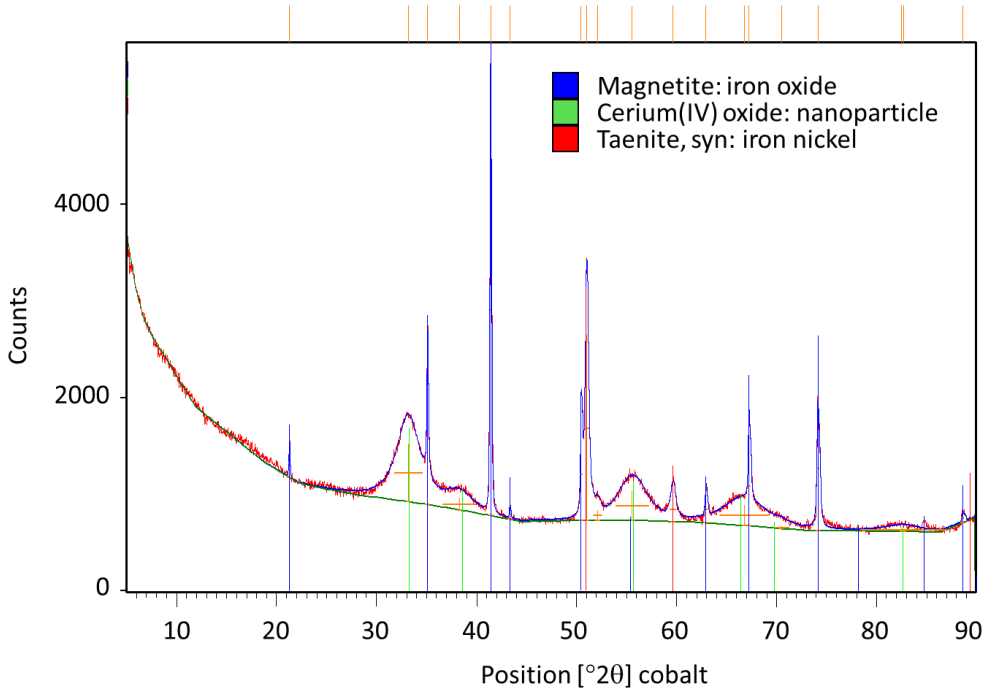

Figure 6-3. XRD pattern of Fe_3O_4@CeO_2/$(OH)_x$.

Table 6-1. Preliminary adsorption results with roasted and unroasted Fe_3O_4@CeO_2/$(OH)_x$ particles for As(III) and As(V) (Experimental conditions: 0.05 g adsorbent; As concentration=100 pm; T=25 °C; pH=9.5; 24 h).

	As (III) adsorbed (mg/g)		As (V) adsorbed (mg/g)	
	Unroasted Fe_3O_4@CeO_2/$(OH)_x$	Roasted Fe_3O_4@CeO_2	Unroasted Fe_3O_4@CeO_2/$(OH)_x$	Roasted Fe_3O_4@CeO_2
Test	78.3	27.0	30.5	11.2
Repeat	81.2	30.1	28.5	10.4

SQUID

Figure 6-4 shows the magnetization curves of the naked magnetite nanoparticles and the cerium coated magnetite microparticles. It is apparent that both Fe_3O_4 and Fe_3O_4@CeO_2/$(OH)_x$ present typical ferromagnetism. The saturation magnetization of

Fe_3O_4 was found to be around 90 emu/g. After the surface coating of cerium species, the maximum magnetization of the material decreased to approximately 40 emu/g. Although a nearly 50% loss of magnetism was caused, the cerium coated magnetite microparticles still could be separated easily from an aqueous solution after adsorption with the help of a handy magnet, as evidenced by Figure 6-5.

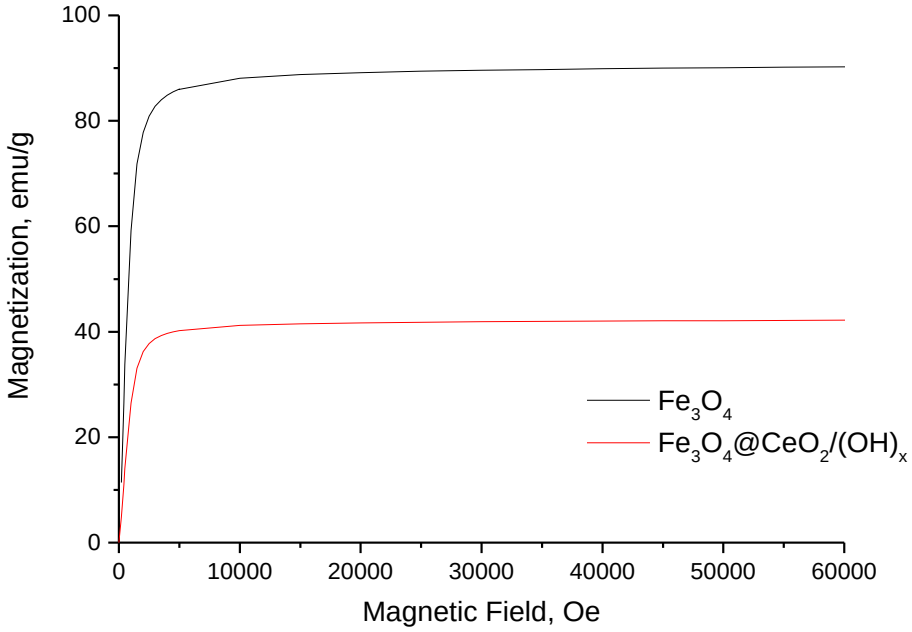

Figure 6-4. Magnetization curves of Fe_3O_4 and $Fe_3O_4@CeO_2/(OH)_x$.

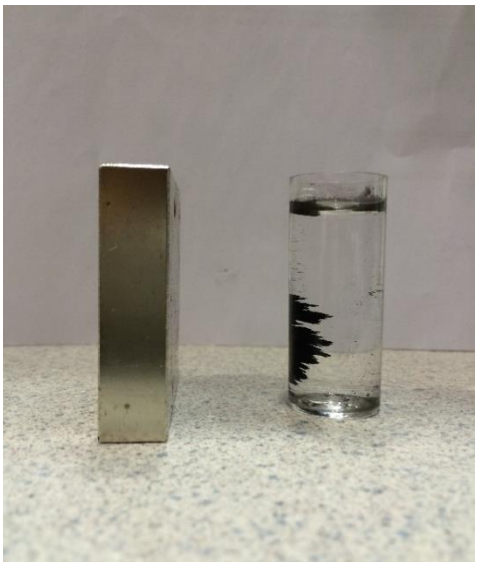

Figure 6-5. Magnetic separation of $Fe_3O_4@CeO_2/(OH)_x$.

BET

The specific surface area of $Fe_3O_4@CeO_2/(OH)_x$ analysed by the BET method was determined to be 91.38 ± 1.47 m^2/g. This is a result of the combined effects of the particle size range of the core material of magnetite (50–100 nm), the amount of the cerium species coated (1:1 mass ratio of shell to core), the aggregation shown in Figure 6-1, etc. The following adsorption tests suggested that such specific surface area was able to provide sufficient active sites for arsenic adsorption.

6.2.2. Adsorption tests

Effect of pH

Batch adsorption tests on the effect of pH were carried out within the pH range of 7 - 11 for 24 h, and the initial concentrations for both As(III) and As(V) were 100 mg/L. Great adsorption results were obtained, as shown in Figure 6-6. Apparently, As(III) was much more attractive to the synthesised cerium-based microparticles than As(V) over the entire pH range studied. Specifically, $Fe_3O_4@CeO_2/(OH)_x$ showed great stability in the adsorption of As(III) when pH values were between 7 and 10, reaching approximately 75 mg/g in average. Nevertheless, a further increase of pH to 11 reduced the adsorption of As(III) to 66.6 mg/g. In comparison, the adsorption of As(V) decreased continuously and slowly, from 36.9 mg/g at neutral pH to 24.1 mg/g at pH 11. The significant differences between the adsorption performances of As(III) and As(V) can be attributed to the effect of pH on the surface charges of the arsenic species and the cerium-based microparticles, leading to different electrostatic interactions.

On the one hand, according to the zeta potential analysis, the point of zero charge of $Fe_3O_4@CeO_2/(OH)_x$ was roughly determined at a pH value between 6 and 7, that is to say, the surfaces of these microparticles were negatively charged under the studied pH range of 7 - 11. On the other hand, H_3AsO_3 is the dominant As(III) species when pH is less than 9.2 while $H_2AsO_3^-$ becomes dominant when pH is between 9.2 and 12.1, and the main form of As(V) species is $HAsO_4^{2-}$ in the pH range of 6.9 - 11.5

(Mohan and Pittman Jr, 2007). Therefore, it is most likely that electrostatic repulsion was the only possible electrostatic interaction between the adsorbents and the adsorbates in this study.

Obviously, the electrostatic repulsion between $H_3AsO_3/H_2AsO_3^-$ and negatively charged $Fe_3O_4@CeO_2/(OH)_x$ was always weaker than that between $HAsO_4^{2-}$ and negatively charged $Fe_3O_4@CeO_2/(OH)_x$, which reasonably explains why the adsorption of As(III) outperformed that of As(V) in the pH range of 7 - 11. Furthermore, when pH was between 7 and 9.2, there was hardly any electrostatic interaction between the dominant As(III) species H_3AsO_3 and $Fe_3O_4@CeO_2/(OH)_x$, so the adsorption of As(III) remained nearly unchanged. However, with a further increase in pH, the increasing electrostatic repulsion between the dominant As(III) species $H_2AsO_3^-$ and negatively charged $Fe_3O_4@CeO_2/(OH)_x$ decreased the adsorption of As(III). By contrast, since negatively charged As(V) species increased with increasing pH, the electrostatic repulsion increased, leading to the decrease in adsorption of As(V).

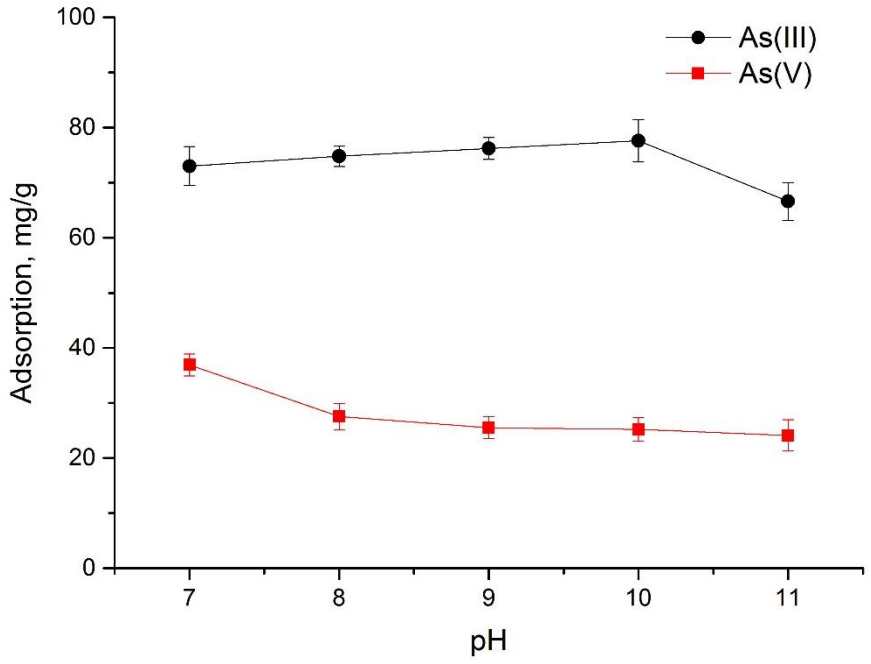

Figure 6-6. Effect of pH on arsenic adsorption (As concentration: 100 mg/L; contact time: 24 h). Bars indicate standard deviations.

Adsorption kinetics

Figure 6-7 shows the kinetics data for arsenic adsorption onto the cerium-based magnetic microparticles. As can be seen, the adsorption processes took place rapidly for both As(III) and As(V), with more than 80% of arsenic species being removed within the first 120 min. Basically, the adsorption equilibrium could be achieved in approximately 240 min, showing high efficiency in practical applications.

The pseudo-second-order kinetic model was fitted to the experimental data of arsenic adsorption onto $Fe_3O_4@CeO_2/(OH)_x$ in order to better understand the adsorption kinetics. The expression of this model can be presented as:

$$\frac{t}{q_t} = \frac{1}{k_2 q_e^2} + \frac{t}{q_e} \quad (1)$$

where q_t (mg/g) is the adsorbed amount at time t (min), q_e (mg/g) is the maximum adsorption capacity, and k_2 (g/mg·min) is the rate constant. The applicability of the pseudo-second-order kinetic model is quantified by the squared correlation coefficient (R^2). The pseudo-second-order kinetic model is based on the assumption that the rate-limiting step tends to be chemisorption (Azizian, 2004).

Table 6-2 shows the kinetics parameters obtained from the fittings in Figure 6-7. The closeness of the R^2 values to 1 indicates that the pseudo-second-order kinetic model fitted the kinetics data accurately. The equilibrium adsorption capacities were estimated as 73.0 mg/g and 26.6 mg/g for As(III) and As(V), respectively. On this basis, it can be concluded that arsenic adsorption onto the cerium-based magnetic microparticles is driven by chemical reactions, which is in line with the arsenic adsorption mechanism onto cerium oxide proposed in the literature (Li et al., 2012).

Table 6-2. Kinetics parameters for arsenic adsorption onto $Fe_3O_4@CeO_2/(OH)_x$.

	q_e, mg/g	**k_2, g/mg·min**	**R^2**
As(III)	73.0	0.00095	0.990
As(V)	26.6	0.00075	0.954

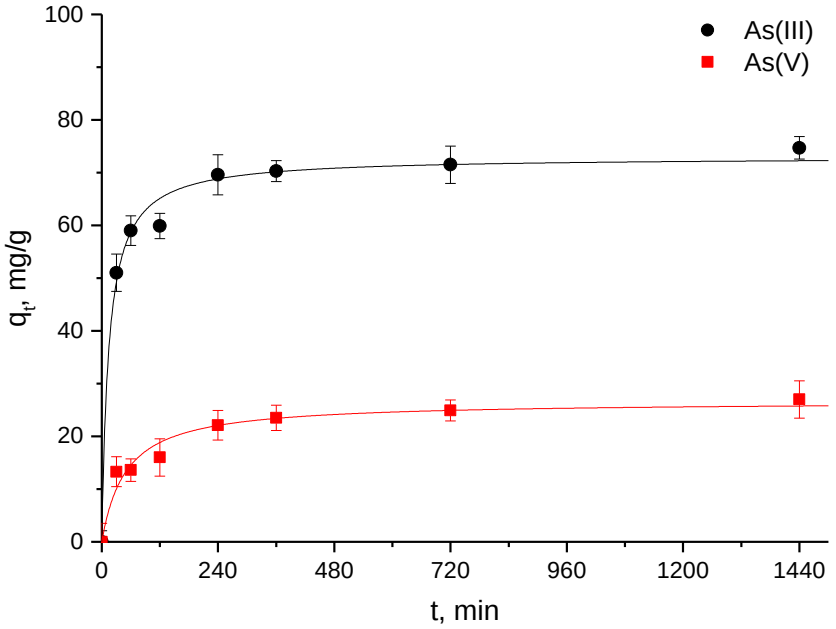

Figure 6-7. Adsorption kinetics data fitted by the pseudo-second-order equation (As concentration: 100 mg/L; pH: 9). Bars indicate standard deviations.

Adsorption isotherms

Batch adsorption tests on isotherms were conducted at 25 °C. Figure 6-8 shows the adsorption isotherms data and the fittings by both Langmuir and Freundlich models, which can be expressed by equations (2) and (3), respectively.

$$Q_e = Q_m \left(\frac{K_L C_e}{1 + K_L C_e} \right) \tag{2}$$

$$Q_e = K_F C_e^{\frac{1}{n}} \tag{3}$$

Where C_e (mg/L) represents the equilibrium arsenic concentration, and Q_e (mg/g) represents the adsorbed amount of arsenic. The maximum adsorption capacity at equilibrium is estimated by the Langmuir parameter Q_m (mg/g), K_L (L/mg) is the Langmuir constant, and n and K_F ($mg^{1-1/n}L^{1/n}g^{-1}$) are parameters of the Freundlich model.

Table 6-3 shows the obtained isotherms parameters in fitting the adsorption data. According to the results, the adsorption data of both As(III) and As(V) could be

better fitted with the Langmuir isotherm, achieving the maximum adsorption capacities of 79.1 mg/g for As(III) and 25.5 mg/g for As(V) at pH 9, which are higher or at least comparable to most reported results (Lata and Samadder, 2016; Ungureanu et al., 2015b).

Table 6-3. Isotherms parameters for arsenic adsorption onto $Fe_3O_4@CeO_2/(OH)_x$.

	Langmuir isotherm			Freundlich isotherm		
	Q_e, mg/g	K_L, L/mg	R^2	n	K_F, $mg^{1-1/n}L^{1/n}g^{-1}$	R^2
As(III)	79.1	0.929	0.982	4.76	36.8	0.894
As(V)	25.5	0.213	0.996	3.50	7.66	0.961

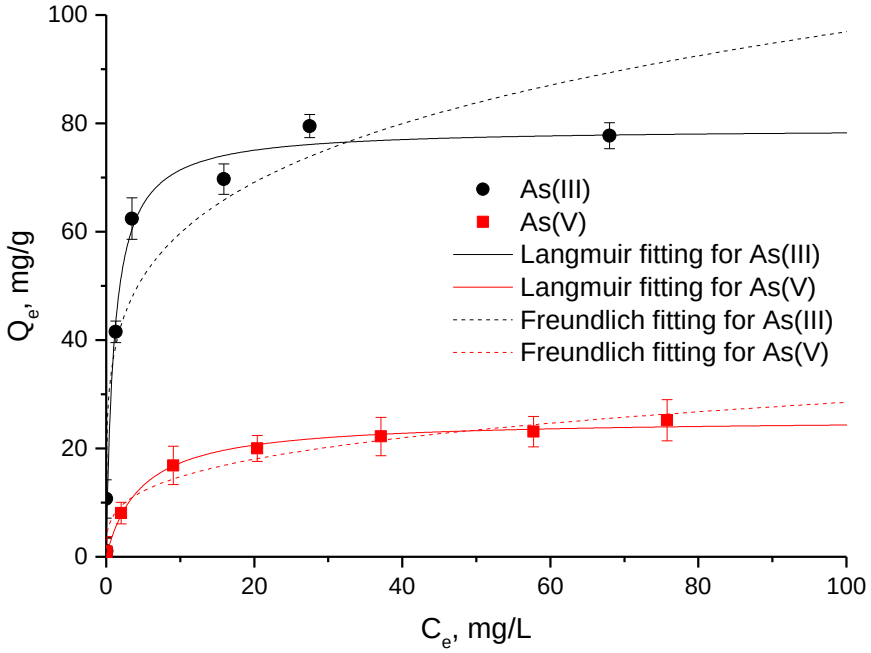

Figure 6-8. Adsorption isotherms data fitted by Langmuir and Freundlich isotherms (pH: 9; contact time: 24 h). Bars indicate standard deviations.

Competitive adsorption

There is no doubt that process waters from gold cyanide leaching are quite complicated, such as high ionic strength and complex chemistry, which could

potentially influence the arsenic adsorption by competitive effects. Consequently, it is necessary to investigate the effect of coexisting ions present in gold cyanidation waters on arsenic adsorption by the cerium-based magnetic microparticles. For this purpose, firstly a synthetic solution was prepared with the recipe given in Table 6-4. This recipe was based on the chemical composition analysis of a process water sample from a Western Australian gold mine. Afterwards, this solution was spiked with arsenite and arsenate in a 1:1 molar ratio of As(III) to As(V). The total arsenic concentration in the final solution was determined to be approximately 90 ppm by ICP-OES. The pH of the synthetic process water sample was found to be 9, which is very close to that of the original process water sample (pH=9).

The competitive adsorption tests were performed using the synthetic solution abovementioned under the identical experimental conditions used in all the other adsorption tests. A simultaneous adsorption of 51.2 mg/g for As(III) and As(V) was attained, demonstrating that the coexisting substances in process waters from gold cyanidation only had a minimal effect on arsenic adsorption by $Fe_3O_4@CeO_2/(OH)_x$. In other words, these synthesised microparticles can be considered as a promising arsenic scavenger in the potential industrial applications.

Table 6-4. The chemical composition of a process water sample from a gold mine in Western Australia.

Analyte	Mg^{2+}	Ca^{2+}	K^{+}	Na^{+}	Cl^{-}	SO_4^{2-}	NO_3^{-}	SCN^{-}	$Fe(CN)_6^{4-}$
Concentration (ppm)	45	1700	250	11000	18000	2600	70	140	36

6.2.3. Regeneration and reuse

In terms of the practicability of the cerium-based magnetic microparticles, exploring regeneration techniques naturally becomes as important as improving the adsorption performance. According to our previous studies, 1.0 mol/L NaOH solution (pH≈13) was used as a regenerant to treat the arsenic-loaded Ti-based and Zr-based microparticles, with good results obtained. Therefore, the same method was applied

in the current study. Five consecutive adsorption-desorption cycles were conducted and the results are shown in Figure 6-9.

As can be seen clearly, over 60% of the initial adsorption capacity of $Fe_3O_4@CeO_2/(OH)_x$ was retained after five cycles of adsorption and desorption, which indicates that a highly alkaline solution could liberate a certain amount of active adsorption sites for arsenic species to be reloaded again. In order to improve the regeneration performance, further investigations should be carried out, for instance, increasing the alkalinity of regenerant, extending the treatment time, seeking for new eluting agents, etc.

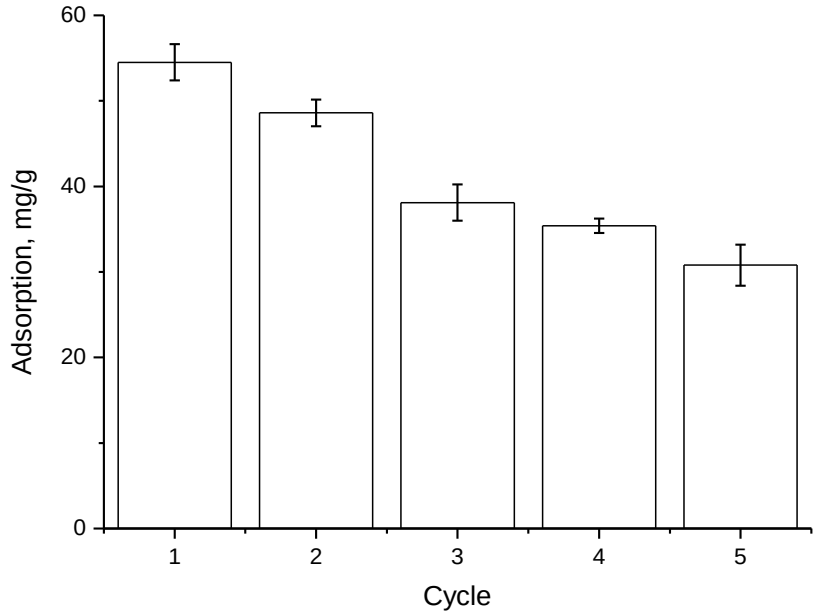

Figure 6-9. Regeneration and reuse of $Fe_3O_4@CeO_2/(OH)_x$. (As concentration: 90 mg/L; pH≈9; contact time: 24 h). Bars indicate standard deviations.

6.3. Summary

- The cerium-based magnetic microparticles were synthesised via a one-step chemical precipitation method at room temperature.
- SEM-EDS analysis showed that the particles had an average particle size of approximately 300 nm in diameter with partly aggregation, and confirmed the successful coating of cerium species. Crystalline magnetite and poorly ordered cerium oxide were identified by the XRD pattern, but amorphous cerium hydroxide could not be ruled out by this analysis. Magnetic analysis by SQUID magnetometer showed both Fe_3O_4 and $Fe_3O_4@CeO_2/(OH)_x$ were ferromagnetic and the latter, with the saturation magnetization of approximately 40 emu/g, could be easily separated by a handy magnet. The specific surface area of $Fe_3O_4@CeO_2/(OH)_x$ was determined to be 91.38 ± 1.47 m^2/g by the BET method.
- According to the results from systematic arsenic adsorption tests, $Fe_3O_4@CeO_2/(OH)_x$ presented rapid adsorption kinetics, great removal capacity and good applicability in the alkaline process waters of gold cyanidation, with the Langmuir adsorption capacities of 79.1 mg/g for As(III) and 25.5 mg/g for As(V) at pH 9.
- Five consecutive adsorption-desorption cycles confirmed the possibility and feasibility of $Fe_3O_4@CeO_2/(OH)_x$ for regeneration and reuse with 1.0 mol/L NaOH solution as a regenerant.

CHAPTER 7 CONCLUSIONS AND FUTURE WORK

The chief objective of this thesis was to propose suitable adsorbents to deal with the arsenic-contaminated process water associated with gold cyanidation circuits. This general objective was expected to be fulfilled by achieving the following sub-targets.

- Design and synthesise several types of functionalised magnetic particles for effectively adsorbing arsenic species from alkaline aqueous solutions.
- Determine their surface properties and structural characteristics by a series of analytical methods.
- Examine their adsorption capacities towards arsenic species in both arsenic-only solutions and simulated process waters from gold cyanidation.
- Understand their adsorption mechanisms.
- Explore the possibilities and feasibilities of regenerating and reusing the synthesised adsorbents.

This chapter are presented in terms of how each of the sub-targets was achieved with some future work recommendations listed in the end.

7.1. Design and synthesis of arsenic adsorbents

Based on the comprehensive literature review on various types of arsenic adsorbents and combining the intrinsic requirement, i.e. alkaline condition, of the gold cyanidation process water, titanium, zirconium and cerium based sorbents were selected as three candidates. In order to facilitate the separation of the solid sorbents from the treated solution, magnetite and maghemite nanoparticles were employed as magnetic core materials to support the functional particles. Eventually, three types of magnetic arsenic adsorbents namely $Fe_3O_4@SiO_2@TiO_2$, γ-$Fe_2O_3@ZrO_2$ and $Fe_3O_4@CeO_2/(OH)_x$, with various core-shell structures were designed.

Specifically, Fe_3O_4@SiO_2@TiO_2 particles were synthesised via conventional sol-gel technique. SiO_2 as the intermediate material was simply served as a linkage between Fe_3O_4 and TiO_2. The adsorbents γ-Fe_2O_3@ZrO_2 particles were obtained by directly coating ZrO_2 onto the surface of γ-Fe_2O_3 nanoparticles through the hydrolysis of $ZrOCl_2 \cdot 8H_2O$. Finally, the Fe_3O_4@CeO_2/$(OH)_x$ adsorbents were synthesised by a simple chemical precipitation method with $Ce(NO_3)_3 \cdot 6H_2O$ and NaOH.

All the preparation processes were straightforward and simple.

7.2. Characterisation of the synthesised arsenic adsorbents

All the synthetic adsorbents were characterised by a series of analytical methods, including SEM-EDS, XRD, SQUID and BET.

The SEM results indicated that the synthesised particles were all in micron-scale with some aggregations. The EDS results confirmed the presence of elements Ti, Zr and Ce in the respective adsorbents.

To confirm the phase compositions of the functionalised magnetic particles, XRD analysis was performed both qualitatively and quantitatively. Inferred by the obtained patterns, Fe_3O_4@SiO_2@TiO_2 mainly consisted of crystalline magnetite and amorphous TiO_2. Similarly, ZrO_2 was mainly amorphous on the surface of crystalline maghemite. As to Fe_3O_4@CeO_2/$(OH)_x$ particles, poorly ordered CeO_2 was identified by the XRD pattern, however, amorphous cerium hydroxides could not be ruled out. The XRD results were also the base for the abbreviated notations of the candidate arsenic adsorbents.

BET analysis was carried out to determine the specific area of the synthesised particles. The results suggested that the specific area of Fe_3O_4@SiO_2@TiO_2, γ-Fe_2O_3@ZrO_2 and Fe_3O_4@CeO_2/$(OH)_x$ was 86.65 m^2/g, 140.03 m^2/g and 91.38 m^2/g, respectively.

The magnetism of the arsenic adsorbents was determined by SQUID. The maximum magnetization of approximately 40 emu/g was retained for all three types of particles, which was enough for easy separation of the arsenic-loaded adsorbents from an aqueous solution by a hand-held magnet.

7.3. Adsorption capacities and mechanisms of the synthesised arsenic adsorbents

Systematic adsorption tests were conducted to determine the adsorption behaviours towards both As(III) and As(V) under alkaline conditions, including the effect of pH on adsorption, adsorption kinetics, adsorption isotherms and competitive adsorption in simulated gold cyanidation process water. The key outcomes of the adsorption tests for $Fe_3O_4@SiO_2@TiO_2$, γ-$Fe_2O_3@ZrO_2$ and $Fe_3O_4@CeO_2/(OH)_x$ are summarised and compared in Table 7-1. In addition, the adsorption tests with various pH values showed similar trends for all three adsorbents. More specifically, for As(III), when pH value was within the range of 7–9, the adsorption performances of the three types of particles were not sensitive to pH changes. However, if the pH of the solution further increased to 10 and 11, the uptake of As(III) onto the adsorbents would be reduced, particularly for the $Fe_3O_4@SiO_2@TiO_2$ particles. In comparison, the adsorptions of As(V) onto the synthesised particles decreased continuously with increasing pH values. Despite the similar trends, $Fe_3O_4@CeO_2/(OH)_x$ presented the highest adsorption of both As(III) and As(V) species under same pH conditions among the three magnetic particles.

Table 7-1. Summary and comparison of the key outcomes of adsorption tests for $Fe_3O_4@SiO_2@TiO_2$, γ-$Fe_2O_3@ZrO_2$ and $Fe_3O_4@CeO_2/(OH)_x$.

		$Fe_3O_4@SiO_2@TiO_2$	γ-$Fe_2O_3@ZrO_2$	$Fe_3O_4@CeO_2/(OH)_x$
Particle size		200–400 nm	20–200 nm	≈300 nm
Specific surface area		86.65 m^2/g	140.03 m^2/g	91.38 m^2/g
Adsorption equilibrium		≈4 h	≈4 h	≈4 h
*Maximum adsorption capacity at pH 9	As(III)-only solution	31.4 mg/g	62.2 mg/g	79.1 mg/g
	As(V)-only solution	10.2 mg/g	18.3 mg/g	25.5 mg/g
Adsorption capacity at pH 9	Simulated solution	15.6 mg/g	42.3 mg/g	51.2 mg/g

* Estimated from Langmuir isotherm model fitting.

Indeed, all three of the functionalised magnetic microparticles can be recognised as effective adsorbents for arsenic species with a certain degree of selectivity under alkaline conditions, showing great potential in practical gold industry. Nevertheless, it is true that the Ce-based adsorbent does seem to be more attractive to arsenic species than the Ti-based and Zr-based ones based on the current research. Even when their specific surface areas are taken into account, the Ce-based adsorbent is still firmly in the lead, as can be seen in Table 7-2. Therefore, it is safe to say that the Ce-based adsorbent possesses the strongest ability to extract arsenic species from alkaline arsenic-containing aqueous solutions in this study. Despite all this, in the present study, it is still impossible to determine if CeO_2 is in nature a better arsenic adsorbent than TiO_2 and ZrO_2 due to many uncertainties, such as concentrations of surface hydroxyl groups, pore structures, M-O bond strength (M=Ti, Zr and Ce), etc.

Table 7-2. The arsenic adsorption capacities per unit surface area of $Fe_3O_4@SiO_2@TiO_2$, γ-$Fe_2O_3@ZrO_2$ and $Fe_3O_4@CeO_2/(OH)_x$.

		$Fe_3O_4@SiO_2@TiO_2$	γ-$Fe_2O_3@ZrO_2$	$Fe_3O_4@CeO_2/(OH)_x$
Adsorption capacity at pH 9	As(III)-only solution	0.38 mg/m^2	0.44 mg/m^2	0.87 mg/m^2
	As(V)-only solution	0.12 mg/m^2	0.13 mg/m^2	0.28 mg/m^2
	Simulated solution	0.18 mg/m^2	0.30 mg/m^2	0.56 mg/m^2

7.4. Regeneration and reuse of the synthesised adsorbents

Desorption tests were carried out using 1 mol/L NaOH solution as the regenerant. After 4 to 5 cycles, all the adsorbents still retained more than 60% of their adsorption capacities, as shown in Table 7-3. This further indicates that all the synthesised magnetic particles are potentially suitable for treating the arsenic contaminated process waters in gold industry.

Table 7-3. Desorption capacities of $Fe_3O_4@SiO_2@TiO_2$, γ-$Fe_2O_3@ZrO_2$ and $Fe_3O_4@CeO_2/(OH)_x$.

	$Fe_3O_4@SiO_2@TiO_2$	γ-$Fe_2O_3@ZrO_2$	$Fe_3O_4@CeO_2/(OH)_x$
Desorption capacity	>60% adsorption capacity retained after 4 cycles	>75% adsorption capacity retained after 5 cycles	>60% adsorption capacity retained after 5 cycles

7.5. Future work

Three different types of functionalised magnetic microparticles were synthesised and used to remove arsenic from gold mining process water. Apart from comparable or even better adsorption capacities than other adsorbents under alkaline conditions, the easy fabrication, good separability and reusability of these adsorbents highlight their potential in real gold mining process. On the foundation of all the promising outcomes of the present thesis, some future work recommendations are listed as follows.

- Simplification and optimisation of synthetic processes for current functionalised magnetic adsorbents. Current synthetic methods were not as complicated as those in other studies in the literature but still could be improved in some respects, particularly the anti-aggregation activity.
- Deeper understanding of current functionalised magnetic adsorbents through further characterisation, such as Raman spectroscopy, X-ray photoelectron spectroscopy, transmission electron microscopy and so forth.
- Further investigation of adsorption kinetics and isotherms for current functionalised magnetic adsorbents. More adsorption data and a series of other common fitting models should be able to reveal more information about adsorption mechanisms.
- Improvement of adsorption capacities for current functionalised magnetic adsorbents, which could be made in two main ways, i.e. expansion of the specific surface area and enhancement of the surface reactivity of the functionalised coatings.
- Systematic study into magnetic separability for current functionalised magnetic adsorbents, which would largely benefit their future industrialisation.
- Further study on interference effects of coexisting ions in gold cyanidation process waters for current functionalised magnetic adsorbents. The possible adverse effect on arsenic adsorption for each type of ion in a typical gold cyanidation liquor should be studied individually, assisting in fully understanding the selectivity of the synthesised adsorbents.
- Since the adsorption mechanisms were not the main focus of the thesis, the investigations in this regard were not in depth. Further exploration of the

established adsorption mechanisms for current functionalised magnetic adsorbents is needed, which would serve to help understand the difference in adsorption capacities among them.

- Enhancement of desorption capacities for current functionalised magnetic adsorbents. Exploratory research could be carried out, such as increasing the alkalinity of the regenerant, extending the treatment time, seeking for new eluting agents, etc.
- Searching for new functionalised magnetic adsorbents, which would inevitably be built on extensive literature survey and numerous experiments.

REFERENCES

Abejón, A., Garea, A., & Irabien, A. (2015). Arsenic removal from drinking water by reverse osmosis: Minimization of costs and energy consumption. *Separation and Purification Technology, 144,* 46-53. doi:http://dx.doi.org/10.1016/j.seppur.2015.02.017

Adams, M. D. (2016). Chapter 54 - Summary of Gold Plants and Processes *Gold Ore Processing (Second Edition)* (pp. 961-984): Elsevier.

Ahn, J. S., Chon, C.-M., Moon, H.-S., & Kim, K.-W. (2003). Arsenic removal using steel manufacturing byproducts as permeable reactive materials in mine tailing containment systems. *Water Research, 37*(10), 2478-2488. doi:http://doi.org/10.1016/S0043-1354(02)00637-1

Akin, I., Arslan, G., Tor, A., Cengeloglu, Y., & Ersoz, M. (2011). Removal of arsenate [As(V)] and arsenite [As(III)] from water by SWHR and BW-30 reverse osmosis. *Desalination, 281,* 88-92. doi:http://dx.doi.org/10.1016/j.desal.2011.07.062

Akin, I., Arslan, G., Tor, A., Ersoz, M., & Cengeloglu, Y. (2012). Arsenic(V) removal from underground water by magnetic nanoparticles synthesized from waste red mud. *Journal of Hazardous Materials, 235–236,* 62-68. doi:http://doi.org/10.1016/j.jhazmat.2012.06.024

Alijani, H., & Shariatinia, Z. (2017). Effective aqueous arsenic removal using zero valent iron doped MWCNT synthesized by in situ CVD method using natural α-Fe2O3 as a precursor. *Chemosphere, 171,* 502-511. doi:http://doi.org/10.1016/j.chemosphere.2016.12.106

Amin, M. N., Kaneco, S., Kitagawa, T., Begum, A., Katsumata, H., Suzuki, T., & Ohta, K. (2006). Removal of Arsenic in Aqueous Solutions by Adsorption onto Waste Rice Husk. *Industrial & Engineering Chemistry Research, 45*(24), 8105-8110. doi:10.1021/ie060344j

Andjelkovic, I., Stankovic, D., Jovic, M., Markovic, M., Krstic, J., Manojlovic, D., & Roglic, G. (2015). Microwave-hydrothermal synthesis of TiO2 and zirconium doped TiO2 adsorbents for removal of As(III) and As(V). *Journal of Saudi Chemical Society*, 19(4), 429-435. doi:https://doi.org/10.1016/j.jscs.2014.05.009

Arcibar-Orozco, J. A., Josue, D.-B., Rios-Hurtado, J. C., & Rangel-Mendez, J. R. (2014). Influence of iron content, surface area and charge distribution in the arsenic removal by activated carbons. *Chemical Engineering Journal, 249*, 201-209. doi:http://dx.doi.org/10.1016/j.cej.2014.03.096

Arehart, G. B., Chryssoulis, S. L., & Kesler, S. E. (1993). Gold and arsenic in iron sulfides from sediment-hosted disseminated gold deposits; implications for depositional processes. *Economic Geology, 88*(1), 171-185. doi:10.2113/gsecongeo.88.1.171

Argos, M., Kalra, T., Rathouz, P. J., Chen, Y., Pierce, B., Parvez, F., Ahsan, H. (2010). Arsenic exposure from drinking water, and all-cause and chronic-disease mortalities in Bangladesh (HEALS): a prospective cohort study. Lancet, 376(9737), 252-258. doi:10.1016/S0140-6736(10)60481-3

Ashley, P. M., & Lottermoser, B. G. (1999). Arsenic contamination at the Mole River mine, northern New South Wales. Australian Journal of Earth Sciences, 46(6), 861-874. doi:10.1046/j.1440-0952.1999.00748.x

Artioli, Y. (2008). Adsorption. In S. E. J. D. Fath (Ed.), *Encyclopedia of Ecology* (pp. 60-65). Oxford: Academic Press.

Arumugam, A., Ponnusami, V., Narendhar, C., & Bhuvaneshvari, T. S. (2013). Novel Waste Water Treatment Strategy Using Titanate Nanofibers in Fixed Bed Reactor. In K. P. Giri, K. D. Goswami, & A. Perumal (Eds.), *Advanced Nanomaterials and Nanotechnology: Proceedings of the 2nd International Conference on Advanced Nanomaterials and Nanotechnology, Dec 8-10, 2011, Guwahati, India* (pp. 589-598). Berlin, Heidelberg: Springer Berlin Heidelberg.

Asadullah, M., Jahan, I., Ahmed, M. B., Adawiyah, P., Malek, N. H., & Rahman, M. S. (2014). Preparation of microporous activated carbon and its modification for arsenic removal from water. *Journal of Industrial and Engineering Chemistry, 20*(3), 887-896. doi:http://dx.doi.org/10.1016/j.jiec.2013.06.019

Asmel, N. K., Yusoff, A. R. M., Sivarama Krishna, L., Majid, Z. A., & Salmiati, S. (2017). High concentration arsenic removal from aqueous solution using nano-iron ion enrich material (NIIEM) super adsorbent. *Chemical Engineering Journal, 317*, 343-355. doi:http://dx.doi.org/10.1016/j.cej.2017.02.039

Asselin, E., & Shaw, R. (2016). Chapter 41 - Developments in Arsenic Management in the Gold Industry A2 - Adams, Mike D *Gold Ore Processing (Second Edition)* (pp. 739-751): Elsevier.

Azizian, S. (2004). Kinetic models of sorption: a theoretical analysis. *Journal of Colloid and Interface Science, 276*(1), 47-52. doi:http://dx.doi.org/10.1016/j.jcis.2004.03.048

Babu, C. M., Vinodh, R., Sundaravel, B., Abidov, A., Peng, M. M., Cha, W. S., & Jang, H.-T. (2016). Characterization of reduced graphene oxide supported mesoporous Fe2O3/TiO2 nanoparticles and adsorption of As(III) and As(V) from potable water. *Journal of the Taiwan Institute of Chemical Engineers, 62*, 199-208. doi:http://doi.org/10.1016/j.jtice.2016.02.005

Badruddoza, A. Z. M., Shawon, Z. B. Z., Rahman, M. T., Hao, K. W., Hidajat, K., & Uddin, M. S. (2013). Ionically modified magnetic nanomaterials for arsenic and chromium removal from water. *Chemical Engineering Journal, 225*, 607-615. doi:10.1016/j.cej.2013.03.114

Baig, S. A., Zhu, J., Muhammad, N., Sheng, T., & Xu, X. (2014). Effect of synthesis methods on magnetic Kans grass biochar for enhanced As(III, V) adsorption from aqueous solutions. *Biomass and Bioenergy, 71*, 299-310. doi:10.1016/j.biombioe.2014.09.027

Balaji, T., & Matsunaga, H. (2002). Adsorption characteristics of As(III) and As(V) with titanium dioxide loaded amberlite XAD-7 resin. *Analytical Sciences, 18*(12), 1345-1349. doi:DOI 10.2116/analsci.18.1345

Bang, S., Patel, M., Lippincott, L., & Meng, X. (2005). Removal of arsenic from groundwater by granular titanium dioxide adsorbent. *Chemosphere, 60*(3), 389-397. doi:http://doi.org/10.1016/j.chemosphere.2004.12.008

Barakat, M. A., & Ismat-Shah, S. (2013). Utilization of anion exchange resin Spectra/Gel for separation of arsenic from water. *Arabian Journal of Chemistry, 6*(3), 307-311. doi:http://doi.org/10.1016/j.arabjc.2010.10.011

Bentahar, Y., Hurel, C., Draoui, K., Khairoun, S., & Marmier, N. (2016). Adsorptive properties of Moroccan clays for the removal of arsenic(V) from aqueous solution. *Applied Clay Science, 119, Part 2*, 385-392. doi:http://doi.org/10.1016/j.clay.2015.11.008

Bhowmick, S., Chakraborty, S., Mondal, P., Van Renterghem, W., Van den Berghe, S., Roman-Ross, G., . . . Iglesias, M. (2014). Montmorillonite-supported

nanoscale zero-valent iron for removal of arsenic from aqueous solution: Kinetics and mechanism. *Chemical Engineering Journal, 243*, 14-23. doi:http://doi.org/10.1016/j.cej.2013.12.049

Bilici Baskan, M., & Pala, A. (2010). A statistical experiment design approach for arsenic removal by coagulation process using aluminum sulfate. *Desalination, 254*(1–3), 42-48. doi:http://dx.doi.org/10.1016/j.desal.2009.12.016

Bissen, M., & Frimmel, F. H. (2003). Arsenic — a Review. Part I: Occurrence, Toxicity, Speciation, Mobility. Acta hydrochimica et hydrobiologica, 31(1), 9-18. doi:10.1002/aheh.200390025

Boddu, V. M., Abburi, K., Talbott, J. L., Smith, E. D., & Haasch, R. (2008). Removal of arsenic (III) and arsenic (V) from aqueous medium using chitosan-coated biosorbent. *Water Research, 42*(3), 633-642. doi:http://doi.org/10.1016/j.watres.2007.08.014

Bortun, A., Bortun, M., Pardini, J., Khainakov, S. A., & García, J. R. (2010). Synthesis and characterization of a mesoporous hydrous zirconium oxide used for arsenic removal from drinking water. *Materials Research Bulletin, 45*(2), 142-148. doi:http://doi.org/10.1016/j.materresbull.2009.09.030

Brahman, K. D., Kazi, T. G., Baig, J. A., Afridi, H. I., Arain, S. S., Saraj, S., . . . Arain, S. A. (2016). Biosorptive removal of inorganic arsenic species and fluoride from aqueous medium by the stem of Tecomella undulate. *Chemosphere, 150*, 320-328. doi:http://doi.org/10.1016/j.chemosphere.2016.02.017

Brammer, H., & Ravenscroft, P. (2009). Arsenic in groundwater: A threat to sustainable agriculture in South and South-east Asia. Environment International, 35(3), 647-654. doi:http://dx.doi.org/10.1016/j.envint.2008.10.004

Bretzler, A., Lalanne, F., Nikiema, J., Podgorski, J., Pfenninger, N., Berg, M., & Schirmer, M. (2017). Groundwater arsenic contamination in Burkina Faso, West Africa: Predicting and verifying regions at risk. Science of The Total Environment, 584–585, 958-970. doi:https://doi.org/10.1016/j.scitotenv.2017.01.147

Chammui, Y., Sooksamiti, P., Naksata, W., Thiansem, S., & Arqueropanyo, O.-a. (2014). Removal of arsenic from aqueous solution by adsorption on

Leonardite. *Chemical Engineering Journal, 240*, 202-210. doi:http://dx.doi.org/10.1016/j.cej.2013.11.083

Chan, B. K. C., & Dudeney, A. W. L. (2008). Reverse osmosis removal of arsenic residues from bioleaching of refractory gold concentrates. *Minerals Engineering, 21*(4), 272-278. doi:http://dx.doi.org/10.1016/j.mineng.2007.10.003

Chang, F.-f., Liu, W.-j., & Wang, X.-m. (2014). Comparison of polyamide nanofiltration and low-pressure reverse osmosis membranes on As(III) rejection under various operational conditions. *Desalination, 334*(1), 10-16. doi:http://dx.doi.org/10.1016/j.desal.2013.11.002

Chaudhry, S. A., Khan, T. A., & Ali, I. Zirconium oxide-coated sand based batch and column adsorptive removal of arsenic from water: Isotherm, kinetic and thermodynamic studies. *Egyptian Journal of Petroleum*. doi:http://doi.org/10.1016/j.ejpe.2016.11.006

Chaudhry, S. A., Khan, T. A., & Ali, I. (2017). Zirconium oxide-coated sand based batch and column adsorptive removal of arsenic from water: Isotherm, kinetic and thermodynamic studies. *Egyptian Journal of Petroleum*. doi:http://dx.doi.org/10.1016/j.ejpe.2016.11.006

Chaudhry, S. A., Zaidi, Z., & Siddiqui, S. I. (2017). Isotherm, kinetic and thermodynamics of arsenic adsorption onto Iron-Zirconium Binary Oxide-Coated Sand (IZBOCS): Modelling and process optimization. *Journal of Molecular Liquids, 229*, 230-240. doi:http://doi.org/10.1016/j.molliq.2016.12.048

Chen, L., Xin, H., Fang, Y., Zhang, C., Zhang, F., Cao, X., . . . Li, X. (2014). Application of Metal Oxide Heterostructures in Arsenic Removal from Contaminated Water. *Journal of Nanomaterials, 2014*, 10. doi:10.1155/2014/793610

Cheng, W., Xu, J., Wang, Y., Wu, F., Xu, X., & Li, J. (2015). Dispersion–precipitation synthesis of nanosized magnetic iron oxide for efficient removal of arsenite in water. *Journal of Colloid and Interface Science, 445*, 93-101. doi:http://dx.doi.org/10.1016/j.jcis.2014.12.082

Çiftçi, T. D., & Henden, E. (2015). Nickel/nickel boride nanoparticles coated resin: A novel adsorbent for arsenic(III) and arsenic(V) removal. *Powder*

Technology, 269, 470-480. doi:http://dx.doi.org/10.1016/j.powtec.2014.09.041

Clifford, D., Chu, P., & Lau, A. (1983). Thermal regeneration of powdered activated carbon (pac) and pac-biological sludge mixtures. *Water Research, 17*(9), 1125-1138. doi:http://dx.doi.org/10.1016/0043-1354(83)90053-2

Conner, J. R., & Hoeffner, S. L. (1998). A Critical Review of Stabilization/Solidification Technology. *Critical Reviews in Environmental Science and Technology, 28*(4), 397-462. doi:10.1080/10643389891254250

Criscuoli, A., Bafaro, P., & Drioli, E. (2013). Vacuum membrane distillation for purifying waters containing arsenic. *Desalination, 323*, 17-21. doi:http://dx.doi.org/10.1016/j.desal.2012.08.004

Cui, H., Li, Q., Gao, S., & Shang, J. K. (2012). Strong adsorption of arsenic species by amorphous zirconium oxide nanoparticles. *Journal of Industrial and Engineering Chemistry, 18*(4), 1418-1427. doi:http://doi.org/10.1016/j.jiec.2012.01.045

Dao, T. D., Laborie, S., & Cabassud, C. (2016). Direct As(III) removal from brackish groundwater by vacuum membrane distillation: Effect of organic matter and salts on membrane fouling. *Separation and Purification Technology, 157*, 35-44. doi:http://dx.doi.org/10.1016/j.seppur.2015.11.018

Deuel, L. E., & Swoboda, A. R. (1972). Arsenic Toxicity to Cotton and Soybeans1. *Journal of Environmental Quality, 1*(3), 317-320. doi:10.2134/jeq1972.00472425000100030026x

Di Natale, F., Erto, A., & Lancia, A. (2013). Desorption of arsenic from exhaust activated carbons used for water purification. *Journal of Hazardous Materials, 260*, 451-458. doi:http://dx.doi.org/10.1016/j.jhazmat.2013.05.055

Diamadopoulos, E., Ioannidis, S., & Sakellaropoulos, G. P. (1993). As(V) removal from aqueous solutions by fly ash. *Water Research, 27*(12), 1773-1777. doi:http://dx.doi.org/10.1016/0043-1354(93)90116-Y

Díaz, X., & Caizaguano, R. (1999). Bioremediation of cyanide leaching residues. In R. Amils & A. Ballester (Eds.), *Process Metallurgy* (Vol. Volume 9, pp. 595-605): Elsevier.

Donia, A. M., Atia, A. A., & Mabrouk, D. H. (2011). Fast kinetic and efficient removal of As(V) from aqueous solution using anion exchange resins.

Journal of Hazardous Materials, 191(1–3), 1-7. doi:http://dx.doi.org/10.1016/j.jhazmat.2011.01.056

Doušová, B., Lhotka, M., Grygar, T., Machovič, V., & Herzogová, L. (2011). In situ co-adsorption of arsenic and iron/manganese ions on raw clays. *Applied Clay Science, 54*(2), 166-171. doi:http://doi.org/10.1016/j.clay.2011.08.004

Drahota, P., & Filippi, M. (2009). Secondary arsenic minerals in the environment: A review. *Environment International, 35*(8), 1243-1255. doi:http://dx.doi.org/10.1016/j.envint.2009.07.004

Dutta, P. K., Ray, A. K., Sharma, V. K., & Millero, F. J. (2004). Adsorption of arsenate and arsenite on titanium dioxide suspensions. *Journal of Colloid and Interface Science,* 278(2), 270-275. doi:https://doi.org/10.1016/j.jcis.2004.06.015

El-Moselhy, M. M., Ates, A., & Çelebi, A. (2017). Synthesis and characterization of hybrid iron oxide silicates for selective removal of arsenic oxyanions from contaminated water. *Journal of Colloid and Interface Science, 488*, 335-347. doi:http://doi.org/10.1016/j.jcis.2016.11.003

Emsley, J. (2001). *Nature's Building Blocks: An A-Z Guide to the Elements*: Oxford University Press.

Emsley, J. (2011). *Nature's building blocks: an AZ guide to the elements*: Oxford University Press.

Fang, J., & Deng, B. (2014). Rejection and modeling of arsenate by nanofiltration: Contributions of convection, diffusion and electromigration to arsenic transport. *Journal of Membrane Science, 453*, 42-51. doi:http://dx.doi.org/10.1016/j.memsci.2013.10.056

Feng, L., Cao, M., Ma, X., Zhu, Y., & Hu, C. (2012). Superparamagnetic high-surface-area Fe3O4 nanoparticles as adsorbents for arsenic removal. *Journal of Hazardous Materials, 217–218,* 439-446. doi:http://doi.org/10.1016/j.jhazmat.2012.03.073

Ferguson, J. F., & Gavis, J. (1972). A review of the arsenic cycle in natural waters. *Water Research, 6*(11), 1259-1274. doi:10.1016/0043-1354(72)90052-8

Figoli, A., Cassano, A., Criscuoli, A., Mozumder, M. S. I., Uddin, M. T., Islam, M. A., & Drioli, E. (2010). Influence of operating parameters on the arsenic removal by nanofiltration. *Water Research, 44*(1), 97-104. doi:http://dx.doi.org/10.1016/j.watres.2009.09.007

Foo, K. Y., & Hameed, B. H. (2010). Insights into the modeling of adsorption isotherm systems. *Chemical Engineering Journal, 156*(1), 2-10. doi:http://dx.doi.org/10.1016/j.cej.2009.09.013

Garcia, S., Sardar, S., Maldonado, S., Garcia, V., Tamez, C., & Parsons, J. G. (2014). Study of As(III) and As(V) oxoanion adsorption onto single and mixed ferrite and hausmannite nanomaterials. *Microchemical Journal, 117*, 52-60. doi:http://dx.doi.org/10.1016/j.microc.2014.06.008

Gholami, M. M., Mokhtari, M. A., Aameri, A., & Alizadeh Fard, M. R. (2006). Application of reverse osmosis technology for arsenic removal from drinking water. *Desalination, 200*(1), 725-727. doi:http://dx.doi.org/10.1016/j.desal.2006.03.504

Gu, Z., Fang, J., & Deng, B. (2005). Preparation and Evaluation of GAC-Based Iron-Containing Adsorbents for Arsenic Removal. *Environmental Science & Technology*, 39(10), 3833-3843. doi:10.1021/es048179r

Guan, X., Du, J., Meng, X., Sun, Y., Sun, B., & Hu, Q. (2012). Application of titanium dioxide in arsenic removal from water: A review. *Journal of Hazardous Materials, 215–216*, 1-16. doi:http://doi.org/10.1016/j.jhazmat.2012.02.069

Guan, X. H., Du, J. S., Meng, X. G., Sun, Y. K., Sun, B., & Hu, Q. H. (2012). Application of titanium dioxide in arsenic removal from water: A review. *Journal of Hazardous Materials, 215*, 1-16. doi:DOI 10.1016/j.jhazmat.2012.02.069

Gupta, A., Vidyarthi, S. R., & Sankararamakrishnan, N. (2015). Concurrent removal of As(III) and As(V) using green low cost functionalized biosorbent – Saccharum officinarum bagasse. *Journal of Environmental Chemical Engineering, 3*(1), 113-121. doi:http://doi.org/10.1016/j.jece.2014.11.023

Gupta, K., Bhattacharya, S., Chattopadhyay, D., Mukhopadhyay, A., Biswas, H., Dutta, J., . . . Ghosh, U. C. (2011). Ceria associated manganese oxide nanoparticles: Synthesis, characterization and arsenic(V) sorption behavior. *Chemical Engineering Journal, 172*(1), 219-229. doi:http://doi.org/10.1016/j.cej.2011.05.092

Gupta, K., Bhattacharya, S., Nandi, D., Dhar, A., Maity, A., Mukhopadhyay, A., . . . Ghosh, U. C. (2012). Arsenic(III) sorption on nanostructured cerium incorporated manganese oxide (NCMO): A physical insight into the

mechanistic pathway. *Journal of Colloid and Interface Science, 377*(1), 269-276. doi:http://doi.org/10.1016/j.jcis.2012.01.066

Gupta, K., Biswas, K., & Ghosh, U. C. (2008). Nanostructure Iron(III)−Zirconium(IV) Binary Mixed Oxide: Synthesis, Characterization, and Physicochemical Aspects of Arsenic(III) Sorption from the Aqueous Solution. *Industrial & Engineering Chemistry Research, 47*(24), 9903-9912. doi:10.1021/ie8002107

Gupta, K., & Ghosh, U. C. (2009). Arsenic removal using hydrous nanostructure iron(III)–titanium(IV) binary mixed oxide from aqueous solution. *Journal of Hazardous Materials, 161*(2–3), 884-892. doi:http://doi.org/10.1016/j.jhazmat.2008.04.034

Han, C., Li, H., Pu, H., Yu, H., Deng, L., Huang, S., & Luo, Y. (2013). Synthesis and characterization of mesoporous alumina and their performances for removing arsenic(V). *Chemical Engineering Journal, 217*, 1-9. doi:http://doi.org/10.1016/j.cej.2012.11.087

Harisha, R. S., Hosamani, K. M., Keri, R. S., Nataraj, S. K., & Aminabhavi, T. M. (2010). Arsenic removal from drinking water using thin film composite nanofiltration membrane. *Desalination, 252*(1–3), 75-80. doi:http://dx.doi.org/10.1016/j.desal.2009.10.022

He, J., Bardelli, F., Gehin, A., Silvester, E., & Charlet, L. (2016). Novel chitosan goethite bionanocomposite beads for arsenic remediation. *Water Research, 101*, 1-9. doi:http://doi.org/10.1016/j.watres.2016.05.032

He, Z., Tian, S., & Ning, P. (2012). Adsorption of arsenate and arsenite from aqueous solutions by cerium-loaded cation exchange resin. *Journal of Rare Earths, 30*(6), 563-572. doi:http://dx.doi.org/10.1016/S1002-0721(12)60092-1

Heikens, A., Panaullah, G. M., & Meharg, A. A. (2007). Arsenic Behaviour from Groundwater and Soil to Crops: Impacts on Agriculture and Food Safety. In D. M. Whitacre, G. W. Ware, H. N. Nigg, D. R. Doerge, L. A. Albert, P. de Voogt, C. P. Gerba, O. Hutzinger, J. B. Knaak, F. L. Mayer, D. P. Morgan, D. L. Park, R. S. Tjeerdema, R. S. H. Yang, & F. A. Gunther (Eds.), Reviews of Environmental Contamination and Toxicology: Continuation of Residue Reviews (pp. 43-87). New York, NY: Springer New York.

Ho, Y. S., & McKay, G. (1998). A Comparison of Chemisorption Kinetic Models Applied to Pollutant Removal on Various Sorbents. *Process Safety and Environmental Protection, 76*(4), 332-340. doi:http://dx.doi.org/10.1205/095758298529696

Hokkanen, S., Repo, E., Lou, S., & Sillanpää, M. (2015). Removal of arsenic(V) by magnetic nanoparticle activated microfibrillated cellulose. *Chemical Engineering Journal, 260*, 886-894. doi:http://dx.doi.org/10.1016/j.cej.2014.08.093

Hou, J., Luo, J., Song, S., Li, Y., & Li, Q. (2017). The remarkable effect of the coexisting arsenite and arsenate species ratios on arsenic removal by manganese oxide. *Chemical Engineering Journal, 315*, 159-166. doi:http://doi.org/10.1016/j.cej.2016.12.115

Huong, P. T. L., Huy, L. T., Phan, V. N., Huy, T. Q., Nam, M. H., Lam, V. D., & Le, A.-T. (2016). Application of Graphene Oxide-MnFe2O4 Magnetic Nanohybrids as Magnetically Separable Adsorbent for Highly Efficient Removal of Arsenic from Water. *Journal of Electronic Materials, 45*(5), 2372-2380. doi:10.1007/s11664-015-4314-3

Jadhav, S. V., Bringas, E., Yadav, G. D., Rathod, V. K., Ortiz, I., & Marathe, K. V. (2015). Arsenic and fluoride contaminated groundwaters: A review of current technologies for contaminants removal. *Journal of Environmental Management, 162*, 306-325. doi:http://dx.doi.org/10.1016/j.jenvman.2015.07.020

Jais, F. M., Ibrahim, S., Yoon, Y., & Jang, M. (2016). Enhanced arsenate removal by lanthanum and nano–magnetite composite incorporated palm shell waste–based activated carbon. *Separation and Purification Technology, 169*, 93-102. doi:http://dx.doi.org/10.1016/j.seppur.2016.05.034

Jegadeesan, G., Al-Abed, S. R., Sundaram, V., Choi, H., Scheckel, K. G., & Dionysiou, D. D. (2010). Arsenic sorption on TiO2 nanoparticles: Size and crystallinity effects. *Water Research, 44*(3), 965-973. doi:10.1016/j.watres.2009.10.047

Jegadeesan, G., Sundaram, V., Choi, H., Dionysiou, D., & Al-Abed, S. R. (2006). Arsenic removal using titanium dioxide nanoparticles synthesized with sol-gel methods. *Abstracts of Papers - American Chemical Society, 232*, 627-627.

Jing, C., Meng, X., Calvache, E., & Jiang, G. (2009). Remediation of organic and inorganic arsenic contaminated groundwater using a nanocrystalline TiO 2-based adsorbent. *Environmental Pollution, 157*(8-9), 2514-2519. doi:10.1016/j.envpol.2009.03.011

Kang, K., Jang, M., Cui, M. C., Qiu, P. P., Park, B., Snyder, S. A., & Khim, J. (2014). Preparation and characterization of magnetic-core titanium dioxide: Implications for photocatalytic removal of ibuprofen. *Journal of Molecular Catalysis a-Chemical, 390*, 178-186. doi:DOI 10.1016/j.molcata.2014.03.023

Kang, M., Kawasaki, M., Tamada, S., Kamei, T., & Magara, Y. (2000). Effect of pH on the removal of arsenic and antimony using reverse osmosis membranes. *Desalination, 131*(1), 293-298. doi:http://dx.doi.org/10.1016/S0011-9164(00)90027-4

Kang, M., Kawasaki, M., Tamada, S., Kamei, T., & Magara, Y. (2001). Effect of pH on the removal of arsenic and antimony using reverse osmosis membranes. *Desalination, 133*(1), 93. doi:http://dx.doi.org/10.1016/S0011-9164(01)00088-1

Karmacharya, M. S., Gupta, V. K., Tyagi, I., Agarwal, S., & Jha, V. K. (2016). Removal of As(III) and As(V) using rubber tire derived activated carbon modified with alumina composite. *Journal of Molecular Liquids, 216*, 836-844. doi:http://dx.doi.org/10.1016/j.molliq.2016.02.025

Ketzial, J. J., & Nesaraj, A. S. (2011). Synthesis of CeO2 nanoparticles by chemical precipitation and the effect of a surfactant on the distribution of particle sizes. *Journal of Ceramic Processing Research, 12*(1), 74-79.

Khalid, N., Ahmad, S., Toheed, A., & Ahmed, J. (1998). Immobilization of Arsenic on Rice Husk. *Adsorption Science & Technology, 16*(8), 655-666. doi:10.1177/026361749801600806

Kilianová, M., Prucek, R., Filip, J., Kolařík, J., Kvítek, L., Panáček, A., . . . Zbořil, R. (2013). Remarkable efficiency of ultrafine superparamagnetic iron(III) oxide nanoparticles toward arsenate removal from aqueous environment. *Chemosphere, 93*(11), 2690-2697. doi:10.1016/j.chemosphere.2013.08.071

Košutić, K., Furač, L., Sipos, L., & Kunst, B. (2005). Removal of arsenic and pesticides from drinking water by nanofiltration membranes. *Separation and Purification Technology, 42*(2), 137-144. doi:http://dx.doi.org/10.1016/j.seppur.2004.07.003

Kumar, S., Nair, R. R., Pillai, P. B., Gupta, S. N., Iyengar, M. A. R., & Sood, A. K. (2014). Graphene oxide-MnFe2O4 magnetic nanohybrids for efficient removal of lead and arsenic from water. *ACS Applied Materials and Interfaces, 6*(20), 17426-17436. doi:10.1021/am504826q

Kundu, S., & Gupta, A. K. (2006). Arsenic adsorption onto iron oxide-coated cement (IOCC): Regression analysis of equilibrium data with several isotherm models and their optimization. *Chemical Engineering Journal, 122*(1-2), 93-106. doi:10.1016/j.cej.2006.06.002

Kwok, K. C. M., Koong, L. F., Chen, G., & McKay, G. (2014). Mechanism of arsenic removal using chitosan and nanochitosan. *Journal of Colloid and Interface Science, 416*, 1-10. doi:http://doi.org/10.1016/j.jcis.2013.10.031

Kwon, O.-H., Kim, J.-O., Cho, D.-W., Kumar, R., Baek, S. H., Kurade, M. B., & Jeon, B.-H. (2016). Adsorption of As(III), As(V) and Cu(II) on zirconium oxide immobilized alginate beads in aqueous phase. *Chemosphere, 160*, 126-133. doi:http://doi.org/10.1016/j.chemosphere.2016.06.074

Kyle, J. H., Breuer, P. L., Bunney, K. G., & Pleysier, R. (2012a). Review of trace toxic elements (Pb, Cd, Hg, As, Sb, Bi, Se, Te) and their deportment in gold processing Part II: Deportment in gold ore processing by cyanidation. *Hydrometallurgy, 111*, 10-21. doi:10.1016/j.hydromet.2011.09.005

Kyle, J. H., Breuer, P. L., Bunney, K. G., & Pleysier, R. (2012b). Review of trace toxic elements (Pb, Cd, Hg, As, Sb, Bi, Se, Te) and their deportment in gold processing: Part II: Deportment in gold ore processing by cyanidation. *Hydrometallurgy, 111–112*, 10-21. doi:http://dx.doi.org/10.1016/j.hydromet.2011.09.005

Lagergren, S. (1898). About the theory of so-called adsorption of soluble substances.

Lalancette, J.-M., Dubreuil, B., & Lemieux, D. (2015). Method and composition for sequestration of arsenic: Google Patents.

Largitte, L., & Pasquier, R. (2016). A review of the kinetics adsorption models and their application to the adsorption of lead by an activated carbon. *Chemical Engineering Research and Design, 109*, 495-504. doi:http://dx.doi.org/10.1016/j.cherd.2016.02.006

Lata, S., & Samadder, S. R. (2016). Removal of arsenic from water using nano adsorbents and challenges: A review. *Journal of Environmental Management, 166*, 387-406. doi:http://dx.doi.org/10.1016/j.jenvman.2015.10.039

Lehmann, E. L., Fostier, A. H., & Arruda, M. A. Z. (2013). Hydride generation using a metallic atomizer after microwave-assisted extraction for inorganic arsenic speciation in biological samples. *Talanta, 104*, 187-192. doi:http://dx.doi.org/10.1016/j.talanta.2012.11.009

Lenoble, V., Chabroullet, C., al Shukry, R., Serpaud, B., Deluchat, V., & Bollinger, J.-C. (2004). Dynamic arsenic removal on a MnO2-loaded resin. *Journal of Colloid and Interface Science, 280*(1), 62-67. doi:http://dx.doi.org/10.1016/j.jcis.2004.07.034

Li, R., Li, Q., Gao, S., & Shang, J. K. (2012). Exceptional arsenic adsorption performance of hydrous cerium oxide nanoparticles: Part A. Adsorption capacity and mechanism. *Chemical Engineering Journal, 185–186*, 127-135. doi:http://doi.org/10.1016/j.cej.2012.01.061

Li, R., Yang, W., Su, Y., Li, Q., Gao, S., & Shang, J. K. (2014). Ionic Potential: A General Material Criterion for the Selection of Highly Efficient Arsenic Adsorbents. *Journal of Materials Science & Technology, 30*(10), 949-953. doi:http://dx.doi.org/10.1016/j.jmst.2014.08.010

Li, W.-G., Gong, X.-J., Wang, K., Zhang, X.-R., & Fan, W.-B. (2014). Adsorption characteristics of arsenic from micro-polluted water by an innovative coal-based mesoporous activated carbon. *Bioresource Technology, 165*, 166-173. doi:http://dx.doi.org/10.1016/j.biortech.2014.02.069

Li, Z., Deng, S., Yu, G., Huang, J., & Lim, V. C. (2010). As(V) and As(III) removal from water by a Ce–Ti oxide adsorbent: Behavior and mechanism. *Chemical Engineering Journal, 161*(1–2), 106-113. doi:http://doi.org/10.1016/j.cej.2010.04.039

Lin, T., Liu, C., & Hsieh, W. (2006). Adsorption kinetics and equilibrium of arsenic onto an iron-based adsorbent and an ion exchange resin. *Water Science and Technology: Water Supply, 6*(2), 201-207.

Ling, L., & Zhang, W.-x. (2014). Sequestration of Arsenate in Zero-Valent Iron Nanoparticles: Visualization of Intraparticle Reactions at Angstrom Resolution. *Environmental Science & Technology Letters, 1*(7), 305-309. doi:10.1021/ez5001512

Litter, M. I., Morgada, M. E., & Bundschuh, J. (2010). Possible treatments for arsenic removal in Latin American waters for human consumption.

Environmental Pollution, 158(5), 1105-1118. doi:http://dx.doi.org/10.1016/j.envpol.2010.01.028

Liu, C.-H., Chuang, Y.-H., Chen, T.-Y., Tian, Y., Li, H., Wang, M.-K., & Zhang, W. (2015). Mechanism of Arsenic Adsorption on Magnetite Nanoparticles from Water: Thermodynamic and Spectroscopic Studies. *Environmental Science & Technology, 49*(13), 7726-7734. doi:10.1021/acs.est.5b00381

Liu, H. F., Jia, Z. G., Ji, S. F., Zheng, Y. Y., Li, M., & Yang, H. (2011). Synthesis of TiO2/SiO2@Fe3O4 magnetic microspheres and their properties of photocatalytic degradation dyestuff. *Catalysis Today, 175*(1), 293-298. doi:10.1016/j.cattod.2011.04.042

Liu, S., Kang, S., Wang, G., Zhao, H., & Cai, W. (2015). Micro/nanostructured porous Fe–Ni binary oxide and its enhanced arsenic adsorption performances. *Journal of Colloid and Interface Science, 458*, 94-102. doi:http://dx.doi.org/10.1016/j.jcis.2015.07.038

Liu, T., Yang, Y., Wang, Z.-L., & Sun, Y. (2016). Remediation of arsenic(III) from aqueous solutions using improved nanoscale zero-valent iron on pumice. *Chemical Engineering Journal, 288*, 739-744. doi:http://doi.org/10.1016/j.cej.2015.12.070

Liu, Z., Lei, H.-y., Bai, T., Wang, W.-z., Chen, K., Chen, J.-j., & Hu, Q.-w. (2015). Microwave-assisted arsenic removal and the magnetic effects of typical arsenopyrite-bearing mine tailings. *Chemical Engineering Journal, 272*, 1-11. doi:http://dx.doi.org/10.1016/j.cej.2015.02.084

Lodeiro, P., Kwan, S. M., Perez, J. T., González, L. F., Gérente, C., Andrès, Y., & McKay, G. (2013). Novel Fe loaded activated carbons with tailored properties for As(V) removal: Adsorption study correlated with carbon surface chemistry. *Chemical Engineering Journal, 215–216*, 105-112. doi:http://dx.doi.org/10.1016/j.cej.2012.11.052

Lohokare, H. R., Muthu, M. R., Agarwal, G. P., & Kharul, U. K. (2008). Effective arsenic removal using polyacrylonitrile-based ultrafiltration (UF) membrane. *Journal of Membrane Science, 320*(1–2), 159-166. doi:http://dx.doi.org/10.1016/j.memsci.2008.03.068

Lorenzen, L., Vandeventer, J. S. J., & Landi, W. M. (1995). Factors Affecting the Mechanism of the Adsorption of Arsenic Species on Activated Carbon.

Minerals Engineering, 8(4-5), 557-569. doi:Doi 10.1016/0892-6875(95)00017-K

Lunge, S., Singh, S., & Sinha, A. (2014). Magnetic iron oxide (Fe3O4) nanoparticles from tea waste for arsenic removal. *Journal of Magnetism and Magnetic Materials, 356*, 21-31. doi:10.1016/j.jmmm.2013.12.008

Luo, X., Wang, C., Wang, L., Deng, F., Luo, S., Tu, X., & Au, C. (2013). Nanocomposites of graphene oxide-hydrated zirconium oxide for simultaneous removal of As(III) and As(V) from water. *Chemical Engineering Journal, 220*, 98-106. doi:http://doi.org/10.1016/j.cej.2013.01.017

Luther, S., Borgfeld, N., Kim, J., & Parsons, J. G. (2012). Removal of arsenic from aqueous solution: A study of the effects of pH and interfering ions using iron oxide nanomaterials. *Microchemical Journal, 101*, 30-36. doi:http://doi.org/10.1016/j.microc.2011.10.001

Ma, J., Zhu, Z. L., Chen, B., Yang, M. X., Zhou, H. M., Li, C., . . . Chen, J. H. (2013). One-pot, large-scale synthesis of magnetic activated carbon nanotubes and their applications for arsenic removal. *Journal of Materials Chemistry A, 1*(15), 4662-4666. doi:10.1039/c3ta10329c

Ma, Y., Zheng, Y.-M., & Chen, J. P. (2011). A zirconium based nanoparticle for significantly enhanced adsorption of arsenate: Synthesis, characterization and performance. *Journal of Colloid and Interface Science, 354*(2), 785-792. doi:http://doi.org/10.1016/j.jcis.2010.10.041

Mahmood, T., Din, S. U., Naeem, A., Tasleem, S., Alum, A., & Mustafa, S. (2014). Kinetics, equilibrium and thermodynamics studies of arsenate adsorption from aqueous solutions onto iron hydroxide. *Journal of Industrial and Engineering Chemistry, 20*(5), 3234-3242. doi:http://doi.org/10.1016/j.jiec.2013.12.004

Manna, A. K., Sen, M., Martin, A. R., & Pal, P. (2010). Removal of arsenic from contaminated groundwater by solar-driven membrane distillation. *Environmental Pollution, 158*(3), 805-811. doi:http://dx.doi.org/10.1016/j.envpol.2009.10.002

Manning, B. A., Fendorf, S. E., & Goldberg, S. (1998). Surface Structures and Stability of Arsenic(III) on Goethite: Spectroscopic Evidence for Inner-

Sphere Complexes. *Environmental Science & Technology, 32*(16), 2383-2388. doi:10.1021/es9802201

Marsden, J., & House, I. (2006). *The Chemistry of Gold Extraction*: Society for Mining, Metallurgy, and Exploration.

Masscheleyn, P. H., Delaune, R. D., & Patrick, W. H. (1991). Effect of redox potential and pH on arsenic speciation and solubility in a contaminated soil. *Environmental Science & Technology, 25*(8), 1414-1419. doi:10.1021/es00020a008

Matović, L. L., Vukelić, N. S., Jovanović, U. D., Kumrić, K. R., Krstić, J. B., Babić, B. M., & Đukić, A. B. (2016). Mechanochemically improved surface properties of activated carbon cloth for the removal of As(V) from aqueous solutions. *Arabian Journal of Chemistry*. doi:http://dx.doi.org/10.1016/j.arabjc.2016.07.004

Matsunaga, H., Yokoyama, T., Eldridge, R. J., & Bolto, B. A. (1996). Adsorption characteristics of arsenic(III) and arsenic(V) on iron(III)-loaded chelating resin having lysine-Nα,Nα-diacetic acid moiety. *Reactive and Functional Polymers, 29*(3), 167-174. doi:http://dx.doi.org/10.1016/1381-5148(96)00041-7

McCreadie, H., Jambor, J.L., Blowes, D.W., Ptacek, C., Hiller, D., 1998. Geochemical behaviour of autoclave-produced ferric arsenates: jarosite in a gold-mine tailings impoundment. In: Petruk, W. (Ed.), Waste Characterization and Treatment, 15th Process Mineralogy Symposium, Society for Mining, Metallurgy, and Exploration, Inc. (SME). Littleton, Colorado, pp. 61–78.

Mehta, D., Mazumdar, S., & Singh, S. K. (2015). Magnetic adsorbents for the treatment of water/wastewater—A review. *Journal of Water Process Engineering, 7*, 244-265. doi:http://doi.org/10.1016/j.jwpe.2015.07.001

Mohan, D., & Pittman, C. U. (2007). Arsenic removal from water/wastewater using adsorbents - A critical review. *Journal of Hazardous Materials, 142*(1-2), 1-53.

Mohan, D., & Pittman Jr, C. U. (2007). Arsenic removal from water/wastewater using adsorbents—A critical review. *Journal of Hazardous Materials, 142*(1–2), 1-53. doi:http://dx.doi.org/10.1016/j.jhazmat.2007.01.006

Mohan, D., Pittman Jr, C. U., Bricka, M., Smith, F., Yancey, B., Mohammad, J., . . . Gong, H. (2007). Sorption of arsenic, cadmium, and lead by chars produced from fast pyrolysis of wood and bark during bio-oil production. *Journal of Colloid and Interface Science, 310*(1), 57-73. doi:http://doi.org/10.1016/j.jcis.2007.01.020

Molinari, R., & Argurio, P. (2017). Arsenic removal from water by coupling photocatalysis and complexation-ultrafiltration processes: A preliminary study. *Water Research, 109*, 327-336. doi:http://dx.doi.org/10.1016/j.watres.2016.11.054

Mondal, P., Bhowmick, S., Chatterjee, D., Figoli, A., & Van der Bruggen, B. (2013). Remediation of inorganic arsenic in groundwater for safe water supply: A critical assessment of technological solutions. *Chemosphere*, 92(2), 157-170. doi:https://doi.org/10.1016/j.chemosphere.2013.01.097

Mondal, P., Hermans, N., Kim Tran, A. T., Zhang, Y., Fang, Y., Wang, X., & Van der Bruggen, B. (2014). Effect of physico-chemical parameters on inorganic arsenic removal from aqueous solution using a forward osmosis membrane. *Journal of Environmental Chemical Engineering, 2*(3), 1309-1316. doi:http://dx.doi.org/10.1016/j.jece.2014.04.015

Mouzourakis, E., Georgiou, Y., Louloudi, M., Konstantinou, I., & Deligiannakis, Y. (2017). Recycled-tire pyrolytic carbon made functional: A high-arsenite [As(III)] uptake material PyrC350®. *Journal of Hazardous Materials, 326*, 177-186. doi:http://dx.doi.org/10.1016/j.jhazmat.2016.12.027

Nabi, D., Aslam, I., & Qazi, I. A. (2009). Evaluation of the adsorption potential of titanium dioxide nanoparticles for arsenic removal. *Journal of Environmental Sciences-China, 21*(3), 402-408. doi:10.1016/S1001-0742(08)62283-4

Nazari, A. M., Radzinski, R., & Ghahreman, A. (2016). Review of arsenic metallurgy: Treatment of arsenical minerals and the immobilization of arsenic. *Hydrometallurgy*. doi:10.1016/j.hydromet.2016.10.011

Ng, M., Kho, E. T., Liu, S., Lim, M., & Amal, R. (2014). Highly adsorptive and regenerative magnetic TiO2 for natural organic matter (NOM) removal in water. *Chemical Engineering Journal, 246*(0), 196-203. doi:http://dx.doi.org/10.1016/j.cej.2014.02.015

Nguyen, C. M., Bang, S., Cho, J., & Kim, K.-W. (2009). Performance and mechanism of arsenic removal from water by a nanofiltration membrane.

Desalination, 245(1), 82-94. doi:http://dx.doi.org/10.1016/j.desal.2008.04.047

Nguyen, V. T., Vigneswaran, S., Ngo, H. H., Shon, H. K., & Kandasamy, J. (2009). Arsenic removal by a membrane hybrid filtration system. *Desalination, 236*(1), 363-369. doi:http://dx.doi.org/10.1016/j.desal.2007.10.088

Nicomel, N., Leus, K., Folens, K., Van Der Voort, P., & Du Laing, G. (2016). Technologies for Arsenic Removal from Water: Current Status and Future Perspectives. *International journal of environmental research and public health, 13*(1), 62.

Nicomel, N. R., Leus, K., Folens, K., Van Der Voort, P., & Du Laing, G. (2015). Technologies for arsenic removal from water: current status and future perspectives. *International journal of environmental research and public health, 13*(1), 62.

Ning, R. Y. (2002). Arsenic removal by reverse osmosis. *Desalination, 143*(3), 237-241. doi:http://dx.doi.org/10.1016/S0011-9164(02)00262-X

Nishimura, T. and Robins, R. G. A Re-evaluation of the Solubility and Stability Regions of Calcium Arsenites and Calcium Arsenates in Aqueous Solution at 25°C. *Mineral Processing and Extractive Metallurgy Review*,18 pp. 283-308, 1998.

Nishimura, T., & Robins, R. G. (2000). Removal of arsenic in gold cyanide processes. *Minor Elements 2000: Processing and Environmental Aspects of as, Sb, Se, Te, and Bi*, 135-140.

Niu, H. Y., Wang, J. M., Shi, Y. L., Cai, Y. Q., & Wei, F. S. (2009). Adsorption behavior of arsenic onto protonated titanate nanotubes prepared via hydrothermal method. *Microporous and Mesoporous Materials, 122*(1-3), 28-35. doi:10.1016/j.micromeso.2009.02.005

O'Day, P. A. (2006). Chemistry and Mineralogy of Arsenic. *Elements, 2*(2), 77-83. doi:10.2113/gselements.2.2.77

Opio, F. (2013). Investigation of Fe (III)-As (III) bearing phases and their potential for arsenic disposal.

Pagana, A. E., Sklari, S. D., Kikkinides, E. S., & Zaspalis, V. T. (2008). Microporous ceramic membrane technology for the removal of arsenic and chromium ions from contaminated water. *Microporous and Mesoporous Materials, 110*(1), 150-156. doi:http://dx.doi.org/10.1016/j.micromeso.2007.10.013

Pal, P., & Manna, A. K. (2010). Removal of arsenic from contaminated groundwater by solar-driven membrane distillation using three different commercial membranes. *Water Research, 44*(19), 5750-5760. doi:http://dx.doi.org/10.1016/j.watres.2010.05.031

Palmer, N. E., Freudenthal, J. H., & von Wandruszka, R. (2006). Reduction of Arsenates by Humic Materials. *Environmental Chemistry, 3*(2), 131-136. doi:http://dx.doi.org/10.1071/EN05081

Pan, B., Li, Z., Zhang, Y., Xu, J., Chen, L., Dong, H., & Zhang, W. (2014). Acid and organic resistant nano-hydrated zirconium oxide (HZO)/polystyrene hybrid adsorbent for arsenic removal from water. *Chemical Engineering Journal, 248*, 290-296. doi:http://doi.org/10.1016/j.cej.2014.02.093

Pena, M., Meng, X., Korfiatis, G. P., & Jing, C. (2006). Adsorption Mechanism of Arsenic on Nanocrystalline Titanium Dioxide. *Environmental Science & Technology, 40*(4), 1257-1262. doi:10.1021/es052040e

Peng, B., Song, T., Wang, T., Chai, L., Yang, W., Li, X., . . . Wang, H. (2016). Facile synthesis of Fe3O4@Cu(OH)2 composites and their arsenic adsorption application. *Chemical Engineering Journal, 299*, 15-22. doi:http://dx.doi.org/10.1016/j.cej.2016.03.135

Peng, X.-T., Jiang, L., Gong, Y., Hu, X.-Z., Peng, L.-J., & Feng, Y.-Q. (2015). Preparation of mesoporous ZrO2-coated magnetic microsphere and its application in the multi-residue analysis of pesticides and PCBs in fish by GC–MS/MS. *Talanta, 132*, 118-125. doi:http://dx.doi.org/10.1016/j.talanta.2014.08.069

Peralta Ramos, M. L., González, J. A., Albornoz, S. G., Pérez, C. J., Villanueva, M. E., Giorgieri, S. A., & Copello, G. J. (2016). Chitin hydrogel reinforced with TiO2 nanoparticles as an arsenic sorbent. *Chemical Engineering Journal, 285*, 581-587. doi:http://doi.org/10.1016/j.cej.2015.10.035

Pérez-Marín, A. B., Zapata, V. M., Ortuño, J. F., Aguilar, M., Sáez, J., & Lloréns, M. (2007). Removal of cadmium from aqueous solutions by adsorption onto orange waste. *Journal of Hazardous Materials, 139*(1), 122-131. doi:10.1016/j.jhazmat.2006.06.008

Podder, M. S., & Majumder, C. B. (2015). Phycoremediation of arsenic from wastewaters by Chlorella pyrenoidosa. *Groundwater for Sustainable Development, 1*(1–2), 78-91. doi:http://doi.org/10.1016/j.gsd.2015.12.003

Podder, M. S., & Majumder, C. B. (2016). Corynebacterium glutamicum MTCC 2745 immobilized on granular activated carbon/MnFe2O4 composite: A novel biosorbent for removal of As(III) and As(V) ions. *Spectrochimica Acta Part A: Molecular and Biomolecular Spectroscopy, 168*, 159-179. doi:http://doi.org/10.1016/j.saa.2016.05.056

Qiu, H., Lv, L., Pan, B.-c., Zhang, Q.-j., Zhang, W.-m., & Zhang, Q.-x. (2009). Critical review in adsorption kinetic models. *Journal of Zhejiang University-SCIENCE A, 10*(5), 716-724. doi:10.1631/jzus.A0820524

Qu, D., Wang, J., Hou, D., Luan, Z., Fan, B., & Zhao, C. (2009). Experimental study of arsenic removal by direct contact membrane distillation. *Journal of Hazardous Materials, 163*(2–3), 874-879. doi:http://dx.doi.org/10.1016/j.jhazmat.2008.07.042

Rahaman, M. S., Basu, A., & Islam, M. R. (2008). The removal of As(III) and As(V) from aqueous solutions by waste materials. *Bioresource Technology*, 99(8), 2815-2823. doi:https://doi.org/10.1016/j.biortech.2007.06.038

Raj, K. R., Kardam, A., & Srivastava, S. (2013). Development of polyethylenimine modified Zea mays as a high capacity biosorbent for the removal of As (III) and As (V) from aqueous system. *International Journal of Mineral Processing, 122*, 66-70. doi:http://doi.org/10.1016/j.minpro.2013.02.010

Ravenscroft, P., Brammer, H., & Richards, K. (2009). *Arsenic pollution: a global synthesis* (Vol. 28): John Wiley & Sons.

Reddy, D. H. K., & Yun, Y.-S. (2016). Spinel ferrite magnetic adsorbents: Alternative future materials for water purification? *Coordination Chemistry Reviews, 315*, 90-111. doi:http://doi.org/10.1016/j.ccr.2016.01.012

Redlich, O., & Peterson, D. L. (1959). A Useful Adsorption Isotherm. *The Journal of Physical Chemistry, 63*(6), 1024-1024. doi:10.1021/j150576a611

Robins, R. G., & Jayaweera, L. D. (1992). Arsenic in Gold Processing. *Mineral Processing and Extractive Metallurgy Review*, 9(1-4), 255-271. doi:10.1080/08827509208952710

Robins, R. G., Nishimura, T., & Singh, P. (2001). *Removal of arsenic from drinking water by precipitation, adsorption or cementation.* Paper presented at the International Workshop on Technologies for Arsenic Removal from Drinking Water, Dhaka.

Rodella, N., Bosio, A., Zacco, A., Borgese, L., Pasquali, M., Dalipi, R., . . . Bontempi, E. (2014). Arsenic stabilization in coal fly ash through the employment of waste materials. *Journal of Environmental Chemical Engineering, 2*(3), 1352-1357. doi:http://doi.org/10.1016/j.jece.2014.05.011

Roy, E., Patra, S., Madhuri, R., & Sharma, P. K. (2016). Europium doped magnetic graphene oxide-MWCNT nanohybrid for estimation and removal of arsenate and arsenite from real water samples. *Chemical Engineering Journal, 299*, 244-254. doi:http://dx.doi.org/10.1016/j.cej.2016.04.051

Saitúa, H., Campderrós, M., Cerutti, S., & Padilla, A. P. (2005). Effect of operating conditions in removal of arsenic from water by nanofiltration membrane. *Desalination, 172*(2), 173-180. doi:http://dx.doi.org/10.1016/j.desal.2004.08.027

Samsuri, A. W., Sadegh-Zadeh, F., & Seh-Bardan, B. J. (2013). Adsorption of As(III) and As(V) by Fe coated biochars and biochars produced from empty fruit bunch and rice husk. *Journal of Environmental Chemical Engineering, 1*(4), 981-988. doi:10.1016/j.jece.2013.08.009

Schmidt, S.-A., Gukelberger, E., Hermann, M., Fiedler, F., Großmann, B., Hoinkis, J., . . . Bundschuh, J. (2016). Pilot study on arsenic removal from groundwater using a small-scale reverse osmosis system—Towards sustainable drinking water production. *Journal of Hazardous Materials, 318*, 671-678. doi:http://dx.doi.org/10.1016/j.jhazmat.2016.06.005

Sen, M., Manna, A., & Pal, P. (2010). Removal of arsenic from contaminated groundwater by membrane-integrated hybrid treatment system. *Journal of Membrane Science, 354*(1–2), 108-113. doi:http://dx.doi.org/10.1016/j.memsci.2010.02.063

Shan, C., & Tong, M. (2013). Efficient removal of trace arsenite through oxidation and adsorption by magnetic nanoparticles modified with Fe-Mn binary oxide. *Water Research, 47*(10), 3411-3421. doi:10.1016/j.watres.2013.03.035

Singh, K., Sinha, T. J. M., & Srivastava, S. (2015). Functionalized nanocrystalline cellulose: Smart biosorbent for decontamination of arsenic. *International Journal of Mineral Processing, 139*, 51-63. doi:http://doi.org/10.1016/j.minpro.2015.04.014

Smith, K., Li, Z., Chen, B., Liang, H., Zhang, X., Xu, R., . . . Liu, S. (2017). Comparison of sand-based water filters for point-of-use arsenic removal in

China. *Chemosphere, 168*, 155-162. doi:http://doi.org/10.1016/j.chemosphere.2016.10.021

Staunton, W. P. (2016). Chapter 30 - Carbon-in-Pulp A2 - Adams, Mike D *Gold Ore Processing (Second Edition)* (pp. 535-552): Elsevier.

Stöber, W., Fink, A., & Bohn, E. (1968). Controlled growth of monodisperse silica spheres in the micron size range. *Journal of Colloid and Interface Science, 26*(1), 62-69. doi:http://dx.doi.org/10.1016/0021-9797(68)90272-5

Sun, T., Zhao, Z., Liang, Z., Liu, J., Shi, W., & Cui, F. (2017). Efficient As(III) removal by magnetic CuO-Fe3O4 nanoparticles through photo-oxidation and adsorption under light irradiation. *Journal of Colloid and Interface Science, 495*, 168-177. doi:http://doi.org/10.1016/j.jcis.2017.01.104

Sun, W., Li, Q., Gao, S., & Shang, J. K. (2012). Exceptional arsenic adsorption performance of hydrous cerium oxide nanoparticles: Part B. Integration with silica monoliths and dynamic treatment. *Chemical Engineering Journal, 185–186*, 136-143. doi:http://doi.org/10.1016/j.cej.2012.01.060

Sun, Y., Chen, S. S., Tsang, D. C. W., Graham, N. J. D., Ok, Y. S., Feng, Y., & Li, X.-D. (2017). Zero-valent iron for the abatement of arsenate and selenate from flowback water of hydraulic fracturing. *Chemosphere, 167*, 163-170. doi:http://doi.org/10.1016/j.chemosphere.2016.09.120

Sun, Z., Yu, Y., Pang, S., & Du, D. (2013). Manganese-modified activated carbon fiber (Mn-ACF): Novel efficient adsorbent for Arsenic. *Applied Surface Science, 284*, 100-106. doi:http://dx.doi.org/10.1016/j.apsusc.2013.07.031

Tahija, D., & Huang, H. H. (2000). Factors influencing arsenic coprecipitation with ferric hydroxide. *Minor Elements 2000: Processing and Environmental Aspects of as, Sb, Se, Te, and Bi*, 149-155.

Tajuddin Sikder, M., Tanaka, S., Saito, T., & Kurasaki, M. (2014). Application of zerovalent iron impregnated chitosan-caboxymethyl-β-cyclodextrin composite beads as arsenic sorbent. *Journal of Environmental Chemical Engineering, 2*(1), 370-376. doi:http://dx.doi.org/10.1016/j.jece.2014.01.009

Tanboonchuy, V., Grisdanurak, N., & Liao, C.-H. (2012). Background species effect on aqueous arsenic removal by nano zero-valent iron using fractional factorial design. *Journal of Hazardous Materials, 205–206*, 40-46. doi:http://doi.org/10.1016/j.jhazmat.2011.11.090

Tang, S. C. N., & Lo, I. M. C. (2013). Magnetic nanoparticles: Essential factors for sustainable environmental applications. *Water Research, 47*(8), 2613-2632. doi:http://doi.org/10.1016/j.watres.2013.02.039

Tang, W., Li, Q., Gao, S., & Shang, J. K. (2011). Arsenic (III,V) removal from aqueous solution by ultrafine α-Fe2O3 nanoparticles synthesized from solvent thermal method. *Journal of Hazardous Materials*, 192(1), 131-138. doi:https://doi.org/10.1016/j.jhazmat.2011.04.111

Tang, W., Su, Y., Li, Q., Gao, S., & Shang, J. K. (2013). Superparamagnetic magnesium ferrite nanoadsorbent for effective arsenic (III, V) removal and easy magnetic separation. *Water Research, 47*(11), 3624-3634. doi:10.1016/j.watres.2013.04.023

Tempkin, M., & Pyzhev, V. (1940). Kinetics of ammonia synthesis on promoted iron catalyst. *Acta Phys. Chim. USSR, 12*(1), 327.

Trois, C., & Cibati, A. (2015). South African sands as an alternative to zero valent iron for arsenic removal from an industrial effluent: Batch experiments. *Journal of Environmental Chemical Engineering, 3*(1), 488-498. doi:http://doi.org/10.1016/j.jece.2014.12.019

Tu, Y. J., You, C. F., Chang, C. K., Wang, S. L., & Chan, T. S. (2013). Adsorption behavior of As(III) onto a copper ferrite generated from printed circuit board industry. *Chemical Engineering Journal, 225*, 433-439. doi:10.1016/j.cej.2013.03.120

Tuna, A. T. A., özdemir, E., şimşek, E. B., & Beker, U. (2013). Removal of As(V) from aqueous solution by activated carbon-based hybrid adsorbents: Impact of experimental conditions. *Chemical Engineering Journal, 223*, 116-128. doi:10.1016/j.cej.2013.02.096

Ungureanu, G., Santos, S., Boaventura, R., & Botelho, C. (2015a). Arsenic and antimony in water and wastewater: Overview of removal techniques with special reference to latest advances in adsorption. *Journal of Environmental Management, 151*(0), 326-342. doi:http://dx.doi.org/10.1016/j.jenvman.2014.12.051

Ungureanu, G., Santos, S., Boaventura, R., & Botelho, C. (2015b). Arsenic and antimony in water and wastewater: Overview of removal techniques with special reference to latest advances in adsorption. *Journal of Environmental*

Management, 151, 326-342. doi:http://dx.doi.org/10.1016/j.jenvman.2014.12.051

Uppal, H., Hemlata, Tawale, J., & Singh, N. (2016). Zinc peroxide functionalized synthetic graphite: An economical and efficient adsorbent for adsorption of arsenic (III) and (V). *Journal of Environmental Chemical Engineering, 4*(3), 2964-2975. doi:http://doi.org/10.1016/j.jece.2016.05.038

Vijayaraghavan, K., Padmesh, T. V. N., Palanivelu, K., & Velan, M. (2006). Biosorption of nickel(II) ions onto Sargassum wightii: Application of two-parameter and three-parameter isotherm models. *Journal of Hazardous Materials, 133*(1-3), 304-308. doi:10.1016/j.jhazmat.2005.10.016

Vitela-Rodriguez, A. V., & Rangel-Mendez, J. R. (2013). Arsenic removal by modified activated carbons with iron hydro(oxide) nanoparticles. *Journal of Environmental Management, 114*, 225-231. doi:http://dx.doi.org/10.1016/j.jenvman.2012.10.004

Vithanage, M., Herath, I., Joseph, S., Bundschuh, J., Bolan, N., Ok, Y. S., . . . Rinklebe, J. (2017). Interaction of arsenic with biochar in soil and water: A critical review. *Carbon, 113*, 219-230. doi:http://doi.org/10.1016/j.carbon.2016.11.032

Wang, J., Gao, X., Xu, Y., Wang, Q., Zhang, Y., Wang, X., & Gao, C. (2016). Ultrasonic-assisted acid cleaning of nanofiltration membranes fouled by inorganic scales in arsenic-rich brackish water. *Desalination, 377*, 172-177. doi:http://dx.doi.org/10.1016/j.desal.2015.09.021

Wang, J., Xu, W., Chen, L., Huang, X., & Liu, J. (2014). Preparation and evaluation of magnetic nanoparticles impregnated chitosan beads for arsenic removal from water. *Chemical Engineering Journal, 251*, 25-34. doi:10.1016/j.cej.2014.04.061

Wang, S., Gao, B., Li, Y., Creamer, A. E., & He, F. (2017). Adsorptive removal of arsenate from aqueous solutions by biochar supported zero-valent iron nanocomposite: Batch and continuous flow tests. *Journal of Hazardous Materials, 322, Part A*, 172-181. doi:http://doi.org/10.1016/j.jhazmat.2016.01.052

Wang, S., Gao, B., Li, Y., Wan, Y., & Creamer, A. E. (2015). Sorption of arsenate onto magnetic iron-manganese (Fe-Mn) biochar composites. *RSC Advances, 5*(83), 67971-67978. doi:10.1039/c5ra12137j

Wang, S., Gao, B., Zimmerman, A. R., Li, Y., Ma, L., Harris, W. G., & Migliaccio, K. W. (2015). Removal of arsenic by magnetic biochar prepared from pinewood and natural hematite. *Bioresource Technology, 175*, 391-395. doi:10.1016/j.biortech.2014.10.104

Wang, Y., Duan, J., Liu, S., Li, W., van Leeuwen, J., & Mulcahy, D. (2014). Removal of As(III) and As(V) by ferric salts coagulation – Implications of particle size and zeta potential of precipitates. *Separation and Purification Technology, 135*, 64-71. doi:http://dx.doi.org/10.1016/j.seppur.2014.08.004

Wen, Z., Zhang, Y., Dai, C., Chen, B., Guo, S., Yu, H., & Wu, D. (2014). Synthesis of ordered mesoporous iron manganese bimetal oxides for arsenic removal from aqueous solutions. *Microporous and Mesoporous Materials, 200*, 235-244. doi:http://doi.org/10.1016/j.micromeso.2014.08.049

Xu, J.-h., Gao, N.-y., Zhao, D.-y., Chu, W.-h., He, G.-c., & Chen, P. (2016). Enhanced iron efficiency of Fe-impregnated granular activated carbon (Fe-GAC) for arsenate removal via Fe(II)–H2O2 method. *Journal of the Taiwan Institute of Chemical Engineers, 67*, 443-452. doi:http://dx.doi.org/10.1016/j.jtice.2016.07.036

Xu, W. H., Wang, J., Wang, L., Sheng, G. P., Liu, J. H., Yu, H. Q., & Huang, X. J. (2013a). Enhanced arsenic removal from water by hierarchically porous CeO2-ZrO2 nanospheres: Role of surface- and structure-dependent properties. *Journal of Hazardous Materials, 260*, 498-507. doi:10.1016/j.jhazmat.2013.06.010

Xu, W. H., Wang, L., Wang, J., Sheng, G. P., Liu, J. H., Yu, H. Q., & Huang, X. J. (2013b). Superparamagnetic mesoporous ferrite nanocrystal clusters for efficient removal of arsenite from water. *CrystEngComm, 15*(39), 7895-7903. doi:10.1039/c3ce40944a

Yan, L., Hu, S., & Jing, C. (2016). Recent progress of arsenic adsorption on TiO2 in the presence of coexisting ions: A review. *Journal of Environmental Sciences, 49*, 74-85. doi:http://doi.org/10.1016/j.jes.2016.07.007

Yan, W., Vasic, R., Frenkel, A. I., & Koel, B. E. (2012). Intraparticle Reduction of Arsenite (As(III)) by Nanoscale Zerovalent Iron (nZVI) Investigated with In Situ X-ray Absorption Spectroscopy. *Environmental Science & Technology, 46*(13), 7018-7026. doi:10.1021/es2039695

Yang, R., Su, Y., Aubrecht, K. B., Wang, X., Ma, H., Grubbs, R. B., . . . Chu, B. (2015). Thiol-functionalized chitin nanofibers for As (III) adsorption. *Polymer, 60*, 9-17. doi:http://doi.org/10.1016/j.polymer.2015.01.025

Ye, S., Jin, W., Huang, Q., Hu, Y., Shah, B. R., Li, Y., & Li, B. (2016). Development of Mag-FMBO in clay-reinforced KGM aerogels for arsenite removal. *International Journal of Biological Macromolecules, 87*, 77-84. doi:http://dx.doi.org/10.1016/j.ijbiomac.2016.01.087

Yoon, J., Amy, G., Chung, J., Sohn, J., & Yoon, Y. (2009). Removal of toxic ions (chromate, arsenate, and perchlorate) using reverse osmosis, nanofiltration, and ultrafiltration membranes. *Chemosphere, 77*(2), 228-235. doi:http://dx.doi.org/10.1016/j.chemosphere.2009.07.028

Yoon, Y., Park, W. K., Hwang, T.-M., Yoon, D. H., Yang, W. S., & Kang, J.-W. (2016). Comparative evaluation of magnetite–graphene oxide and magnetite-reduced graphene oxide composite for As(III) and As(V) removal. *Journal of Hazardous Materials, 304*, 196-204. doi:http://dx.doi.org/10.1016/j.jhazmat.2015.10.053

Yu, L., Peng, X., Ni, F., Li, J., Wang, D., & Luan, Z. (2013). Arsenite removal from aqueous solutions by γ-Fe2O3-TiO2 magnetic nanoparticles through simultaneous photocatalytic oxidation and adsorption. *Journal of Hazardous Materials, 246-247*, 10-17. doi:10.1016/j.jhazmat.2012.12.007

Yu, Y., Zhang, C., Yang, L., & Paul Chen, J. (2017). Cerium oxide modified activated carbon as an efficient and effective adsorbent for rapid uptake of arsenate and arsenite: Material development and study of performance and mechanisms. *Chemical Engineering Journal, 315*, 630-638. doi:http://doi.org/10.1016/j.cej.2016.09.068

Yürüm, A., Kocabaş-Ataklı, Z. Ö., Sezen, M., Semiat, R., & Yürüm, Y. (2014). Fast deposition of porous iron oxide on activated carbon by microwave heating and arsenic (V) removal from water. *Chemical Engineering Journal, 242*, 321-332. doi:http://dx.doi.org/10.1016/j.cej.2014.01.005

Zhang, C., Shan, C., Jin, Y., & Tong, M. (2014). Enhanced removal of trace arsenate by magnetic nanoparticles modified with arginine and lysine. *Chemical Engineering Journal, 254*, 340-348. doi:http://dx.doi.org/10.1016/j.cej.2014.05.133

Zhang, G., Qu, J., Liu, H., Liu, R., & Wu, R. (2007). Preparation and evaluation of a novel Fe–Mn binary oxide adsorbent for effective arsenite removal. *Water Research, 41*(9), 1921-1928. doi:http://doi.org/10.1016/j.watres.2007.02.009

Zhang, G., Ren, Z., Zhang, X., & Chen, J. (2013). Nanostructured iron(III)-copper(II) binary oxide: A novel adsorbent for enhanced arsenic removal from aqueous solutions. *Water Research, 47*(12), 4022-4031. doi:http://dx.doi.org/10.1016/j.watres.2012.11.059

Zhang, L., Zhu, T., Liu, X., & Zhang, W. (2016). Simultaneous oxidation and adsorption of As(III) from water by cerium modified chitosan ultrafine nanobiosorbent. *Journal of Hazardous Materials, 308*, 1-10. doi:http://doi.org/10.1016/j.jhazmat.2016.01.015

Zhang, M., Gao, B., Varnoosfaderani, S., Hebard, A., Yao, Y., & Inyang, M. (2013). Preparation and characterization of a novel magnetic biochar for arsenic removal. *Bioresource Technology, 130*, 457-462. doi:10.1016/j.biortech.2012.11.132

Zhang, M., He, G., & Pan, G. (2009). Combined DFT and IR evidence on metastable-equilibrium adsorption of arsenate on TiO2 surfaces. *Journal of Colloid and Interface Science, 338*(1), 284-286. doi:http://doi.org/10.1016/j.jcis.2009.06.024

Zheng, Y.-M., Yu, L., & Chen, J. P. (2012). Removal of methylated arsenic using a nanostructured zirconia-based sorbent: Process performance and adsorption chemistry. *Journal of Colloid and Interface Science, 367*(1), 362-369. doi:http://dx.doi.org/10.1016/j.jcis.2011.10.007

Zheng, Y.-M., Yu, L., Wu, D., & Paul Chen, J. (2012). Removal of arsenite from aqueous solution by a zirconia nanoparticle. *Chemical Engineering Journal, 188*, 15-22. doi:http://dx.doi.org/10.1016/j.cej.2011.12.054

Zhou, Y., Gao, B., Zimmerman, A. R., Chen, H., Zhang, M., & Cao, X. (2014). Biochar-supported zerovalent iron for removal of various contaminants from aqueous solutions. *Bioresource Technology, 152*, 538-542. doi:10.1016/j.biortech.2013.11.021

Zhou, Z., Liu, Y.-g., Liu, S.-b., Liu, H.-y., Zeng, G.-m., Tan, X.-f., . . . Cai, X.-x. (2017). Sorption performance and mechanisms of arsenic(V) removal by magnetic gelatin-modified biochar. *Chemical Engineering Journal, 314*, 223-231. doi:http://doi.org/10.1016/j.cej.2016.12.113

APPENDIX

This appendix mainly shows the information about the magnetic core materials and the arsenic adsorption performances of them as well as the arsenic uptake abilities of the as-purchased commercial titania, zirconia and ceria particles. The preliminary adsorption tests shown in this appendix were not conducted with systematically designed experimental conditions.

I. Fe_3O_4

SEM

The SEM image (Figure A-1) shows that the commercial grade magnetite particles have an octahedral shape and the particle size is around 50-100 nm. These nanoparticles show some degree of aggregation, which would probably reduce their adsorption capacity and reactivity, and also affect further functionalization.

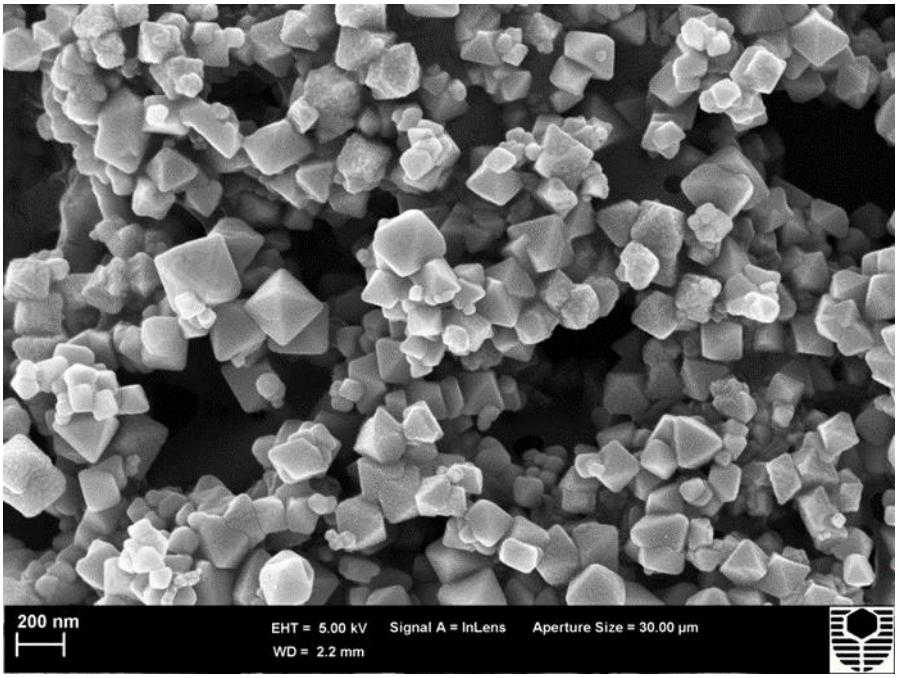

Figure A-1. SEM image of Fe_3O_4.

XRD

Figure A-2 shows the quantitative XRD analysis for the magnetite sample acquired from Sigma-Aldrich. The sample is composed of 98 wt% magnetite, 0.5 wt% quartz and 1.5 wt% amorphous content, which is in line with the description from the supplier.

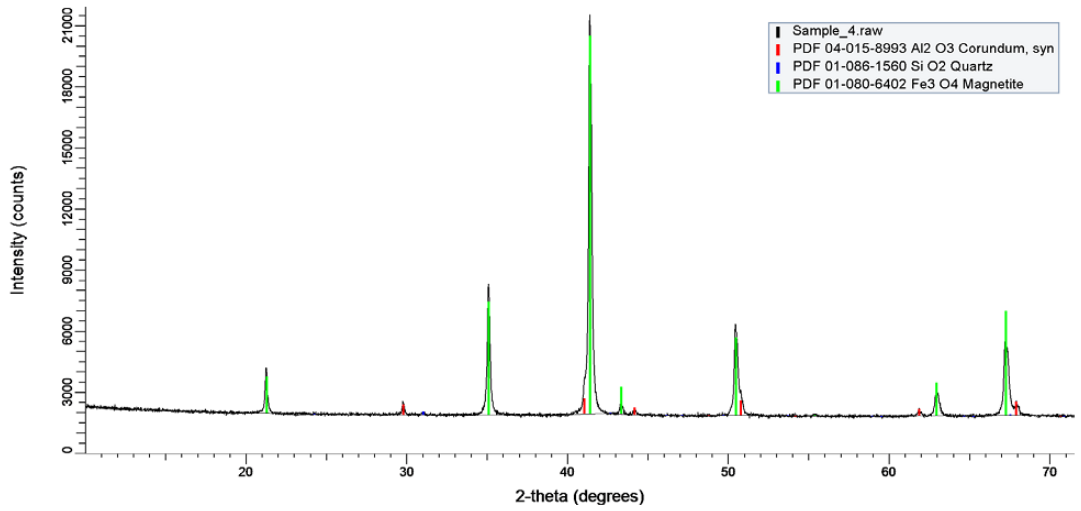

Figure A-2. Quantitative XRD spectrum of Fe_3O_4.

Adsorption tests

Table A-1 shows the results of adsorption tests without SCN^- and CNO^- in the system.

Table A-1. ICP-OES analysis results for Fe_3O_4 (without NaSCN and NaCNO). Experimental conditions: As concentration 10 ppm; Dosage 0.05 g; 24 h.

Arsenic	Initial pH	Removal/%	Capacity/mg·g^{-1}
As(III)	7	9.50	1.70
	8	11.17	2.00
	9	14.53	2.60
	10	10.61	1.90
As(V)	7	8.02	1.30
	8	11.11	1.80
	9	8.64	1.40
	10	6.17	1.00

Table A-2 shows the results of adsorption tests with 50 ppm SCN^- and CNO^- in the system. In combination with Table A-1, it can be seen that naked Fe_3O_4 nanoparticles can only adsorb a limited amount of As(III)/As(V) with a removal capacity of less than 3 mg·g^{-1} under alkaline conditions, with or without the presence of SCN^- and CNO^-. In addition, an increased dosage of adsorbents did not improve the removal rate and capacity for As (III). For As(V), removal was worse.

Table A-2. ICP-OES analysis results for Fe_3O_4 (with 50 ppm NaSCN and NaCNO). Experimental conditions: As concentration 100 ppm; pH 9.5.

Arsenic	Dosage/g	Time/h	Removal/%	Capacity/mg·g^{-1}
As(III)	0.1	4	5.53	2.75
As(III)	0.2	4	13.17	3.28
As(V)	0.1	1	1.96	1.00
	0.1	2	0.98	0.50
	0.1	4	0.00	0.00
As(V)	0.2	4	4.51	1.15
As(V)	0.5	1	7.49	0.73
	0.5	4	7.70	0.75

II. γ-Fe_2O_3

SEM

Figure A-3 shows the morphology of the as-purchased γ-Fe_2O_3 nanoparticles. Similar to the Fe_3O_4 particles, aggregation is observed. The particle size is approximately 20–40 nm.

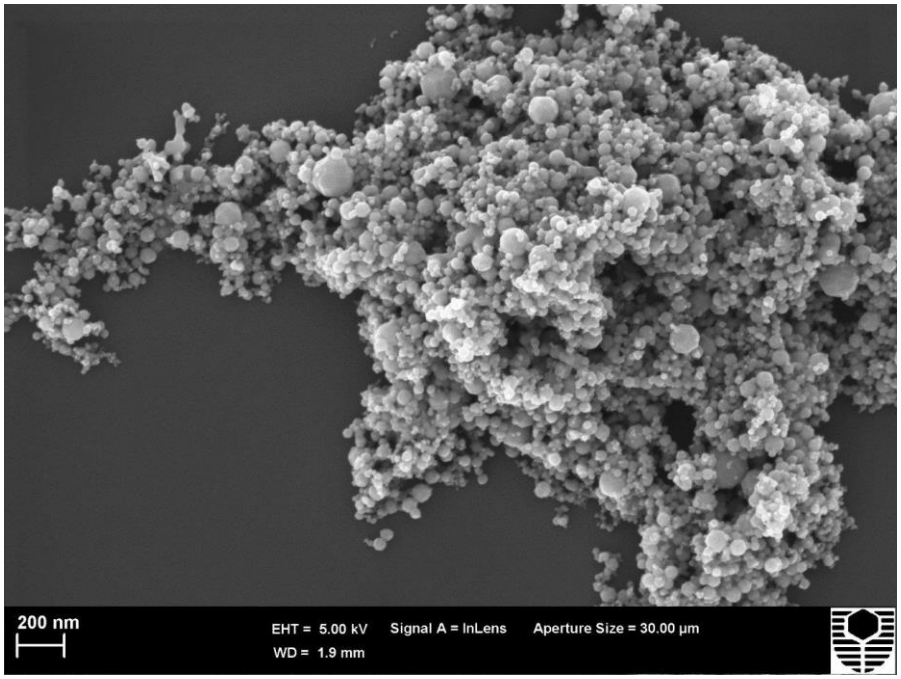

Figure A-3. SEM image of the commercial γ-Fe_2O_3 nanoparticles.

III. TiO_2

SEM

Figure A-4 shows the morphology of the commercial grade titanium dioxide nanoparticles. They are by and large spherical with a uniform size distribution (50-100 nm). These nanoparticles were also well-dispersed, compared with the magnetic particles.

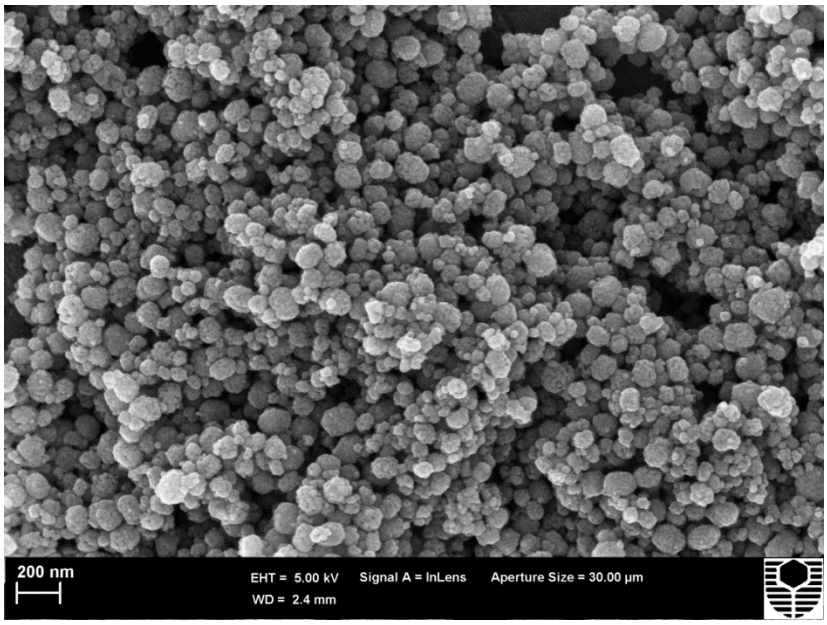

Figure A-4. SEM image of TiO_2 nanoparticles.

Figure A-5 shows the XRD patterns for the TiO_2 nanoparticles. As can be seen, the particles are composed of a mixture of rutile and anatase, with a ratio of 1:4 through a semi-quantitative method, where the amounts of the phases present have been normalised to 100%. This does not incorporate the amount of amorphous content, nor does it take into account any unfitted phases, nor the discrepancy between the calculated and the experimental data. However, it does give an estimate of a relative amount of each crystalline phase identified.

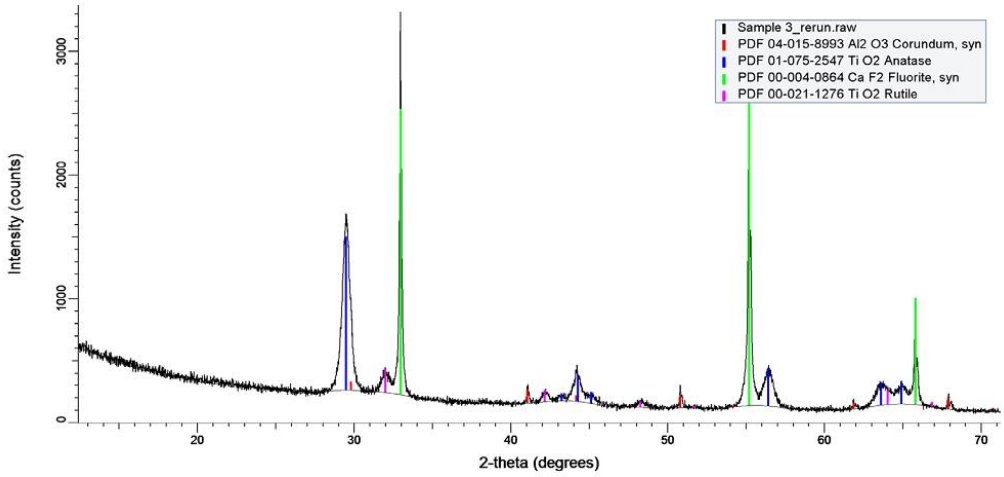

Figure A-5. Semi-quantitative XRD patterns for the commercial TiO_2 nanoparticles.

Adsorption tests

Table A-3 shows the ICP-OES results of adsorption tests for the commercial TiO_2 particles with 50 ppm SCN^- and CNO^- in the system, indicating low adsorption capacity.

Table A-3. ICP-OES analysis results for TiO_2.
(with 50 ppm NaSCN and NaCNO)
Experimental conditions: As concentration 100 ppm; pH 9.5.

Arsenic	Time/h	Dosage/g	Removal/%	Capacity/mg·g^{-1}
As(III)	4	0.1	27.34	13.60
As(III)	4	0.2	42.11	10.47
As(V)	1	0.1	8.73	4.45
	2	0.1	10.39	5.30
	4	0.1	6.67	3.40
As(V)	4	0.2	16.37	4.17
As(V)	1	0.5	47.57	4.59
	4	0.5	48.66	4.70

IV. ZrO_2

Adsorption tests

Table A-4 shows the ICP-OES results of adsorption tests for the commercial ZrO_2 particles with 50 ppm SCN^- and CNO^- in the system, indicating low adsorption capacity.

Table A-4. ICP-OES analysis results for ZrO_2 (with 50 ppm NaSCN and NaCNO). Experimental conditions: As concentration 100 ppm; pH 9.5.

Arsenic	Time/h	Dosage/g	Removal/%	Capacity/mg·g^{-1}
As(III)	1	0.1	14.81	7.25
	2	0.1	15.22	7.45
	4	0.1	14.30	7.00
As(III)	4	0.2	30.85	7.55
As(V)	1	0.1	7.2	3.60
	2	0.1	7.3	3.65
	4	0.1	7.8	3.90
As(V)	4	0.2	14.3	3.58

V. CeO_2

Adsorption tests

Only one group of adsorption tests were carried out to check the arsenic removal performance of the commercial CeO_2 particles. As(III)-only and As(V)-only solutions with initial concentrations of 100 ppm and initial pH value of 9.5 (approx.) were treated with 0.05 g CeO_2 sorbents for 24 h. The adsorption capacity obtained was 6.1 mg·g^{-1} and 4.0 mg·g^{-1} for As(III) and As(V), respectively.